Medizinische Fakultät der Otto-von-Guericke-Universität Magdeburg

in Zusammenarbeit mit dem

Cardiovascular Research Institute der University of Vermont

Mapping of Human Atrial Fibrillation –

Constraints of Dominant Frequency and Complex Fractionated Atrial Electrograms

Dissertation

zur Erlangung des Doktorgrades

Dr.med.

(doctor medicinae)

an der Medizinischen Fakultät

der Otto-von-Guericke-Universität Magdeburg

vorgelegt von Nicole Habel

Magdeburg, 2020

Bibliographische Beschreibung

Habel, Nicole:

Mapping of Human Atrial Fibrillation – Constraints of Dominant Frequency and Complex Fractionated Atrial Electrograms. - 2020. – 103 Bl., 27 Abb., 4 Tab.

Kurzreferat

Vorhofflimmern (VHF) ist eine der häufigsten Herzrhythmusstörungen, von der über 6,8 Millionen Menschen in Europa und den Vereinigten Staaten betroffen sind. Die medikamentöse Behandlung ist meist unzureichend, und mit steigender Belastung an Vorhofflimmern liefern derzeitige Ablationsverfahren nur unbefriedigende Ergebnisse. Dies ist auf inadäquate Ausführung der bestehenden Ablationsstrategien zurückzuführen und/oder deuted darauf hin, dass derzeitige Strategien unzureichend sind. Da die räumlich-zeitliche Komplexität von VHF eine große Anzahl von Elektroden erfordern würde um ein genaues Bild der gesamten Vorhoferregung zu erstellen, werden Ersatzparameter, wie dominante Frequenz (DF) und komplex fraktionierte atriale Elektrogramme (CFAE) verwendet, um kritische Bereiche zu identifizieren, die für die Aufrechterhaltung von VHF ausschlaggebend erscheinen. Allerdings haben auch diese Verfahren ihre Schwachstellen.

Die folgende Reihe von Studien ist darauf ausgerichtet, die Grenzen des Mapping von DF und CFAE mit heutigen Methoden zu erforschen. Außerdem untersuchen wir die fundamentalen Komponenten der räumlichen Auflösung von Elektroden[43], sowie deren Einfluss auf die Messwerte von Frequenz[113] und Fraktionierung[44]. Ausserdem wird ein Computermodell vorgestellt, das für die Untersuchung der Erregungsausbreitung und des daraus resultierenden Potentialfeldes entwickelt wurde. Dieses Modell wird dann in den folgenden Studien angewendet.

Ehrenerklärung

Ich erkläre, dass ich die der Medizinischen Fakultät der Otto-von-Guericke-Universität zur Promotion eingereichte Dissertation mit dem Titel

"Mapping of Human Atrial Fibrillation - Constraints of Dominant Frequency and Complex Fractionated Atrial Electrograms"

im Cardiovascular Research Institute der University of Vermont mit der Unterstützung durch Dr. Peter Spector und Prof. Helmut Klein ohne sonstige Hilfe durchgeführt und bei der Abfassung der Dissertation keine anderen als die dort aufgeführten Hilfsmittel benutzt habe.

Bei der Abfassung der Dissertation sind Rechte Dritter nicht verletzt worden.

Ich habe diese Dissertation bisher an keiner in-oder ausländischen Hochschule zur Promotion eingereicht. Ich übertrage der Medizinischen Fakultät das Recht, weitere Kopien meiner Dissertation herzustellen und zu vertreiben.

Colchester, Vermont (USA), den 28. Januar 2020

Nicole Habel

KEY WORDS

Ablation

Atrial Fibrillation

Autonomic nervous system

Complex Fractionated Atrial Electrograms

Computational Modeling

Dominant Frequency

Electrode Resolution

Intracardiac Electrograms

Mapping

Parasympathetic Blockade

Spatio-Temporal Variability

Sympathetic Blockade

Mapping of Human Atrial Fibrillation - Constraints of Dominant Frequency and Complex Fractionated Atrial Electrograms

Table of Contents

ABBREVIATIONS

AF   Atrial Fibrillation

AFCL   Atrial Fibrillation Cycle Length

AIPI   Average inter-potential interval

ANS   Autonomic nervous system

CA   Continuous Activity

CFAE   Complex Fractionated Atrial Electrograms

CV   Coefficient of variation

DF   Dominant Frequency

GP   Ganglionated plexi

HF   High Frequency

ICL   Interval confidence level

ICT   Intra-complex peak to peak time

IES   Interelectrode spacing

PAB   Pharmacologic autonomic blockade

PCL   Pacing cycle length

PPI   Post-pacing interval

PV   Pulmonary veins

PVI   Pulmonary vein isolation

SD   Standard deviation

TCL   Tachycardia cycle length

1. INTRODUCTION

Improvements in the treatment of atrial fibrillation are warranted

Atrial Fibrillation (AF) is one of the most common heart rhythm disturbances afflicting over 6.8 million people in Europe and the Unites States.[1,2] While AF itself is not immediately life threatening it is associated with an increased risk of stroke and can lead to tachycardia induced cardiomyopathy.[3] A wide ranges of symptoms including a fast heart rate, light-headedness, palpitations and shortness of breath can impact patients' lives. The frequency and duration of AF episodes vary from patient to patient and can progress over time. Patients can generally be categorized as having paroxysmal AF (self-terminating episodes, each lasting less than 7 days), persistent AF (episodes lasting more than 7 days and likely to require electrical or pharmacological cardioversion in order to restore sinus rhythm) or long-standing persistent/chronic AF (episodes can last several months and are virtually resistant to cardioversion).[4]

Pharmacologic treatment achieves rhythm control in 52% of patients, but its use can be limited by major side effects.[5] Catheter ablation on the other hand attains a 70% success rate for paroxysmal AF patients with pulmonary vein isolation (PVI) alone.[6] However, success rates decline with increased AF burden. Even though more extensive ablation lesions are delivered when treating patients with persistent or long-standing persistent AF success rates remain low (64.8% and 63.1%, respectively).[7]

Contributing factors for this dissatisfying outcome of catheter ablation are the following: Either the existing strategies for AF ablation are inadequately executed and/or the current strategies themselves are insufficient.

(1) Inadequate execution: Incomplete ablation lines not only result in treatment failure but also have the potential to be pro-arrhythmic. Studies investigating the fundamental relationship between power of energy delivery[8], duration of energy delivery[9], convective cooling[10], electrode size[11], contact force[12,13] and lesion size have improved our understanding of the biophysics of ablation and yielded increased precision of radiofrequency energy delivery through the development of catheters utilizing contact force sensing[14]. Analogous principles apply to the use of cyroablation.[15] Despite these advancements, we still lack the ability to accurately and reliably assess intra-operative lesion size three dimensionally;[16] the use of MR thermography[17] and real-time MRI[18] are currently under investigation.

(2) <u>Insufficient strategies:</u> The general practice of medicine involves a diagnostic measure and a treatment that is tailored to the findings of that diagnostic test. Unfortunately, this is currently not routinely employed in the treatment of atrial fibrillation. While rotor mapping has been the latest approach to target drivers of atrial fibrillation, the techniques are not without flaws and have yielded mixed results.[19,20] To date the standard approach involves PVI, linear lesions emulating the surgical Maze procedure and frequently "substrate modification", e.g. targeting dominant frequency (DF) or complex fractionated atrial electrograms (CFAEs).[21]

The first step in changing from this standard "one-size fits all" ablation to an individualized lesion set requires a mechanistic understanding of the initiation and maintenance of AF in the individual patient.

Current understanding of the mechanisms underlying atrial fibrillation

Atrial fibrillation is characterized by electrical derangement, with its initiation being dependent on triggers and its maintenance requiring the appropriate pro-arrhythmic substrate. Focal firing from the pulmonary veins is a major contributor to AF initiation. Hence, circumferential electrical isolation of the pulmonary vein musculature is used to quarantine these triggers.[22] In addition to the pulmonary veins other sites such as the Ligament of Marshall[23] and areas under the influence of ganglionated plexi can also exhibit abnormal automaticity and may be considered as target for ablation.[24]

While the importance of impulse initiation is widely recognized, there is still much controversy as to the mechanisms responsible for maintaining AF in humans. In 1914 Garrey[25] demonstrated that the persistence of fibrillation is independent of its initiation site and established that a critical tissue mass is needed to support fibrillation. He also found that altering the shape of the tissue impacts its ability to fibrillate (the narrower the tissue the less likely it is to sustain fibrillation). In 1962 Moe proposed the multiple wavelet hypothesis of atrial fibrillation[26] and subsequently gathered evidence for several co-existing reentrant waves sustaining AF using a computer model of electrical propagation.[27] With the advancements in electronics and computer technology Allessie and colleagues[28] were able to create activation maps of AF in the isolated canine heart: With the use of 192 simultaneous endocardial recordings these investigators were able to demonstrate multiple co-existing wavelets of varying size and conduction velocity. They further established that a critical number of wavelets is needed to maintain fibrillation. Hence, the balance of new wavelet formation to wavelet extinction determines the duration

of any given AF episode. These early studies paved the way for the Cox-Maze procedure, first performed in 1987. Incisional scars create lines of conduction block and alter the probability of wavelet formation vs. termination.

In 1993 Schuessler et al.[29] further elucidated the three-dimensional complexity of AF by simultaneously mapping the epicardial and endocardial activation sequence in the right atrium of canines. This study emphasizes that the heterogeneity in electrophysiological structure and function gives rise to spatio-temporal complexity of AF. Konings and colleagues at the Cardiovascular Research Institute in Masstricht[30] were the first to utilize high-density mapping of *human* AF. This landmark study supports the multi-wavelet hypothesis of atrial fibrillation but also demonstrated large inter-individual differences in the complexity of atrial activation.

A co-existent or alternative mechanism for the perpetuation of atrial fibrillation, namely rotors with fibrillatory conduction, has been extensively investigated by Jalife and colleagues[31,32]. Rotors are variants of functional reentry[33] and can either be stationary, meandering or anchor to structural obstacles. Utilizing high density electrical mapping of the isolated canine right atrium Schuessler et al.[34] demonstrated that increasing concentrations of acetylcholine can induce a state change from multiple reentrant wavelets to a single, relatively stable circuit. Optical mapping data from the isolated sheep heart[35] further suggests stationary rotors as one mechanism for the maintenance of AF. Clinical data has provided some indirect evidence for localized stable drivers.[36] However, limitations in acquiring detailed mapping information of human AF keeps the controversy about the individual mechanism maintaining atrial fibrillation alive.

Challenges in mapping of human atrial fibrillation

The spatio-temporal complexity and inter-individual variability of AF[30] make it difficult to distinguish between mechanistic drivers of AF and bystander activity. Hence, selecting appropriate targets for ablation remain challenging to date. While optical mapping allows for the direct visualization of myocardial excitation, it is only feasible in animal models. An indirect measure of electrical activity can be obtained using electrogram recordings. Unfortunately, reconstruction of the complex activation pattern of atrial fibrillation based on electrograms has practical limitations. A large number of electrodes would be required in order to obtain an exact picture of the beat to beat activity. An alternative approach to the

complete reconstruction of electrical activity during AF seeks the identification of surrogate markers that are critical to the perpetuation of the rhythm.

Based on optical mapping data in the isolated sheep heart[35] dominant frequency (DF) mapping has been proposed as a tool for identification of AF driver sites. Nademanee and colleagues[37] suggested that complex fractionated atrial electrograms (CFAE) represent areas of wavelet reentry and if targeted prevent perpetuation of AF. Initial studies provided promising result – CFAE ablation achieved 91% freedom of AF at 1 year follow-up[37] and targeting high DF sites resulted in freedom of AF in 88% of paroxysmal and 56% of persistent AF patients at a mean follow up of 9.3 ± 5.4 months.[38] However, subsequent studies of DF guided ablation[39,40] and a meta-analysis of 13 studies of CFAE ablation[41] concluded that targeting either surrogate may not provide any additional benefit over PVI alone.

The present work highlights several constraints encountered with DF and CFAE mapping: Both measures are not temporally stable[42], vary with the spatial resolution of the recording electrodes[43,44] and change unpredictably with autonomic tone[45]. These limitations may explain why substrate modification does not consistently improve outcomes.

2. STUDY AIMS

Targeted ablation of atrial fibrillation is desirable; however, the complexity of electrical activity makes it challenging to identify the underlying circuitry. In contrast, delineating the critical limb of other arrhythmias, such as atrial flutter, AVNRT or orthodromic reentrant tachycardia is comparatively straight forward. Additionally, there is much controversy around what drives atrial fibrillation in the individual patient. The ambiguity in identifying appropriate targets hinges on our inability to routinely use high-resolution, high-density mapping in every-day clinical practice. Such tools are currently not available for the clinical realm of transvenous EP studies. In lieu of complete data, clinical studies of atrial fibrillation have turned to surrogates, such as mapping of dominant frequency and complex fractionated atrial electrograms to identify targets for ablation.

The following series of studies is aimed at highlighting the limitations of mapping DF and CFAEs with current techniques and technologies. We further explore the underlying components of electrode spatial resolution, and how it influences measures of frequency and fractionation. We start by discussing a computational model designed for the study of electrical propagation and the electrical field it creates. This model is then utilized in the studies to follow.

Nicole Habel contributed to the following aspects of the individual studies:

- *"Emergence of complex behavior: An interactive model of cardiac excitation provides a powerful tool for understanding electric propagation"*: **Computational programming, model design, testing of the model, manuscript.**

- *"The temporal variability of Dominant Frequency and Complex Fractionated Atrial Electrograms constrains the validity of sequential mapping of human atrial fibrillation"*: **Data analysis, manuscript.**

- *"The impact of pharmacologic sympathetic and parasympathetic blockade on atrial electrogram characteristics in patients with atrial fibrillation"*: **Data analysis, manuscript**.

- *"Effects of electrode size and spacing on the resolution of intracardiac electrograms"*: **Study design, data analysis, manuscript.**

- *"Electrogram fractionation: The relationship between spatiotemporal variation in tissue excitation and electrode spatial resolution"*: **Study design, computational programming, data analysis, manuscript.**

3. COMPUTATIONAL MODELING

Introduction

Mathematical models are an ever-evolving component of biomedical science. Hodgkin and Huxley[46] were the first to describe the initiation and propagation of electrical activity as a product of the cellular electrical components (e.g. ion channels, ion concentrations inside and outside the cell and capacitance of the cell membrane). Over the past several decades sophisticated computational models have been developed to study individual ion channels[47–49], cardiac cells and the resultant action potential as a composite of their electrical components[50,51], excitation through a finite amount of tissue[27,52,53] up to whole-heart electrical activity[54].

The aim of the following study was to develop a physics based cellular automaton which allows for the study of electrical activity in two dimensions and the electric field it generates. The electric field can be sampled with electrodes of custom configuration (e.g. varying electrode size, inter-electrode spacing, unipolar or bipolar recording), thereby allowing for direct correlation of tissue behavior and electrograms. As is the nature with any computational model, it is only an approximation of cardiac tissue, and was designed with the intention to maximize simulation speed while accepting the trade off to omit certain details, such as current flow across individual ion channels.[55] Instead, cells are modeled to have several states (e.g. quiescent or excited with modulation of absolute and relative refractoriness) and are electrically connected with their neighbors through resistive pathways. The following study demonstrates that despite the limited set of rules, complex tissue behavior can emerge, comparable to more detailed computational models but with the benefit of being able to conduct experiments in quick succession without alteration of the starting conditions from one experiment to the other. Furthermore, it permits direct knowledge of tissue properties (e.g. action potential duration) and enables us to control components of interest *independently* from one another.

The computational model described in the following study has been utilized to study the impact of temporal variation, spatiotemporal variation and inter-electrode spacing on electrogram fractionation[44] (Section 6) as well as in the study of wave dynamics in atrial fibrillation.[56,57]

Emergence of complex behavior: An interactive model of cardiac excitation provides a powerful tool for understanding electric propagation[58]

Authors: Peter S. Spector, Nicole Habel, Burton E. Sobel, Jason H.T. Bates

We have developed a straightforward, physiologically based mathematical in silico model of cardiac electric activity to facilitate understanding of the fundamental principles that determine how excitation propagates through the heart. Despite its simplicity, the model provides a very powerful teaching tool. In fact, its simplicity is integral to the model's utility. The contrast between the minimal set of rules that govern the model's function and the widely varied complex behaviors it can manifest offers insight into the nature of emergent behavior in wave propagation. Emergence in this context refers to the richness of the tissue activation patterns that arise from the aggregate behavior of the simple cells that comprise the tissue. Each cell can be active, inactive, or refractory and interacts only with its immediate neighbors. From these simple building blocks, very elaborate global behaviors emerge.

MODEL UTILITY

From the perspective of the electrophysiology student, the notion of emergent properties can act as a Rosetta stone for deciphering electrophysiological behavior. The spread of electric excitation through the intricate 3D structure of the heart can take widely varied forms, ranging from the orderly propagation seen during sinus rhythm to the marked disorganization seen during ventricular fibrillation. Observation of the diverse and sometimes complex patterns of conduction (e.g. unidirectional block, reentry, spiral waves) as well as the responses to pacing maneuvers (e.g. entrainment) suggests to the electrophysiology student a nearly infinite array of possibilities, the mastery of which can be daunting. However, with study, it becomes apparent that one need not memorize every possible cardiac behavior. Instead, there are overarching principles of cardiac excitation and propagation[31] from which these varied phenomena emerge and through which one can understand and predict rather than memorize electrophysiological behavior. Understanding these fundamental principles is integral to mastering electrophysiology.

A framework for interpreting clinical observations predicated on these principles has been formalized in the computer model we have developed. The interactive nature of the model provides a substrate for active learning rather than passive observation. The student can simulate complex conduction, such as unidirectional block and reentry. This requires grappling with identification of the conditions that are fundamental to reentry, thereby providing a durable learning experience. Experimentation with the model facilitates learning and appreciation of the principles responsible for electrophysiological behaviors.

In the material to follow, we review the conceptual design of our model. We show several examples of how use of the model demonstrates important electrophysiological principles. What is provided, however, is not intended to be an exhaustive review of the lessons that can be learned from use of the model; rather, it serves as an introduction to the ways in which the model can be instructive.

MODEL DESIGN

There are an enormous number of aspects to any complex system that can be described mathematically. How comprehensively one designs a model of such a system depends on the desired use of the model's output. As a guiding principle, a model should be as simple as possible while maintaining sufficient detail to achieve simulation of the desired aspects of the system. The advantage of the simplest model is that it can be used more rapidly and easily than a complex model. There is a deeper conceptual utility conferred by simplicity that is succinctly expressed in a quote attributed to Albert Einstein: "Everything should be made as simple as possible, but not simpler." The phrase "as simple as possible" implies capturing the very essence of a system, excluding all that is incidental or derivative, whereas the phrase "but not simpler" implies leaving out nothing that is fundamental.

What we modeled

We defined a set of rules that govern the behavior of individual "cells" and how they interact with their immediate neighbors.

What we did not model

We did not explicitly model the global behavior of the tissue once it was excited. The spread of electric activity in our model is entirely an emergent property that arises from the programmed behavior of the

individual cells and their interactions. We also did not model the details of how cells become excited (i.e. the kinetics of ion channels), resorting instead to merely specifying a set of rules that each cell obeys depending on its circumstances. Somewhat surprisingly, the intricate details of how the excitation of a cell is achieved are not critical to the production of a vast array of clinically relevant macroscopic tissue behaviors.

THE BEHAVIOR OF THE MODEL

The properties of conduction in the tissue

For electric activation to propagate through tissue, current must flow from excited cells to adjacent quiescent, but excitable cells. A group of excited cells is referred to as a source, whereas a group of electrically connected adjacent, but unexcited cells are referred to as a sink. The relative sizes of a source and sink determine the success or failure and the rate of propagation.[59] Accordingly, the geometric arrangement of groups of cells and their interconnections influence the source/sink balance. For example, a wedge-shaped accessory pathway can exhibit unidirectional conduction as a consequence of its geometry, as illustrated in Figure 3.1. Here, a wavefront successfully propagates from the atrium into the wide end of the accessory pathway because the source (comprising the atrial cells surrounding the entrance to the pathway) is larger than the sink (made up of the 3 cells spanning the wide end of the pathway itself). This sink then becomes the source for the narrower region deeper within the pathway, and so on, until the narrowest part of the pathway is reached at the entrance to the ventricle. Now, however, the sink suddenly becomes very large, comprising the ventricular cells fanning out from the end of the pathway. At this point, the single cell in the source at the end of the pathway cannot generate enough current to activate the 3 cells in the sink, and propagation fails. The overall result is conduction block from an accessory pathway to the ventricle. But now consider what happens when activation proceeds in the opposite direction. For the most part, the scenario is the same except in reverse, until the activation is ready to leave the wide end of the pathway and enter the atrium. At this point, there are 3 cells in the source attempting to excite 5 cells in the sink, a more favorable ratio than the previous 1:3 situation, and propagation proceeds. The unidirectional block created by this pathway geometry can provide one of the conditions necessary for initiation and maintenance of reentry.[60]
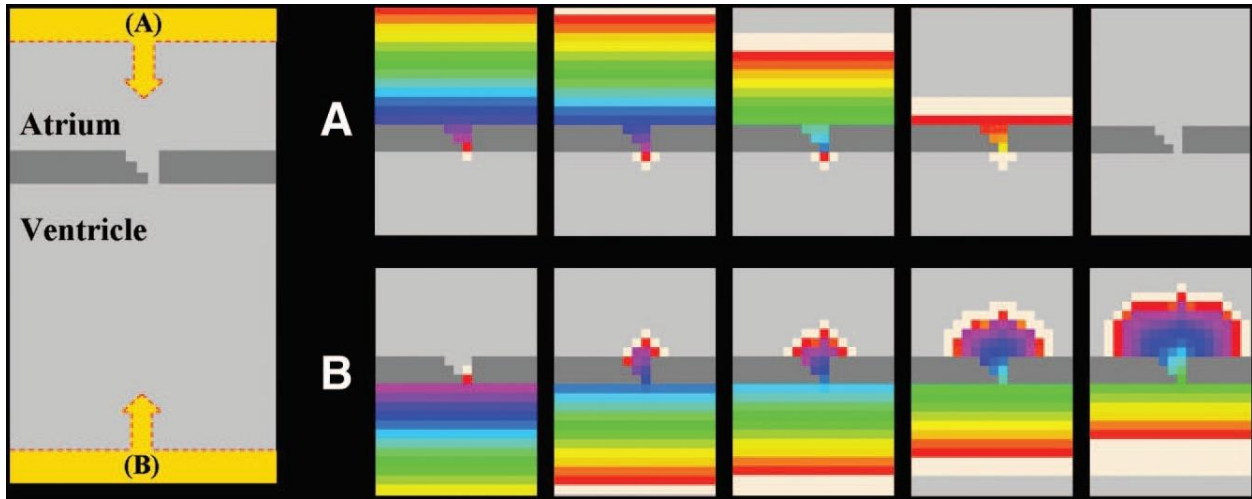
Figure 3.1. Source/sink relationships and unidirectional block. The geometry of a wedge shaped pathway determines its source/sink relationships creating unidirectional block. **A**, Atrium-to-ventricle conduction fails: At the ventricular insertion site of the pathway, the small source (1 cell) cannot depolarize the large sink (3 cells). **B**, Ventricle-to-atrium conduction succeeds: At the ventricular insertion site, there is a 3:1 source/sink ratio, and at the atrial insertion site, there is a 3:5 ratio. In both cases, the source/sink ratio is sufficient to allow propagation.

Reentry occurs when excitation travels along a path that ends where it began such that propagation repetitively transverses the circuit. Reentry is only possible when the conduction time around the loop is less than (or equal to) the time required for each cell in the circuit to recover excitability (refractory period). If the conduction time is shorter than the refractory period, the wavefront will encounter unexcitable tissue and extinguish. It is customary for electrophysiologists to express these parameters in terms of distances (*circuit length*, the physical distance over which electric activity must travel; *wavelength*, the distance from the leading edge to the trailing edge of the wavefront). The model can be used to explore these principles of reentry (Figure 3.2)
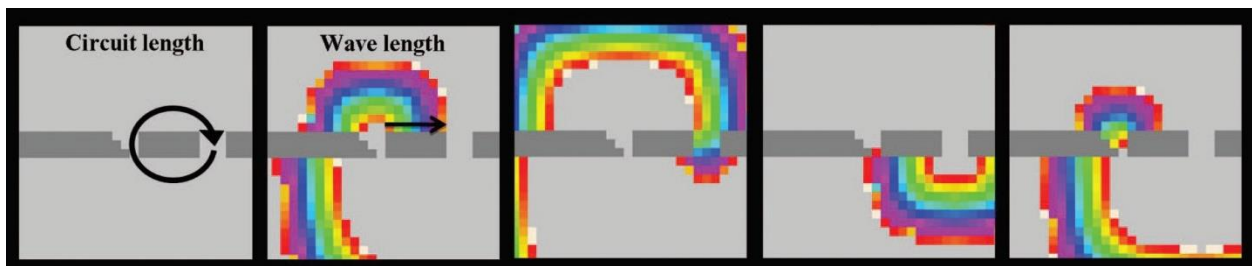

Figure 3.2. Reentry secondary to a fixed, anatomic substrate. Circuit length is the physical distance around the path of the reentry loop. Wavelength is the distance from the leading to the trailing edge of the excitation wavefront.

With the freedom to manipulate the characteristics of tissue conduction and refractoriness as well as the geometric distribution of healthy and diseased tissue, students can discover for themselves the fundamental conditions required for initiation, maintenance, and termination of reentry. The type of reentry described thus far has a fixed anatomic substrate (i.e., there is a physically determined circuit). There is a second type of reentry, however, that has a dynamic, functional substrate. In this latter case, the source/sink relationships determined by the shape of an activation wavefront produce the conditions responsible for reentry (reduced conduction velocity and block). By virtue of its geometry, a flat wavefront has an equal source and sink. A convex wavefront, on the other hand, has a larger sink than source, which causes it to propagate slowly, whereas the opposite is true for a concave wavefront. This situation is illustrated in Figure 3.3, which shows an initially planar wavefront moving to the right past a vertical linear segment of scar tissue. As the leading edges of the wavefront make their way past the scar, they develop a convex curvature because of the movement of activation into the region to the right of the scar. The concave portions travel the fastest, which eventually causes the wavefront to become planar again once it has moved far enough past the scar. Conduction velocity, and ultimately the success or failure of conduction, are thus function of wavefront curvature.[61]
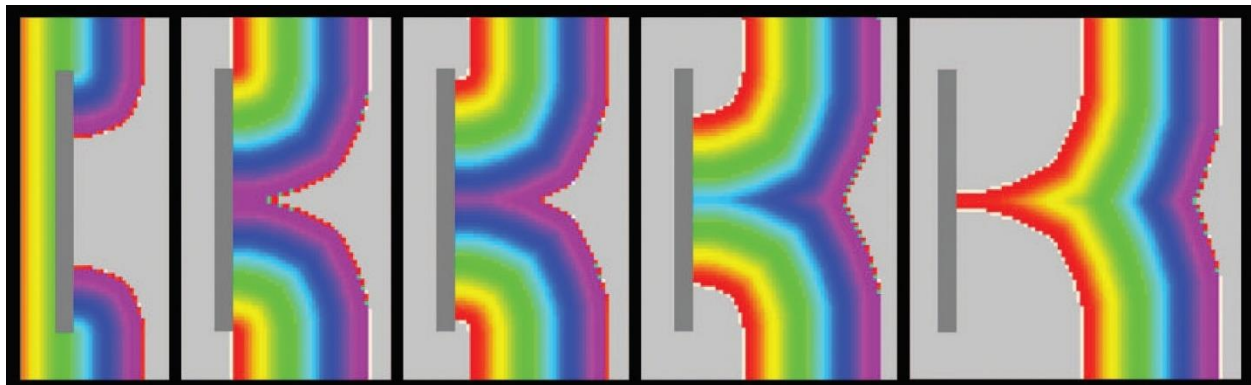

Figure 3.3. The effects of curvature on conduction velocity. As excitation spreads around a linear scar, two curved wavefronts coalesce, forming a concave leading edge. The source/sink ratio is greatest at the concave center, which therefore propagates more rapidly than the flatter portions of the wavefront. As a result, the wavefront becomes progressively less concave.

An extreme example of the effects of curvature is illustrated in Figure 3.4, which shows a spiral excitation wave, or rotor. The innermost portions of the rotor maintain a curvature so great that propagation fails (secondary to source/sink mismatch), creating a central area of excitable, but unexcited tissue around which the rotor spins. Manipulation of the model's initial conditions allows users to create multiple rotors that can degenerate into "daughter waves" that in turn can persist, divide, coalesce, or extinguish. Users can then explore the relationships between wavelength and circuit length, confirming for themselves the validity of the mass hypothesis of atrial fibrillation.[25]
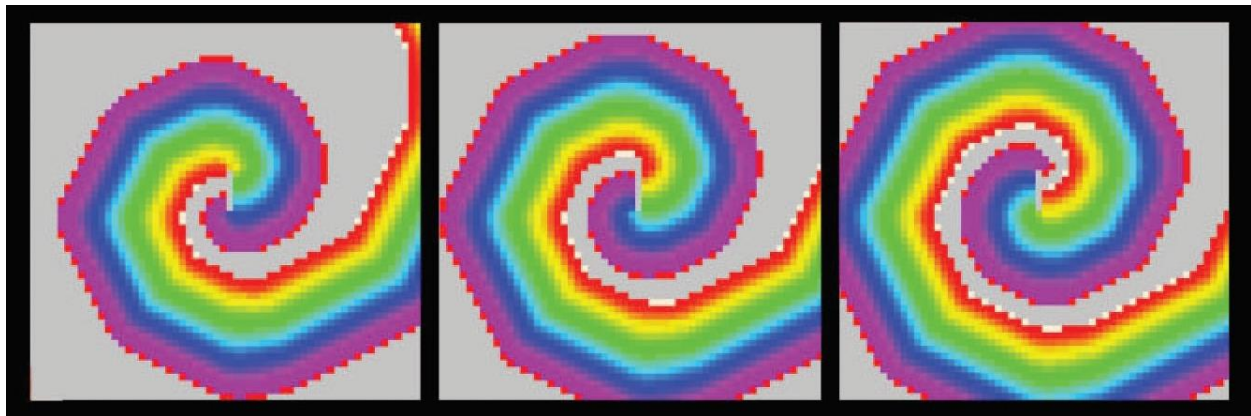

Figure 3.4. Reentry secondary to dynamic, functional substrate. The extreme curvature (center) results in propagation failure and a region of unexcited cells. A curved wavefront propagates around this area of functional block.

The Response to Pacing Maneuvers

Mapping provides a means of deducing the underlying activation pattern of the heart, but sometimes even an accurate activation map is insufficient for discerning which areas are responsible for driving an arrhythmia. For example, in the absence of conduction block, all areas of the heart are excited with each beat. However, only some areas of tissue are involved in the maintenance of an arrhythmia (i.e., are in the circuit), whereas others are simply passively driven as a result of activity emanating from the arrhythmogenic region (i.e., are out of the circuit). Entrainment mapping[62,63], is a clever means of using the response to pacing maneuvers to determine whether a pacing site is in or out of the tachycardia circuit (Figure 3.5). During entrainment mapping, one paces the heart at a cycle length slightly shorter than the tachycardia cycle length, which allows one to "capture" the circuit (activation occurs as a result of the paced wavefront rather than of the tachycardia wavefront). Pacing is then stopped, and the time from the last paced beat to the subsequent tachycardia beat, the postpacing interval, is measured. After the final

paced beat, activation proceeds from the pacing site to the circuit, around the circuit, and back to the pacing site. If the pacing site is in the circuit, then the time from the pacing site to the circuit (and back) is 0. If the conduction velocity around the circuit is the same during tachycardia as it is during pacing, then the time around the circuit is, by definition, equal to the tachycardia cycle length. Thus, if the postpacing interval is equal to the tachycardia cycle length, then the pacing site is in the circuit. If the postpacing interval is greater than the tachycardia cycle length, then either (1) the pacing site is out of the circuit or (2) the conduction velocity around the circuit is slower during pacing than during tachycardia (decremental conduction secondary to functional refractoriness).

Using the model, one can create a reentrant arrhythmia with both passive and active components and then pace at user-defined rates and locations. Examination of the response to pacing can elucidate the concepts integral to understanding entrainment mapping (Figure 3.5). Entrainment requires an electrically stable reentrant circuit (same cycle length and activation sequence with each beat) and an excitable gap (a period of time during which cells have recovered excitability after 1 excitation and before the arrival of the next wavefront).

The preceding are just a few examples of ways in which cardiac electrophysiology can be explored using the model. We invite the reader to experiment with the model on their own.
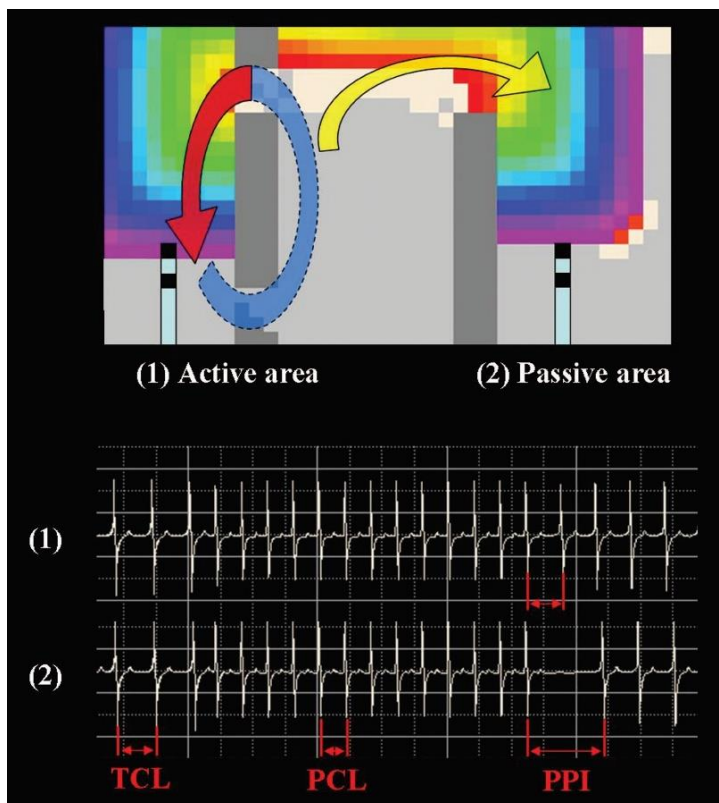

Figure 3.5. Entrainment mapping. A reentry circuit is shown wherein the reentrant wavelenght is indicated by the red arrow, the excitable gap is indicated by the blue tail, and the passive wavefront is indicated by the yellow arrow. Although every cell is activated with every beat, only the left side of the tissue (1, active area) is "in the circuit", whereas the right side of the tissue (2, passive area) is "out of the circuit". When pacing from the circuit (top tracing) the PPI is equal to the TCL. When pacing from outside the circuit (bottom tracing), the PPI is much longer than the TCL. PPI indicates postpacing interval; PCL, pace cycle length; TCL, tachycardia cycle length.

MODEL LIMITATIONS

Although our computational model exhibits a wide range of useful realistic behaviors, we must remain cognizant of the fact that it is far from a perfect representation of real cardiac tissue. Indeed, our emphasis has been on simplicity for ease of use and speed of operation, so there are numerous known details of cardiac electrophysiology that are not included. For example, we have not explicitly modeled the behavior of the numerous ion channels that dynamically regulate the flow of ions across cell boundaries. A great deal is known about these channels, which have been incorporated in other models.[50,64,65] Of course, the multiscale nature of biological systems means that we can, to a useful degree, replace the myriad details of these channels and their microscopic behavior with a set of empirical rules. These rules encapsulate most of the mesoscopic consequences of channel physiology, which in turn give rise to the macroscopic electric activity of the model. Nevertheless, our model does not link macroscopic electric activity directly to the microscopic behavior that causes it in a real heart. Another limitation of our model is its geometry; we consider merely a rectangular, 2D sheet of tissue. It is important to remember that the tissue geometry in 3 dimensions can be a critical factor in arrhythmogenesis[66], and even inclusion of a realistic curvature and topology in 2 dimensions has been used to advantage in previous models.[65,67] These various limitations of our model reflect the practical tradeoffs we have made in devising a convenient and manageable teaching tool.

DISCUSSION

Modeling of ion channels and action potentials got its start with the Hodgkin and Huxley[46] model for the behavior of ion channels in the giant axon of the squid. Very powerful models of cardiac cells were subsequently developed that used partial differential equations to describe ion channel behavior.[51,68] The accuracy of these models improved as data became available from voltage clamp experiments. These models provided a robust mathematical description of cardiac cell membrane behavior. By linking cells together through resistive gap junctions, such models could provide the building blocks for study of propagation through cardiac tissue.[69] Although such model designs provide a relatively detailed accounting of tissue behavior and are well suited to examine the effects of various physiological perturbations (e.g. pharmacological interventions or ischemia), they come at a very high computational cost.

Different model designs were developed that attempted to preserve much of the functional accuracy of

tissue behavior but at reduced computational burden. Models using differential equations that describe dampened oscillators[70–72] were developed and manifest many of the complex emergent properties of tissue propagation seen with ion channel-based models but with fewer variables and lower processing requirements.[73] An even greater level of design simplification makes use of cellular automata to study propagation in cardiac tissue.[27,74–76] Cellular automaton models (like ours) use (1) discrete cell states (quiescent, excited, refractory), (2) a simple lattice structure (generally square or hexagonal), and (3) a simplified set of rules that govern the way that cells update their state as a function of interaction with the state of their neighbors. The first application of cellular automata to cardiac propagation was conceived by Wiener and Rosenblueth[74] in 1946. Several subsequent modifications of this original cellular automata model have enhanced our understanding of the relationship between various functional parameters (e.g. excitability, dispersion, restitution) and complex propagation patterns. Moe et al.[27] incorporated a partially refractory state and demonstrated the role of dispersion of refractoriness in vortex formation. Fast et al.[75] expanded the neighborhood beyond the immediately adjacent cells and provided weighted coupling between cells. They and others made various modifications to the cellular automata rules to more accurately mimic tissue properties such as source/sink relationships and restitution.[75,76] With these modifications, they beautifully demonstrated emergent behaviors, including conduction velocity dependence on wave curvature, and excitation frequency and the dependence of rotor core trajectory on tissue excitability.

Each of these cellular automata models have a purely excitation state-based rule for propagation. The number of neighbors required to excite a cell vary from model to model. Some incorporate a larger neighborhood and a weighting function to determine the connectivity between cells. The present model is a variation on this theme in which cells have an "intrinsic" voltage that varies with time. Cells are electrically connected to their neighbors, and current shifts between cells according to Ohm's law. Thus, the intrinsic cell voltage (action potential) is altered through electrotonic interactions with the cell's neighbors during active as well as passive intercellular current flows. To the best of our knowledge, this agent-based model is the first to use such an approach. In so doing, the model allows current to accumulate over several time steps, ultimately reaching threshold for excitation. In this way, a cell's state depends on the state of its neighbors over several time steps. The present model thus exploits the computational efficiency of a cellular automaton for most of its behavior while gaining the precision afforded by differential equations to account for intercellular current flow.

21

CONCLUSIONS

The model described provides a concrete example of how guiding principles offer a means to decipher electrophysiologic behavior. Experimentation with the model enables students to interactively use the principles to explore electric propagation through excitable tissue. The model provides several advantages over in vivo laboratory demonstrations, including convenience, speed, flexibility, and independent control of relevant parameters. The speed of the model (related in part to its simplicity) facilitates interaction. Because students can conceive of an experiment, perform it, and observe its results in just a few minutes, the ability to learn iteratively is enhanced compared with the pace of learning from in vivo experimentation. Additionally, as opposed to in vivo experimentation, in silico experiments have the advantage that the initial conditions of one experiment are independent of the final conditions of the prior experiment. We hasten to point out that, of course, computer simulations are simply enhanced thought experiments and cannot be used to replace biological experiments. Rather, scientific discovery benefits from the interaction between experimentation and theoretical work (including computer simulations).

This computer model is simply a formalization of our understanding of the principles that govern macroscopic behavior of electric propagation, embodied in a set of rules obeyed by each cell in the model. The appropriateness of these rules is reflected in the extent to which the model behaves realistically under those circumstances that we deem to be of interest. Importantly, even the very minimal set of rules we have used here is adequate to produce a staggering array of complex emergent behavior at the level of the whole tissue. Thus, this model serves not only as a teaching tool for cardiac electrophysiology, but also as an example of how multiscale emergent behavior can arise in complex biological systems.

4. TEMPORAL VARIABILITY OF DOMINANT FREQUENCY AND COMPLEX FRACTIONATED ATRIAL ELECTROGRAMS

INTRODUCTION

It has been established that pulmonary vein firing is a major contributor to the initiation of atrial fibrillation and pulmonary vein isolation (PVI) is an effective means to quarantine these triggers.[22] On the other hand, when atrial fibrillation persists beyond PVI, the approach that follows is less well defined. Unfortunately, the complex activation pattern of atrial fibrillation precludes mapping of local activation time as it would require hundreds of closely spaced electrodes across the entire atria to create an accurate activation map. Instead, surrogate markers such as dominant frequency (DF) and complex fractionated atrial electrograms (CFAEs) have been proposed to identify areas critical to the maintenance of atrial fibrillation.[37,77]

Dominant Frequency Mapping

Mapping high frequency sites is thought to identify driver sites responsible for the maintenance of atrial fibrillation, as demonstrated in a sheep model by Mandapati and colleagues.[35] However, due to the complex nature of atrial activation during AF, which results in varying signal amplitude and morphology, time domain analysis (i.e. measuring the local activation time to determine the rate of activation) is not feasible. To overcome this barrier frequency domain analysis has been employed. An electrogram (i.e. contiguous signal) can be viewed as the summation of weighted sinusoidal functions (Fourier transform). If the signal has certain regularity (i.e. periodicity) over a long time, the magnitude of this frequency is scaled up in the power spectrum. The dominant frequency is then defined as the highest peak in the power spectrum.[78] A caveat to frequency analysis is high variability in activation intervals and inter-beat variation in morphology (e.g. split potentials) as these signals are not easily characterized by sine waves and may lead to multiple peaks in the power spectrum. The regularity index, defined as the ratio of the power at the dominant frequency band to the power of the whole frequency band, has been used as a metric to determine the reliability of the dominant frequency as the "true" atrial frequency.

Mapping of Complex Fractionated Atrial Electrograms

Fractionation, defined as repetitive high-frequency, low amplitude signal, is thought to be a substrate relevant to an arrhythmia circuit, as traditionally seen in mapping studies of scar based ventricular

tachycardia.[79] As we will explore later, there are multiple etiologies that can result in the phenotype of fractionation[44,80] and not all sites exhibiting CFAEs may be appropriate targets for ablation.

The prerequisite for considering dominant frequency and complex fractionated atrial electrograms as targets for ablation is that they must be temporally stable in order to acquire a global map sequentially. Optical mapping data by Kalifa et al.[81] demonstrated episodes of AF that are highly periodic, however the duration of observation has only been on the order of seconds. Similarly, mapping of DF and CFAE in human AF has been performed over five to ten second increments. In the following study, we sought to examine whether frequency and fractionation vary over time, utilizing multisite simultaneous electrogram recordings during 5 minutes of human atrial fibrillation. We found that both DF and CFAE sites which would be targeted for ablation under existing protocols are highly variable over the time course of 5 minutes. We conclude that DF and CFAE cannot be reliably mapped in a sequential manner with the standard catheter design.

The temporal variability of dominant frequency and complex fractionated atrial electrograms constrains the validity of sequential mapping in human atrial fibrillation[42]

Article in Heart Rhythm, May 2010

Authors: Nicole Habel, Pierre Znojkiewicz, Nathaniel Thompson, Joachim G. Müller, Bryan Mason, James Calame, Susan Calame, Shruti Sharma, Gagan Mirchandani, Deborah Janks, Jason Bates, Arshia Noori, Andreas Karnbach, Daniel L Lustgarten, Burton E. Sobel, Peter Spector

It has been postulated that mapping of dominant frequency (DF)[77] or complex fractionated atrial electrograms (CFAE)[37] can identify target sites for ablation in patients with atrial fibrillation (AF). In DF mapping, focal drivers are identified based upon radially distributed frequency gradients.[77,82] CFAE mapping identifies repetitive low-amplitude high-frequency electrograms as ablation targets.[37] In both mapping strategies, electrogram recordings are sequentially acquired with a roving catheter and thus are valid only if DF and CFAE remain stable over the timescale of the mapping procedure. We postulate that frequency and fractionation vary over time (Figure 4.1) and that, accordingly, the distribution of DF or CFAE on a sequentially acquired map will be influenced by the times at which points are sampled. As a consequence, sequential mapping may yield misleading results regarding the loci involved in the initiation or persistence of AF.
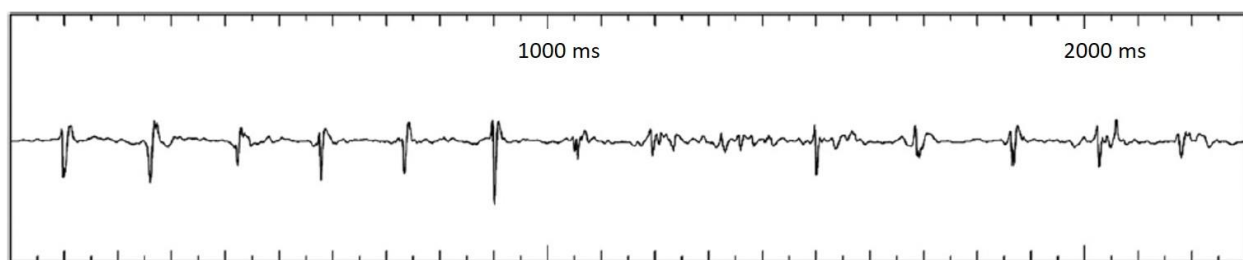

Figure 4.1. Example of the temporal variability of frequency and fractionation recorded on a bipolar electrogram from the basket catheter. Activation is slower and less fractionated in the beginning of the tracing and faster and more fractionated in the middle and slower by the end.

Recording from multiple sites simultaneously allows analysis of spatial frequency distribution without the confounding effects of variation in time. In the present study, we acquired spatially stable multi-electrode recordings with the use of a 64-electrode basket catheter. By virtue of leaving electrodes in the same position for 5 minutes, we were able to determine the stability of frequency and fractionation over much

longer time intervals than with a standard approach to mapping (~5 seconds/site). We created DF and CFAE maps using simultaneously acquired data and simulated sequential maps from the same data set. From these maps, we quantified the accuracy of sequential mapping for identification of DF and CFAE sites.

METHODS

Study Population

Eighteen patients presenting for ablation of symptomatic drug-refractory AF were studied (six paroxysmal, ten persistent, two long-standing persistent). The characteristics of the patients are summarized in Table 4.1. All patients provided written and informed consent. The study was approved by the Institutional Review Committee on Human Research.

Table 4.1 Patient characteristics (n = 18)	
Age, mean ± SD	59.7 ± 9.7
Female sex	6 (33%)
Coronary artery disease	1 (5%)
Hypertension	11 (59%)
Diabetes mellitus	2 (9%)
Sleep apnea	2 (9%)
AF duration, months	61.5 ± 73.4
AF type:	
Paroxysmal	6 (33%)
Persistent	10 (55%)
Long-standing persistent	2 (11 %)
Left ventricular ejection fraction	58.1 ± 12.8

Electrophysiologic studies

All patients were anticoagulated for ≥ 1 month before the study. Antiarrhythmic medications were stopped at least 5 days before the study, and amiodarone was discontinued for at least 3 weeks. Patients were anesthetized with desflurane, fentanyl, and rocuronium and intubated. Patients were enrolled in the study only if they had spontaneous or induced AF that lasted for at least 5 minutes. A double transseptal procedure was performed, and a 64-electrode basket catheter (1.25 mm ring electrodes;

Boston Scientific, Natick, MA) was placed in the left atrium and positioned to maximize the number of electrodes in stable contact with the myocardium (Figure 4.2). Basket size was chosen based on atrial dimensions as measured on a pre-procedural computed tomography scan. Basket dimension were 38, 48, 60, or 75 mm with inter-electrode spacing of 3, 4, 5, or 7 mm, respectively. Initial catheter position was recorded with the use of biplane cineangiography and then periodically checked with biplane fluoroscopy to confirm stability. In five randomly selected patients, electrode positions were monitored continuously with the NavEx system (St. Jude Medical, St. Paul, MN). Electrode movement was analyzed off-line and compared with the temporal changes in DF and CFAE.

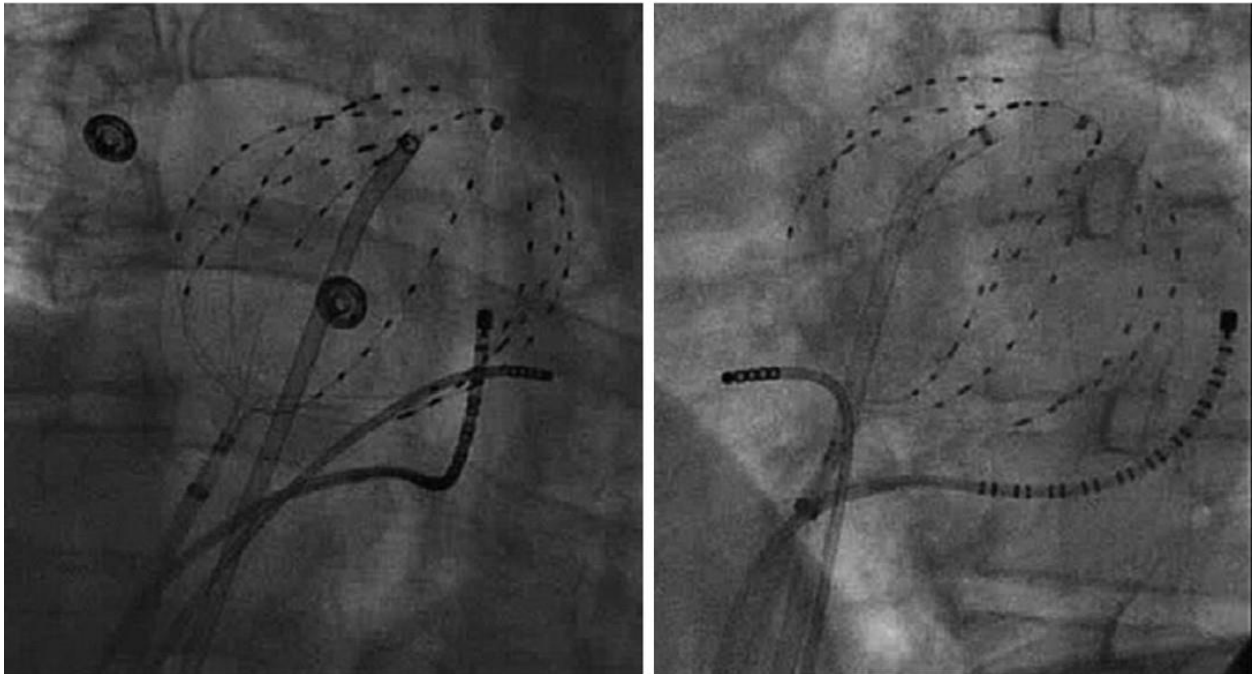**Figure 4.2.** Right anterior oblique (RAO) and left anterior oblique (LAO) fluoroscopic view of the basket catheter placed in the left atrium.

Study protocol

With the catheter in a stable position, electrograms were recorded for 5 minutes. After acquisition of the data, the basket catheter was removed. The planned clinical ablation procedure was then performed without regard to the basket recordings.

Data acquisition

Bipolar signals were sampled at 1 kHz and filtered from 30 to 500 Hz (Bard EP, Lowell, MA). Signals were exported and analyzed off-line with the use of MATLAB software (MathWorks, Natick, MA). Channels with obviously technically compromised signals were excluded from further analysis.

Signal processing and spectral analysis

DF analysis

DF analysis was performed with the use of the methods described by Sanders et al.[77] Signals were Hanning windowed, rectified, and band-pass filtered (3-15Hz). A 4096-point fast Fourier transformation was performed for each 5-second interval. The DF was defined as the maximum amplitude in the magnitude squared spectrum. DF values were excluded if the regularity index was less than 0.2.

Frequency maps

For each patient, we used the DF values calculated as described above to generate two kinds of frequency distribution maps: simultaneous maps in which the frequency at each site (bipolar electrode pair) was calculated from signals acquired during the same 5-second recording period for all 32 electrode pairs and sequential maps in which the frequency at each electrode pair was calculated from sequential 5-second recording periods. A random number generator was used to select the order in which points were chosen for the sequential maps (location and time segment). For each patient, 10 separate sequential maps were generated with different sequences of data points for each map. Simultaneous maps were produced for each 5-second interval during the 5-minute recording period (i.e. 60 simultaneous maps per patient).

DF sites

Using the methods of Sander et al.[77] a site was defined as a DF site if its DF was at least 20% greater than the DF of its closest neighbors (i.e. the eight electrode pairs adjacent to the recording site). Sites were included only if data were available from three or more of the nearest neighbor sites.

CFAE analysis

Electrograms were analyzed with custom software modified from a commercially available automated CFAE detection algorithm (Biosense Webster, Diamond Bar, CA) and divided into 2.5-second segments.

Deflections that were greater than 0.05 mV but less than 0.15 mV were tagged.[83,84] Duration of the intervals between these deflections was then measured. Intervals greater than 70ms but less than 120ms were defined as CFAEs.[84] The number of CFAEs per 2.5-second segment (interval confidence level [ICL] and the inter-potential intervals were recorded.

CFAE sites

A site was defined as a CFAE site based upon two previously reported definitions: ICL ≥ 5[84] and an average inter-potential interval (AIPI) of < 100 ms.[85]

False-positive and false-negative sites

The purpose of DF and CFAE mapping is the identification of sites that participate in maintaining AF so that they can be targeted for ablation. As such, any site that demonstrates the potential to drive AF *at any time* qualifies as an ablation target. For our analysis, we therefore considered sites that met the above criteria for DF and CFAE sites as "true positives" if they were positive on the simultaneous map at any time throughout the 5-minute recording. Accordingly, a site was defined as false negative if it was not identified as DF/CFAE site on the sequential map but was identified on *any* of the simultaneous maps. A site was considered a false positive if it was identified as a DF site on a sequential map but not on *any* of the simultaneous maps.

Electrode movement compared with temporal changes in DF and CFAE

DF, AIPI, and ICL were measured using a sliding window, offset by 13 ms. The x, y and z coordinates for each electrode (sampled every 13ms by the NavEx system) were used to calculate its position relative to its initial location. DF and CFAE measurements as well as position data were plotted against time and then underwent frequency analysis using fast Fourier transformation. The frequency resolution was adapted to the sampling frequency and the number of sampled data points. Linear correlation analysis was then performed on the resulting power spectra (DF, AIPI, and ICL vs. electrode position). Mean and standard deviation (SD) of Pearson's correlation coefficient were calculated over all sites.

Analyses for comparison with previous studies

For the purpose of direct comparison with prior studies of the temporal stability of DF and CFAE, we performed several analyses analogous to those performed in these studies. For comparison with Sander et al.[77] we examined DF during the first and second 5-second time segments of 10 randomly selected 10-

second intervals. For comparison with Scherr et al.[84] we analyzed 10 randomly selected pairs of time points from each map location in all 18 patients. In addition, for comparison with Verma et al.[86] we analyzed the first time sample from each minute of our data.

Statistical analysis

Data are reported using descriptive statistics (mean ± SD), and to further describe the dispersion of measurements, the coefficient of variation (CV) was calculated. The CV is a normalized measure defined as the ratio of the SD to the mean. Wilcoxon signed-rank test and Friedman test were performed with the PRISM (version 5.01) statistical software package (GraphPad Inc., La Jolla, CA). $P < 0.5$ was considered statistically significant.

RESULTS

Recordings

We recorded 32 bipolar electrograms per patient (64 electrodes). DF and CFAE analysis was performed only on signal with adequate signal-to-noise ratio (an average of 21.6 ± 4.3 bipolar electrograms per patient).

Dominant Frequency

We assessed the DF at each recording site during the 60 sequential 5-second time segments of the 5-minute recording. Analysis of these DFs revealed marked variation from time segment to time segment (temporal variability) and from recording site to recording site (spatial variability; Figure 4.3).
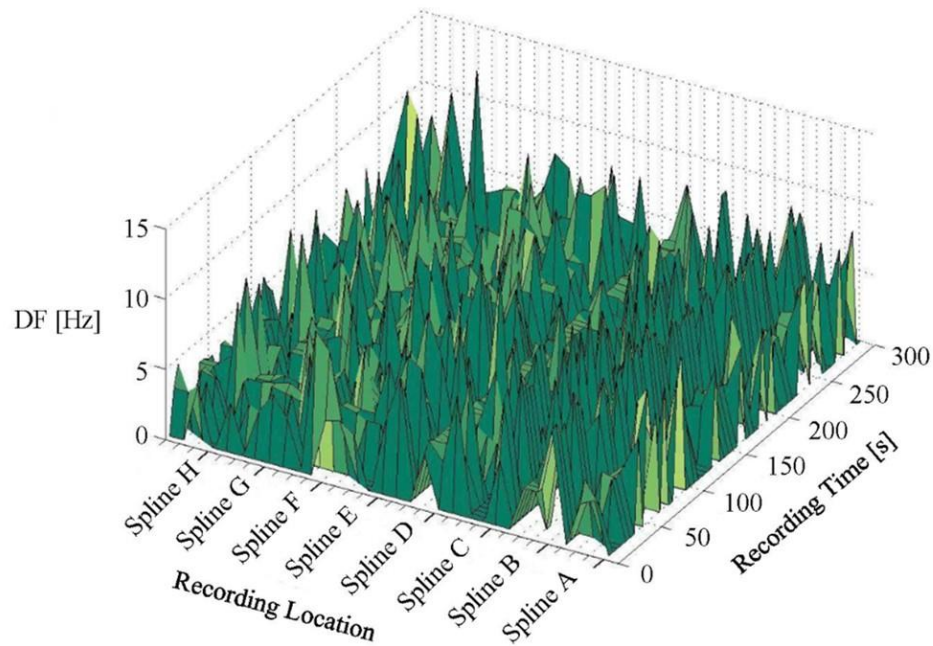
Spatial and Temporal Variability of DF

Figure 4.3. Example of DF variability (in patient 15) plotted over time and space. Graphed from right to left on each spline are electrode pairs 1 to 4. Zeros indicate poor signal quality or regularity index < 0.2.

Temporal variability of DF

To quantify temporal variability, we calculated the coefficient of variation (SD/mean) over 5 minutes for each recording site. There was significant variation of DF over time: the average temporal coefficient of variation (all sites, all patients) was 22.7 ± 5.4%. As indicated by SD and range of the coefficients themselves, there were also significant differences in the amount of variation from site to site (P ≤ 0.02 for all patients) and patient to patient (P = 0.008; Figure 4.4).
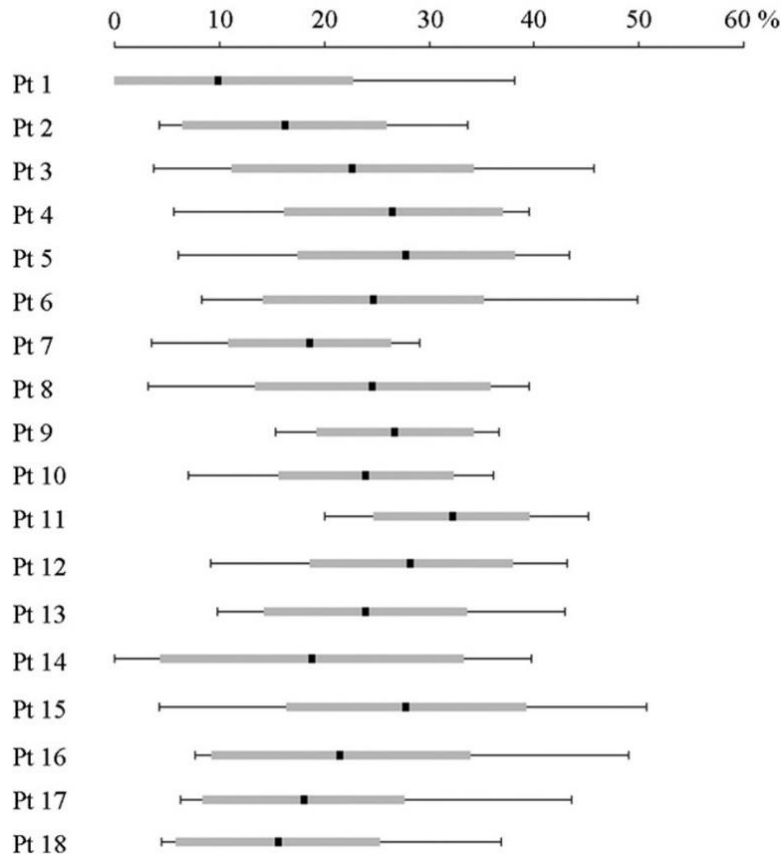
Figure 4.4. Temporal coefficient of variation (CV) of DF. The *center square* (■) indicates mean CV over all sites; the *thick grey bar* indicates SD; the *thin black line* indicates range.

Spatial variability of DF

The spatial coefficient of variation across all recording sites for each 5-second segment was calculated to quantify spatial variability. This analysis revealed marked variation of DF across the atrium: the average spatial coefficient of variation was $26.9 \pm 6.6\%$. There were significant differences between time segments ($P < 0.001$ for all patients) and between patients ($P = 0.008$).

DF site identification was time dependent

Simultaneous maps were created of each 5-second time segment (i.e. 60 maps were created for each patient; Figure 4.5). As a consequence of temporal variation of DF, DF sites were present during some time segments but not during others.

An average of 11.4 out of 32 sites (36%) was identified as DF sites after 5 minutes of continuous simultaneous recording. DF sites were transient, on average lasting only 22.1 seconds out of 5 minutes. Therefore, selection of a single 5-second sample by sequential mapping would yield only a 7.4% probability of identifying these DF sites.

DF site identification was sequence dependent

As a result of temporal variability, the value of DF at any site depended on the time at which that site was sampled. Therefore, sequential maps could yield misleading results (e.g. by sampling fast areas when they are slow and slow areas when they are fast). Sequential maps differed from simultaneous maps, sometimes correctly and sometimes falsely identifying DF sites. The 10 random sequential maps also differed from each other, that is, the DF sites were not the same on all of these 10 maps.

The probability that sequential mapping would fail to identify DF sites was 93%. In contrast, sequential mapping rarely mistakenly labeled non-DF loci as DF sites (probability 0.3%).
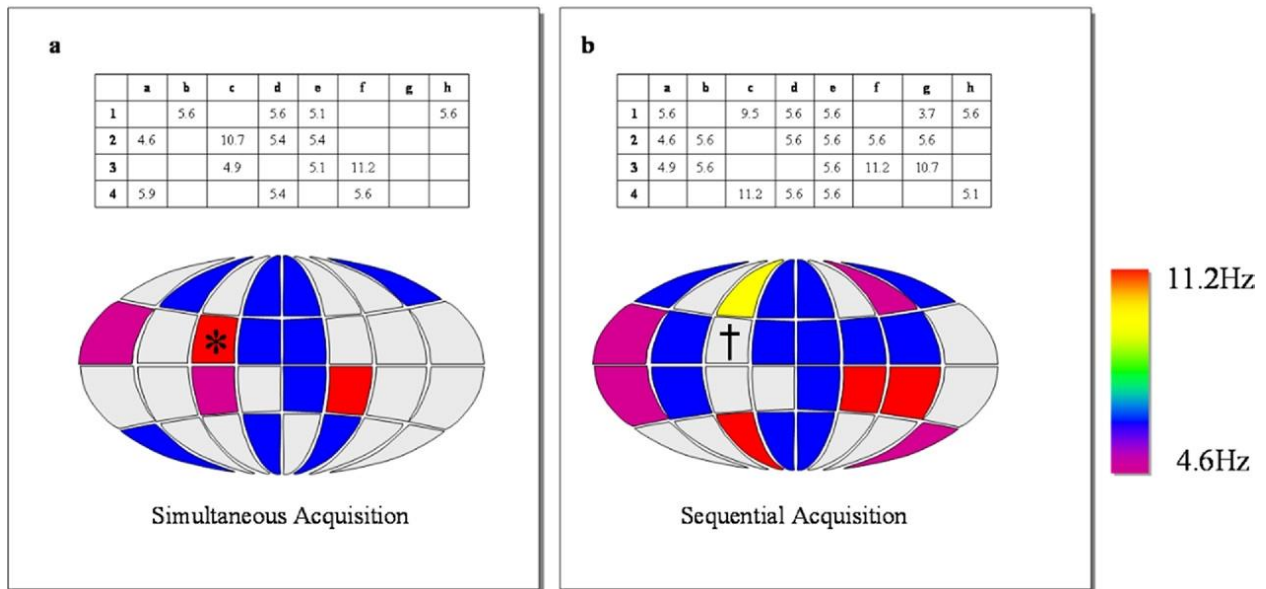

a

	a	b	c	d	e	f	g	h
1		5.6		5.6	5.1			5.6
2	4.6		10.7	5.4	5.4			
3			4.9		5.1	11.2		
4	5.9			5.4		5.6		

b

	a	b	c	d	e	f	g	h
1	5.6		9.5	5.6	5.6		3.7	5.6
2	4.6	5.6		5.6	5.6	5.6	5.6	
3	4.9	5.6			5.6	11.2	10.7	
4			11.2	5.6	5.6			5.1

Simultaneous Acquisition

Sequential Acquisition

11.2Hz

4.6Hz

Figure 4.5. Simultaneous versus sequential maps. (a) Example of a simultaneous acquisition (same 5-second time segment all sites) Top panel: DF values from each electrode pair simultaneously acquired (blanks represent poor signal quality or regularity index <0.2). Bottom panel: color-coded frequency map (top to bottom = electrode pairs 1-4, left to right = spline a-h; note spline A is adjacent to spline H). (b) Example of sequential acquisition (different 5-second time segments each site). Top panel: DF values acquired sequentially. Bottom panel: color-coded frequency map. (Note that DF values do not necessarily correspond with those acquired simultaneously.) The DF site at C2 on the simultaneous map (*) is not identified on the sequential map (†, i.e. false negative).

33

CFAE vary over time

We assessed the number of CFAEs and the interpotential intervals at each recording site during the 120 sequential 0.5-second time segments of our 5-minute recording. Both analyses revealed spatial and temporal variability.

CFAE sites defined by ICL ≥ 5

Out of all sites, 51 ± 33% were identified as CFAE sites. CFAE sites were transient; the average time to first CFAE was 11.1 ± 37.1 seconds. The average duration that a site continuously met criteria as a CFAE site was 8.8 ± 11.3 seconds. The average duration for which a CFAE site did not meet criteria (i.e., the time during which it could be falsely classified as a "non-CFAE site") was 6.8 ± 15.7 seconds. CFAE site identification was sequence dependent. Sequential maps failed to correctly identify 35.9 ± 14.9% of CFAE sites.

CFAE sites defined by AIPI ≤ 100 ms

A total of 47 ± 41% of sites were CFAE sites. The average observation time required to first meet these criteria was 10.8 ± 36.6 seconds. The average duration that sites continuously met CFAE site criteria was 47.2 ± 79.7 seconds. The average duration that a CFAE site failed to meet criteria was 20.7 ± 37.6 seconds. CFAE site identification was sequence dependent; sequential maps failed to correctly identify 38 ± 16% of CFAE sites.

Temporal variations of DF and CFAE were not related to catheter movement

The average electrode movement was ± 1.56, 0.98, and 1.73 mm along the x, y, and z axes, respectively. Analysis of electrode position versus time revealed a periodicity at the frequency of respiration (all patients were mechanically ventilated). In contrast, analysis of DF, AIPI, and ICL versus time revealed no periodicity. There was no correlation between electrode movement and changes in DF, AIPI, and ICL, r = 0.24 ± 0.20, 0.21 ± 0.19, and 0.24 ± 0.23 with $P < 0.05$ in 98%, 100% and 99% of all sites, respectively (Figure 4.6).

**Power Spectra of Electrode Movement
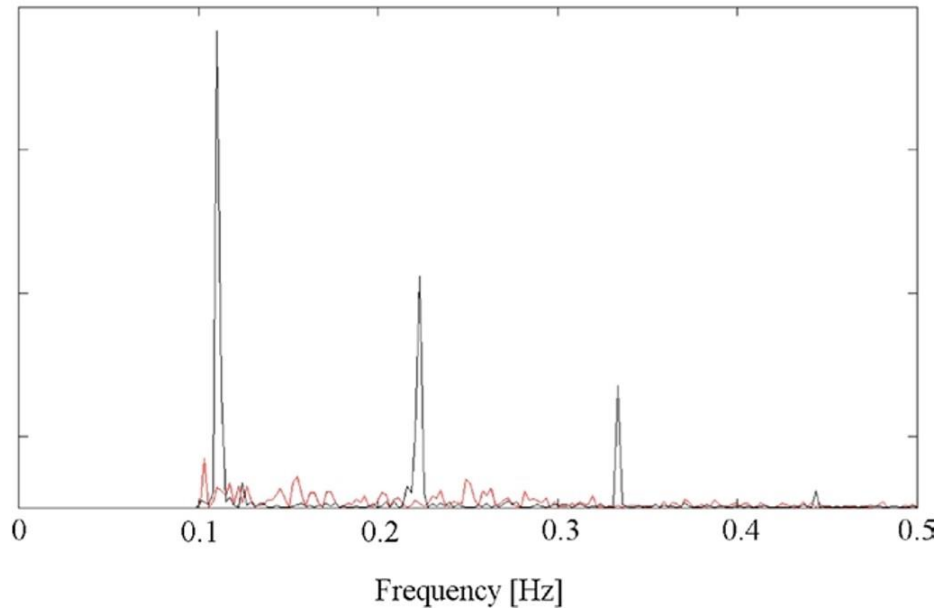and Change of DF over Time**

Frequency [Hz]

Figure 4.6. Examples of the frequency content of electrode movement and of change of DF over time. The red line represents the power spectrum of the DF versus time plot. The black line represents the power spectrum of the electrode position versus time plot. Linear correlation analysis reveals significant non correlation (R = 0.2339, P < 0.001).

Comparison with previous studied

Consistent with the findings of Sanders et al.[77], when we compared only the first and second 5-second time segments of 10 randomly selected 10-second windows we found no significant variability (5.55 ± 1.82 vs 5.55 ± 1.84 Hz, respectively; P = 0.60). Similarly, in an examination analogous to that of Scherr et al.[85], when we compared 10 randomly selected pairs of time points from each map (in all patients), we found that 83 ± 3% of sites initially defined as CFAE sites (defined by AIPI < 100 ms) remained CFAE sites, while 17 ± 3% did not meet criteria as CFAE sites during the second time point. Finally, similar to the results from Verma et al.[86], analysis of the first time sample from each minute of our data revealed a mean change in cycle length of 14.6 ± 14.1 ms (P = 0.10).

DISCUSSION

Given the prevalence of AF[87], its impact on patients and the health care system[88], and the relatively poor efficacy of antiarrhythmic medications[5,89], ablation has been vigorously pursued as a therapeutic approach. Indeed, ablation for AF has met with significant success over the past 10 years. Nevertheless, cure rates remain less than ideal[4,5], owing in part to our limited ability to accurately delineate the spread of electrical activity during AF in each individual patient. Typically, ablation procedures begin with diagnostic mapping maneuvers designed to define the electrical circuitry underlying the arrhythmia. However, this approach is not used in ablation for AF because the activation sequence during fibrillation is not temporally stable and the substrate is functional and dynamic rather than anatomic and fixed.

We believe that an ideal strategy for ablation of AF requires knowledge of its mechanism on a patient-by-patient basis: in short, mapping for electrical guidance. Adequate mapping requires electrogram sampling with sufficient spatial and temporal resolution to identify variations in excitation state. Unfortunately, because of practical limitations which constrain the number of electrodes that can be deployed transvenously, it is difficult to simultaneously record from a sufficiently large number of atrial sites to identify activation patterns occurring during AF. In most noncomplex arrhythmias, the challenge of adequate spatial sampling is overcome by sequential mapping (so that a single roving catheter can be used to sample a wide distribution of sites). The changing activation sequences associated with AF, however, preclude valid sequential activation mapping. Consequently, alternatives to the use of local activation time have been sought for AF mapping. Two examples are DF and CFAE. The tacit presumption underlying these approaches to AF mapping is that DF and CFAE are temporally stable and can therefore be sampled sequentially yet still accurately reflect underlying electrical activity.

CONCLUSION

Multisite simultaneous mapping of DF and CFAE derived from bipolar electrograms (Basket Catheter) demonstrates that these measures vary over time, contrary to preexistent belief. Previous investigations are limited by relatively short sampling period and sequential data acquisition. Our analysis reveals that sequential maps fail to identify a significant portion of DF and CFAE sites as compared to simultaneous acquired data.

5. AUTONOMIC TONE ALTERS DOMINANT FREQUENCY AND COMPLEX FRACTIONATED ELECTROGRAMS IN AN UNPREDICTABLE MANNER

INTRODUCTION

Cardiac function is strongly modulated by the autonomic nervous system. Numerous studies of the cellular physiology have established that both sympathetic and parasympathetic stimulation have a pro-fibrillatory impact on atrial myocardium by shortening of action potential duration and increasing heterogeneity[A] of refractoriness.[90,91] Animal studies further demonstrated that modulation of the autonomic nervous system can alter inducibility of AF.[92] For example, atrial fibrillation can be sustained in dogs as long as the vagus nerve is continuously stimulated[93] and conversely, vagal nerve ablation renders the dog heart non-inducible for atrial fibrillation.[94] Similarly, I_{KACh}-deficient knockout mice do not exhibit atrial fibrillation.[95]

These findings stimulated the hypothesis that elimination of autonomic inputs via ablation of ganglionated plexi (GP) can abolish or diminish triggers for AF and alter the substrate such that there is a decreased likelihood for maintenance of AF. While clinical studies have provided encouraging results for such an approach[24,96], one has to bear in mind that GP ablation alters not only the autonomic nervous system, but directly modifies the atrial myocardium as well. Hence, the effect of sole withdrawal of the autonomic nervous system on the dynamic behavior of atrial fibrillation in humans is not well defined.

The following study sought to examine the impact of pharmacologic autonomic blockade on surrogate markers of AF dynamics, namely dominant frequency and complex fractionated atrial electrograms. Extrapolating from the influence of the ANS on cellular physiology, one would expect that pharmacologic autonomic blockade results in decreased DF and less fractionation. Interestingly, this is not universally the case – we found acceleration of local frequencies in 32% of sites and increased dyssynchrony (i.e. more fractionation) in 29% of all sites.

[A] The heterogeneity in refractoriness may be due to the heterogeneity in (1) postganglionic vagal nerve endings, (2) muscarinergic receptors, (3) expression of acetylcholine dependent potassium channels (I_{KACh}) or a combination thereof.

The impact of pharmacologic sympathetic and parasympathetic blockade on atrial electrogram characteristics in patients with atrial fibrillation[45]

Article in Pacing and Clinical Electrophysiology, September 2011

Authors: Nicole Habel, Joachim G. Müller, Pierre Znojkiewicz, Nathaniel Thompson, James Calame, Susan Calame, Arshia Noori, Annemarie Gallo, Daniel L. Lustgarten, Burton E. Sobel, Peter S. Spector

Much has been learned about atrial fibrillation since its first description by Mackenzie in 1890,[97] and it is now generally accepted that mechanisms underlying this arrhythmia include multiwavelet reentry and focal drivers with fibrillatory conduction. The influence of the autonomic nervous system (ANS) and neurotransmitters on the heart was first elegantly demonstrated in 1921 by Otto Loewi.[98] The dependence of chronotropic, bathmotropic, dromotropic, inotropic, and lusitropic phenomena on the ANS underscores its importance in modulating cardiac function.

The parasympathetic and sympathetic nervous system and the neurotransmitters involved can facilitate induction and maintenance of AF.[99,100] Recent animal studies suggest that the ANS plays a critical role in triggered firing from the pulmonary veins (PV) (and to a lesser extent from non-PV sites).[101–103] In the presence of these triggers (i.e., premature atrial contractions), sympathetic and parasympathetic ANS stimulation exerts profibrillatory effects via shortening of atrial refractory period and increases dispersion of refractoriness.[104] Vagal stimulation alone shortens atrial action potential duration and increases the heterogeneity of atrial refractoriness. By contrast, sympathetic stimulation alone leads to a more homogeneous shortening of action potential duration.[104,105] Finally, it has been demonstrated that the cardiac neural network is under the influence of other (non-cholinergic, non-adrenergic) factors (e.g. vasoactive intestinal peptide).[106]

Ablation of atrial autonomic inputs (ganglionated plexi) has been reported to increase the success rate of paroxysmal AF ablation procedures.[107,108] However, because GP ablation destroys myocardium as well as autonomic inputs,[109] the impact of autonomic blockade *per se* on human AF remains poorly defined.

The present study was performed to characterize the effects of pharmacologic blockade of the sympathetic and parasympathetic nervous system in patients with AF. Multisite simultaneous recordings were acquired to delineate the impact of pharmacologic autonomic blockade (PAB) on atrial electrograms.

METHODS

Study Population

Nineteen patients presenting to the electrophysiologic laboratory for ablation of symptomatic drug-refractory AF were studied (eight paroxysmal, nine persistent, and two long-standing persistent with a mean AF duration of 125 ± 90 months, 31 ± 31 months, and 57 ± 39 months, respectively). AF type was defined according to the ACC/AHA guidelines.[4] Patient characteristics are summarized in Table 5.1. All patients provided written informed consent. The study protocol was approved by the Institutional Review Committee on Human Research.

Table 5.1	Patient characteristics (n = 19)
Age, mean ± SD	59.9 ± 9.4
Female sex	7 (37%)
AF duration, months	71.6 ± 80.5
AF type:	
Paroxysmal	8 (42%)
Persistent	9 (47%)
Long-standing persistent	2 (11 %)
Coronary artery disease	1 (5%)
Hypertension	11 (58%)
Diabetes mellitus	2 (11%)
Sleep apnea	2 (11%)
Left ventricular ejection fraction	45.3 ± 8.8

Electrophysiologic Studies

Antiarrhythmic drugs were withdrawn at least 5 days before each study. Amiodarone was discontinued for at least 3 weeks. All patients were anticoagulation for ≥ 1 month before the study. Patients were anesthetized with desflurane, fentanyl, and rocuronium and intubated.

Multisite simultaneous recordings (Figure 5.1) were acquired from the left atrium with the use of a 64-electrode basket catheter (1.25 mm ring electrodes; Boston Scientific, Natick, MA, USA), from the coronary sinus with the use of a 20-pole catheter (3-mm tip electrode, 1-3-1 mm interelectrode spacing; Biosense Webster, Diamond Bar, CA, USA), and from the right atrium with the use of a 5-pole catheter (1-

mm tip electrode, 2.5-mm interelectrode spacing; Biosense Webster). Basket size was chosen based on atrial dimensions as measured on a preprocedural computed tomography scan. Basket dimension were 38, 40, 60 or 75 mm with interelectrode spacing of 3, 4, 5, or 7 mm, respectively. Initial catheter position was recorded with the use of biplane cineangiography and then periodically checked with biplane fluoroscopy to confirm positional stability.
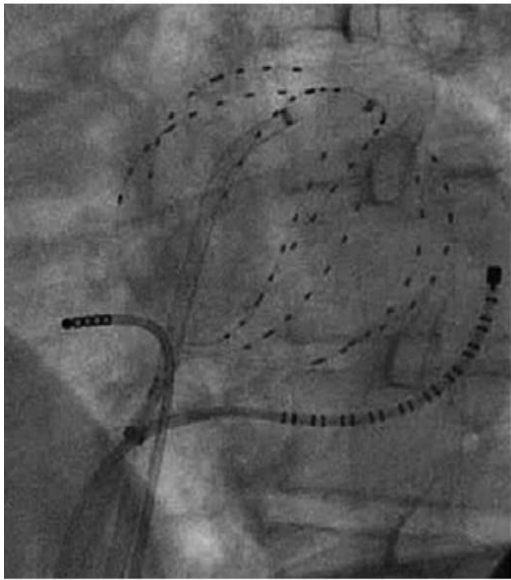

Figure 5.1. A cineangiogram in the left anterior oblique projection demonstrating a 64-electrode basket catheter in the left atrium, a 20-pole catheter in the coronary sinus, and 5-pole catheter in the right atrium.

Study Protocol

Atrial fibrillation had to be induced in five of 19 patients (burst pacing) and was spontaneous in the remaining 14. With the catheters in a stable position, electrograms were recorded for 5 minutes before and 5 minutes during (sympathetic and parasympathetic) autonomic blockade. To achieve balanced autonomic blockade, we first titrated an esmolol infusion to decrease the ventricular rate by 50% and then administered atropine titrated to increase the ventricular rate back to baseline. After acquisition of the data, the basket catheter was removed. The planned clinical ablation procedure was then performed without regard to the data that had been acquired during the study.

Data Acquisition

Bipolar signals were sampled at 1 kHz and filtered from 30-500 Hz (Bard EP, Lowell, MA, USA). Signals were exported and analyzed off-line with the use of MATLAB software (MathWorks, Natick, MA, USA). Channels with technically compromised signals were excluded from further analysis.

Signal Processing

Dominant Frequency (DF) and Atrial Fibrillation Cycle Length (AFCL)

The DF was determined as previously described by Sanders et al.[77] In brief, 5-second segments of electrogram signals were Hanning windowed, rectified, subjected to a 4096-point fast Fourier transformation and filtered from 3-15 Hz. The DF was defined as the maximum amplitude in the magnitude-squared spectrum. The inverse of the resultant DF defined AFCL.

"Driver sites"

The electrogram recordings were of insufficient resolution to directly identify rotors based upon activation sequence. It has been proposed that sites of high DF surrounded by a radially decreasing frequency gradient can be used as a surrogate for identification of driver sites.[77] Therefore, commensurate with the methods of Sanders et al., we identified all such sites provided data were available from two or more of the nearest neighbor sites and criteria were met for at least 30 seconds within the 5-minute recording.

Continuous Activity (CA)

Using the methods of Takahashi et al.[110], CA was defined for each 4-second interval as the percentage of time the electrogram was fractionated. Deflections > 0.05 mV were tagged, and the intervals between deflections were measured, excluding isoelectric segments ≥ 50 ms.

Temporal and Spatial Variability

Temporal and spatial variability of DF and CA were assessed before and during PAB by calculating coefficients of variation (CV) – a normalized measure defined as the ratio of the standard deviation to the mean. In order to distinguish random temporal variability (of DF/CA) from changes due to PAB, we compared the first and second 2.5 minutes of the baseline recording (site-by-site comparison of DF and CA values) using a nonparametric statistical test (Mann-Whitney).

DF and CA before and during PAB

DF and CA values derived from continuous 5-minute recordings were compared before and during PAB.

DF and CA before PAB, during sympathetic blockade and during PAB

One-minute subset of baseline, sympathetic blockade, and PAB recordings were compared using DF and CA analysis.

Statistical Analysis

Data were characterized with descriptive statistics (mean ± standard deviation) unless indicated otherwise. Wilcoxon signed-rank tests, Mann-Whitney tests, and Friedman tests were performed with the PRISM (version 5.01) statistical software (GraphPad Inc., La Jolla, CA, USA). P-values < 0.05 were considered to be statistically significant.

RESULTS

Recordings

In the 17 patients analyzed, a total of 731 channels were recorded (43 bipolar electrograms in each patient; 32 electrode pairs in the left atrium, 10 in the coronary sinus, and one electrode pair in the right atrium). DF and CA analysis was performed only on signals with adequate signal-to-noise ratios (a total of 537 channels; an average of 31.6 ± 3.8 bipolar electrograms per patient). A total of 194 channels had to be excluded.

The Impact of PAB

In two patients (one with persistent and one with induced paroxysmal AF), AF terminated during sympathetic autonomic blockade (after 4 minutes and 1 minute, respectively). A 5-minute recording during balanced sympathetic and parasympathetic autonomic blockade could not be obtained in these patients. Therefore, data from these two patients were excluded from the analysis below, which is based on the remaining 17 patients.

42

Effects of PAB on DF

There was as statistically significant global decrease of DF observed in response to PAB: mean DF (all sites, all patients) decreased during PAB from 5.61 ± 1.08 Hz to 5.43 ± 1.06 Hz, P < 0.001 (corresponding AFCL 178 ± 93 ms vs. 184 ± 94 ms). However, changes in DF varied from patient to patient and from site to site. In 13 of the 17 patients mean DF decreased (statistically significant in nine patients, P ≤ 0.046) and increased in the remaining four patients (Figure 5.2). All patients exhibited sites with increasing as well decreasing mean DF in response to PAB (Figure 5.3 illustrates one example). The extent of change in DF during PAB varied between patients (Δ mean DF ranged from 0.03 Hz to 0.66 Hz) and between sites (Figure 5.4).
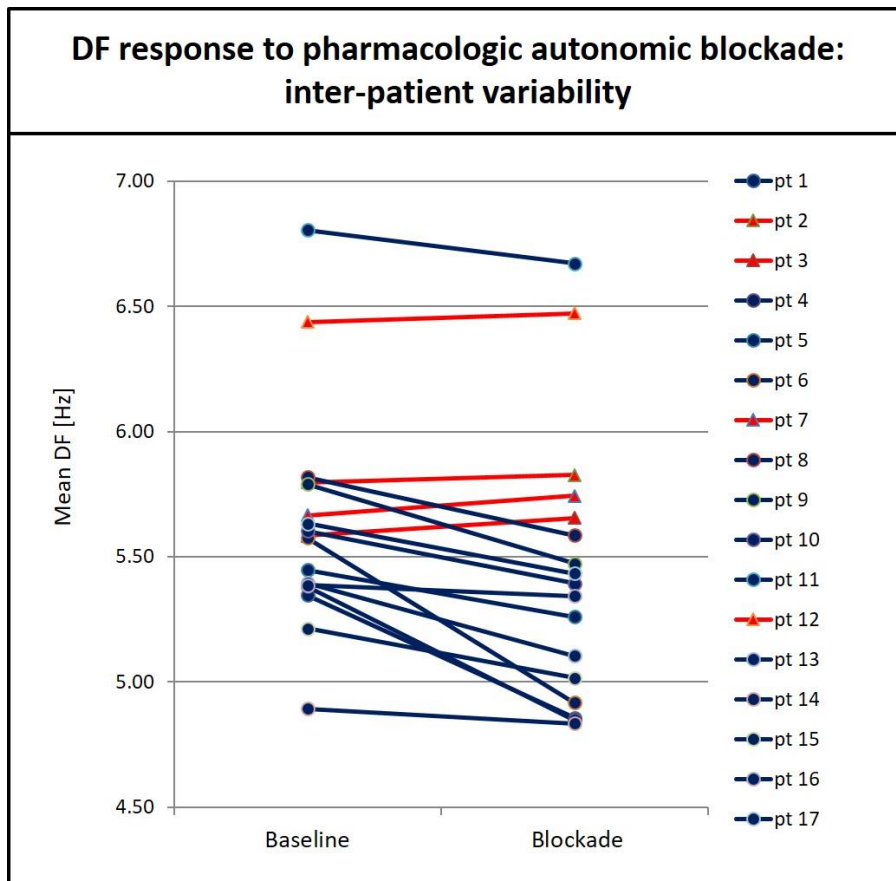

Figure 5.2. The impact of PAB on mean DF varied from patient to patient. Red bars indicate increases in mean DF, blue bars indicate decreases in DF in response to PAB.
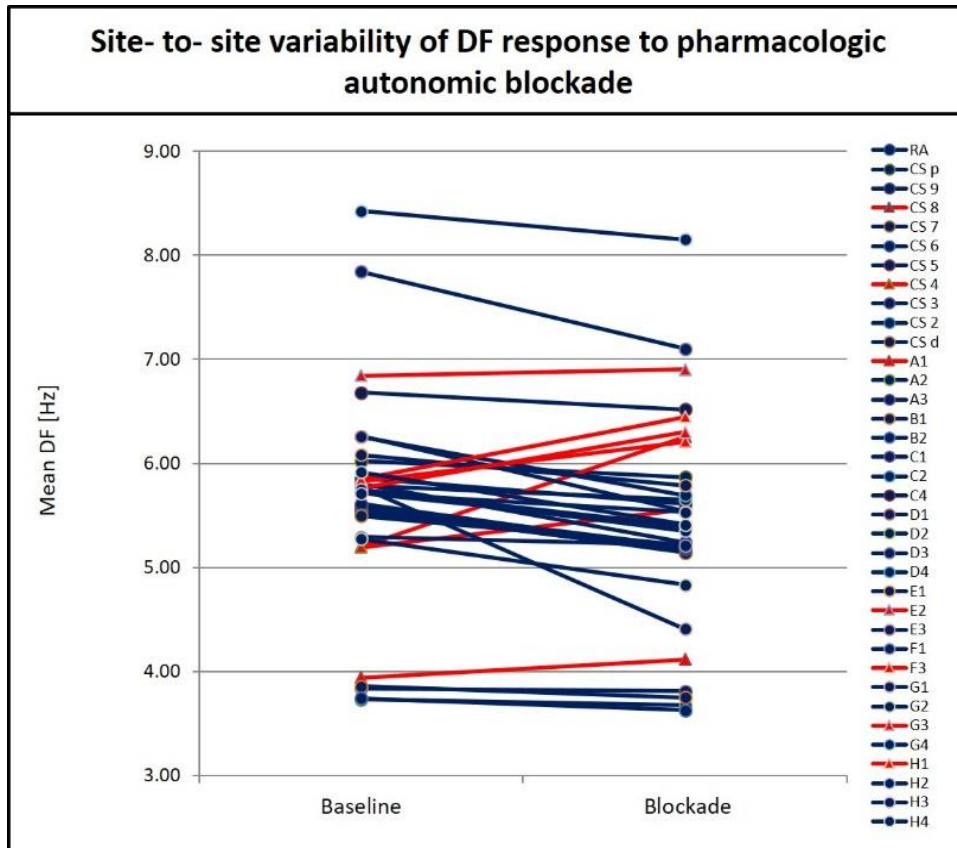
Figure 5.3. Example of the site-dependent effects of PAB (patient 17). Red bars indicate increases in mean DF, blue bars indicate decreases in mean DF in response to PAB.

Effects of PAB on "Driver sites"

A total of 356 left atrial sites were examined; an average of 3.21 ± 0.69 and 3.15 ± 0.73 coexisting "driver sites" could be identified at baseline and during PAB, respectively (p = 0.979). Each "driver site" was surrounded by a mean of 4.8 ± 1.5 (out of a maximum of eight) neighbor sites with adequate signal-to-noise ratio. The following changes in spatial distribution of "driver sites" were seen: a total of 198 "driver sites" were identified at baseline. Of those, 161 remained "driver sites", whereas 37 terminated with PAB. In addition, 45 sites became new "driver sites" during PAB.

The mean DF of "driver sites" remained unchanged during PAB, 9.10 ± 1.49 Hz versus 9.08 ± 1.55 Hz (p = 0.967). "Driver sites" were present for 23 ± 14% and 22 ± 12% of the 5-minute recording during baseline and PAB, respectively (p = 0.335). The average duration of "driver sites" (7.21 ± 5.46 seconds vs. 6.78 ± 1.91 seconds, p 0.678) remained unchanged during PAB.

Spatiotemporal Variability of DF

The overall spatiotemporal variability did not significantly change during PAB, 26 ± 12% vs 27 ± 12% (p = 0.077). However, temporal CV increased by 13 ± 7% in 28% of all sites and decreased by 12 ± 8% in 23% of all sites, whereas in the remaining 49% of sites, CV remained stable within a range of ± 5%.

The average spatial CV of DF in the subset of "non-driver sites" decreased in nine of 17 patients by a mean of 2% (statistically significant in two patients [p ≤ 0.001]), indicating a small decrease in heterogeneity of local frequencies.

	Mean DF, baseline	Mean DF, PAB	% of sites with ↑ DF	Δ DF of sites with ↑ DF	% of sites with ↓ DF	Δ DF of sites with ↓ DF
Change in DF in response to pharmacologic autonomic blockade					

	Mean DF, baseline	Mean DF, PAB	% of sites with ↑ DF	Δ DF of sites with ↑ DF	% of sites with ↓ DF	Δ DF of sites with ↓ DF
1	5.35 Hz	4.86 Hz	11 %	1.43 ± 0.73 Hz	89 %	0.73 ± 1.04 Hz
2	5.80 Hz	5.83 Hz	33 %	0.70 ± 1.18 Hz	67 %	0.31 ± 0.17 Hz
3	5.58 Hz	5.66 Hz	53 %	0.47 ± 0.66 Hz	47 %	0.38 ± 0.46 Hz
4	5.38 Hz	4.85 Hz	13 %	0.09 ± 0.03 Hz	88 %	0.62 ± 0.50 Hz
5	5.45 Hz	5.26 Hz	35 %	0.31 ± 0.20 Hz	65 %	0.46 ± 0.32 Hz
6	5.58 Hz	4.92 Hz	13 %	0.89 ± 0.53 Hz	88 %	0.88 ± 0.46 Hz
7	5.67 Hz	5.74 Hz	55 %	0.42 ± 0.45 Hz	45 %	0.34 ± 0.29 Hz
8	5.82 Hz	5.59 Hz	25 %	0.32 ± 0.19 Hz	75 %	0.42 ± 0.29 Hz
9	5.79 Hz	5.47 Hz	29 %	0.22 ± 0.23 Hz	71 %	0.54 ± 0.41 Hz
10	5.60 Hz	5.39 Hz	16 %	0.90 ± 0.93 Hz	84 %	0.42 ± 0.37 Hz
11	6.81 Hz	6.67 Hz	38 %	0.23 ± 0.11 Hz	63 %	0.35 ± 0.23Hz
12	6.44 Hz	6.47 Hz	47 %	0.40 ± 0.35 Hz	53 %	0.29 ± 0.30 Hz
13	5.40 Hz	5.10 Hz	24 %	1.05 ± 0.84 Hz	58 %	0.95 ± 1.16 Hz
14	4.89 Hz	4.83 Hz	51 %	0.26 ± 0.35 Hz	49 %	0.40 ± 0.49 Hz
15	5.21 Hz	5.02 Hz	30 %	0.35 ± 0.24 Hz	70 %	0.43 ± 0.35 Hz
16	5.39 Hz	5.34 Hz	42 %	0.33 ± 0.49 Hz	58 %	0.32 ± 0.27 Hz
17	5.63 Hz	5.43 Hz	19 %	0.45 ± 0.30 Hz	81 %	0.36 ± 0.26 Hz

Figure 4.4. The change in DF in response to PAB varied from patient to patient and from site to site. Increases in mean DF are highlighted in red. The extent of change in DF differed between sites and between patients.

Temporal Variability of DF and CA at Baseline versus changes with PAB

Although there is variability in DF and CA over time (mean CV, 26%) in 93% and 80% of all sites, mean DF and CA were not significantly different during the first and second 2.5 minutes baseline recording, respectively. However, the change in mean DF and CA during PAB was statistically significant in 49% and 73% of all sites, respectively.

The Heterogeneous Effect of PAB on Local Frequency

The change of DF in response to PAB was not similar at all sites. A total of 537 sites were analyzed; 67% slowed by 0.45 ± 0.59 Hz, while 32% increased by 0.49 ± 0.55 Hz. The change in frequency was statistically significant in 49% of all sites.

The group of sites with decreasing DF (group A) had a significantly higher DF at baseline than the group with increasing DF (group B): 5.74 ± 1.11 Hz vs 5.41 ± 0.95 Hz (p < 0.001). The changes of DF were related to the response of "driver sites" and "non-driver sites" to PAB. Analysis of all 356 left atrial sites indicated that in the majority of cases DF decreased due to "driver site" slowing or termination (45% and 16%, respectively) or "non-driver site" slowing (32%). By contrast, DF increased because of acceleration of "driver sites" (54%), "non-driver sites" becoming new "driver sites" (25%), and "non-driver sites" showing an increased response rate or being driven by a faster driver during PAB (20%).

Effects of PAB on Fractionation

Median CA (all sites, all patients) significantly decreased during PAB from 31 ± 21% to 26 ± 20% (p < 0.001). In 13 of the 17 patients, median CA decreased (statistically significantly in 10 patients [p ≤ 0.038]). Median CA increased in the remaining four patients. Fractionation decreased in 71% of all sites by 7 ± 8%, whereas in 29% CA increased by 3 ± 4%. The change in CA was statistically significant in 73% of all sites.

Sympathetic Blockade Alone Compared with Combined Sympathetic and Parasympathetic Blockade

The decrease in DF from baseline (5.60 ± 1.22 Hz) to sympathetic blockade (5.56 ± 1.18 Hz) and PAB (5.45 ± 1.19 Hz) was statistically significant (p < 0.001). A concordant decrease in frequency with respect to both sympathetic and parasympathetic blockade was present in only 24% of all sites. A discordant change in DF was found in 60% of all sites and a concordant *increase* in DF was found in 14%.

Similar changes were observed for fractionation. CA at baseline (35 ± 21%) was statistically significantly different from CA during sympathetic blockade (33 ± 21%) and during PAB (32 ± 20%), p < 0.001. A concordant decrease in fractionation occurred in only 36% of all sites. The remaining sites exhibited a discordant change (51%) or a concordant *increase* in CA (13%).

DISCUSSION

AF is the most common sustained cardiac arrhythmia afflicting over 6.7 million people in the United States and Europe.[4] AF can lead to cardiomyopathy, hemodynamic impairment, and thromboembolism and therefore constitutes a major health-care burden. Despite the enormous impact of AF, cure rates remain less than ideal. A better understanding of the mechanisms responsible for initiation and maintenance of AF is likely to be valuable in increasing safety and efficacy of antifibrillatory treatment.

Our data demonstrate that PAB results in a global slowing of DF and an increase in AFCL (consistent with increasing action potential duration). However, the changes in DF were nonhomogeneous and indicate a more complex modulation of atrial electrophysiology than that expected based on observations at the cellular level. Complete withdrawal of sympathetic and parasympathetic inputs is anticipated to cause prolongation of action potential duration and an increased homogeneity of refractoriness. Instead of observing the corresponding effects at the tissue level – a decrease in DF at all sites – we detected a decrease in only 67% and an increase of local frequency in 32% of all sites. At such sites "drivers" accelerated (54%) or new "drivers" developed (25%). These findings are consistent with a complex alteration of AF substrate, secondary to a compound modulation of the interactions between myocytes. Additionally, the influence of other neuromodulating factors (i.e., vasoactive intestinal peptide) may have impacted the heterogeneity of substrate modulation in response to PAB.

A "non-driver site" can accelerate (20%), either because it is driven by a faster driver or this response rate to its initial driver more closely approaches a 1:1 relationship (as the driver site slows). Decreasing DF was associated with slowing of "driver" and "non-driver" sites as well as "driver site" termination. Spatiotemporal variability of DF was not significantly different before and during PAB. The small decrease in spatial variability of DF seen and "non-driver sites" is consistent with decreased heterogeneity of refractoriness during autonomic blockade.

Fractionation occurs when dyssynchronous electrical events are present in the recording region of a single electrode pair. As such, fractionation can in part reflect the extent of local atrial dyssynchrony. The present results demonstrate a decrease in CA in the majority of sites, which is consistent with an increase in synchrony between atrial myocytes. However, an increase in fractionation during PAB was observed in 29% of all sites.

Although the sympathetic and parasympathetic nervous systems act similarly on atrial myocytes (i.e., stimulation of either leads to shortening of action potential duration), the majority of sites exhibited a discordant change in both DF and fractionation, further underscoring the complexity of modulation of atrial electrophysiology.

Comparison with Previous Studies

Katritsis et al.[111] examined the effect of pharmacologic parasympathetic withdrawal on complex fractionated atrial electrograms at GP sites and found no significant decrease of fractionation when comparing "electrogram samples" before and after administration of atropine. The absence of decreased fractionation in this study may in part be artefactual, resulting from inadequate sampling in the presence of temporal variability of fractionation.[42] The present study has the advantage of comparing high volume datasets of continuous measurements before and during PAB acquired during multisite simultaneous mapping, which reduces the chances for sampling error due to temporal variability of fractionation while identifying changes due to PAB.

Knecht et al.[112] used sequential electroanatomic mapping to investigate the effects of PAB on the characteristics of complex fractionated atrial electrograms and established a significant decrease in fractionation in the group of patients with paroxysmal but not in the group of patients with persistent AF. They found a significant decrease in fractionation only if AFCL increase by at least 6ms. Our data demonstrate changes in DF and fractionation during PAB regardless of AF type (Figure 5.4). Furthermore, we observed changes in fractionation independent of the degree or direction of changes in DF (related to the inverse of AFCL). These discrepancies may be attributed to study-specific variation in location of data point acquisition, sampling duration (relative to temporal variability of fractionation), and/or variation of ANS effects in individual patients.

Limitations

DF and fractionation maps in human AF are used by some operators to identify ablation targets. We previously demonstrated that because of spatial and temporal variation, the use of multisite simultaneous mapping is required to unambiguously identify the spatial distribution of DF and fractionation sites.[42] Accordingly, in the present study, we used a commercially available 64-electrode basket catheter for left atrial recordings. Unfortunately, this catheter is not an ideal mapping tool. Sufficient endocardial contact cannot be achieved at all sites. Electrograms from the septum, the PVs, and the left atrial appendage are difficult to assess with the basket catheter. The interelectrode spacing and distribution of electrodes provides limited spatial resolution and relatively sparse sampling of atrial activation. Despite these well-recognized limitations, the basket catheter provides the ability to determine changes in DF and fractionation in response to PAB and the ability to assess temporal and spatial variability.

The acquisition of bipolar electrograms is beneficial for elimination of far-field contamination of the local electrogram, but the frequency retrieved from bipolar recordings may not necessarily accurately reflect the periodicity of activation of the tissue.[113] Frequency and fractionation are influenced by interelectrode spacing. However, the use of catheters with varied interelectrode spacing does not influence the electrogram analysis in our study, because comparisons were never made between different catheters. Comparisons were only made before and during PAB with the same catheter (i.e., same interelectrode spacing) in a stable position.

Spectral analysis offers a powerful research tool for extracting information from electrograms in the presence of complex tissue activation patterns. However, because the relationship between tissue activation and electrogram frequency characteristics is nonunique, one cannot unambiguously predict the activation pattern that generated a particular electrogram. Interpretation of spectral analysis can yield helpful but indirect insight into underlying electrophysiology. Further study will be required to delineate the clinical significance of spectral analysis.

The small size of our study population, as well as possible differences in the underlying AF mechanism (i.e., induced vs spontaneous AF), limits our ability to relate patient characteristics (e.g., AF type) to the changes in electrogram characteristics that occur in response to PAB.

All patients underwent general anesthesia with rocuronium. Its vagolytic effect may have influenced the absolute values assessed for DF and fractionation. A definitive measurement of the extent of PAB achieved in each individual patient was not available. Therefore, we cannot determine whether the ANS plays a

critical role in the maintenance of AF, although this possibility is consistent with the termination of AF in two patients in whom it occurred during sympathetic blockade. It has been demonstrated that ablation of the fat pad at the right PV-atrial junction leads to incomplete autonomic blockade, thereby increasing dispersion of refractoriness and resulting in a profibrillatory effect.[114] Although incomplete PAB may not exhibit the same effect of *spatial* heterogeneity of dispersion of refractoriness as isolated autonomic denervation of the high right atrium, we cannot exclude the possibility that the heterogeneous effects of PAB on DF and CA result from incomplete autonomic blockade if the execution was insufficient. It is also possible that the heterogeneous effects observed in our study reflect the limitation of autonomic blockade using cholinergic and adrenergic blockers while ignoring the role of factors such as vasoactive intestinal peptide.

In our study, as well as numerous elegant studies of GP ablation, ANS withdrawal was not sufficient to terminate AF in all patients.[115–117] These findings are consistent with two possible explanations: the strategy of ANS withdrawal is inadequate or, alternatively, the strategy is inadequately executed.

CONCLUSION

The present study demonstrates that given the complexity of the interactions between individual cells throughout the atria, the effects of PAB on global atrial behavior are far more heterogeneous than the direct effects of PAB on individual cells. This latter phenomenon underscores the challenges of relating measurements of macroscopic behavior (e.g., DF and fractionation) directly to the underlying atrial electrophysiology. It is clear that AF is not a single pathophysiologic entity; rather there are several avenues by which atrial electrical activity can become disorganized. The profibrillatory potential of ANS stimulation is clear based upon its effects on atrial cellular physiology. It nonetheless remains a challenge to determine the role that the ANS plays in individual patient with AF. Our data demonstrate a high degree of interpatient variability of the macroscopic behavior (as measured by DF and fractionation) in response to PAB. This suggests that the ANS is not of equal importance in every patient. However, it remains unclear whether complete ANS withdrawal is necessary or sufficient to preclude AF.

6. ELECTRODE RESOLUTION AND INTRACARDIAC ELECTROGRAMS

INTRODUCTION

Spatial resolution refers to the ability to differentiate between two entities – in the context of electrophysiology that is to delineate between two separate excitations within the recording region of an electrode. The recording region of an electrode exceeds its physical dimension as the electric potential field measured by that electrode spreads through space (the strength of the potential field diminishes with distance from the electric currents that generated it). For example, an electrode physically located in the atrium can record both, local atrial activation and far field ventricular excitation.

The electric potential recorded is not only dependent on the currents that generated it, but also changes with the electrode's configuration (electrode size, height above the tissue and inter-electrode spacing when bipolar recordings are obtained). This begets the challenge that the underlying tissue activation cannot easily be reconstructed from the electrogram it generated, a phenomenon mathematically known as the inverse problem. Particularly when mapping atrial fibrillation, the complex activation patterns preclude the creation of an accurate map of electrical activity. Dyssynchrony within the recording region of an electrode results in fractionation and prohibits identification of local activation time. In lieu of activation mapping, identification of surrogate markers, such as dominant frequency[77] or complex fractionated atrial electrograms[37] have been proposed as targets for ablation. However, the spatial resolution of an electrode can also alter measurements of dominant frequency and fractionation. Low spatial resolution may result in the lack of discrimination between two separate excitations thereby missing high frequency areas. The converse is also possible: ambiguity between near field and far field events can lead to over-counting resulting in falsely identifying high frequency sites. While bipolar recordings are generally thought to have higher spatial resolution (due to far field 'cancellation') the nature of a bipolar electrogram resulting from the subtraction of the electric potential recorded by two closely spaced electrodes introduces another pitfall for over-counting: When simulating bipolar electrograms along a linear scar during single loop reentry (Figure 6.1) the biphasic components of the electrogram represent activation from one and then the other side of the circuit. As the time between peaks of the biphasic electrogram approaches half the tachycardia cycle length each component can be misinterpreted as a separate wave front, increasing the chance of over-counting. This discrepancy between electrogram frequency and tissue frequency can lead to inaccurate frequency maps and inappropriate identification of ablation targets.[113]
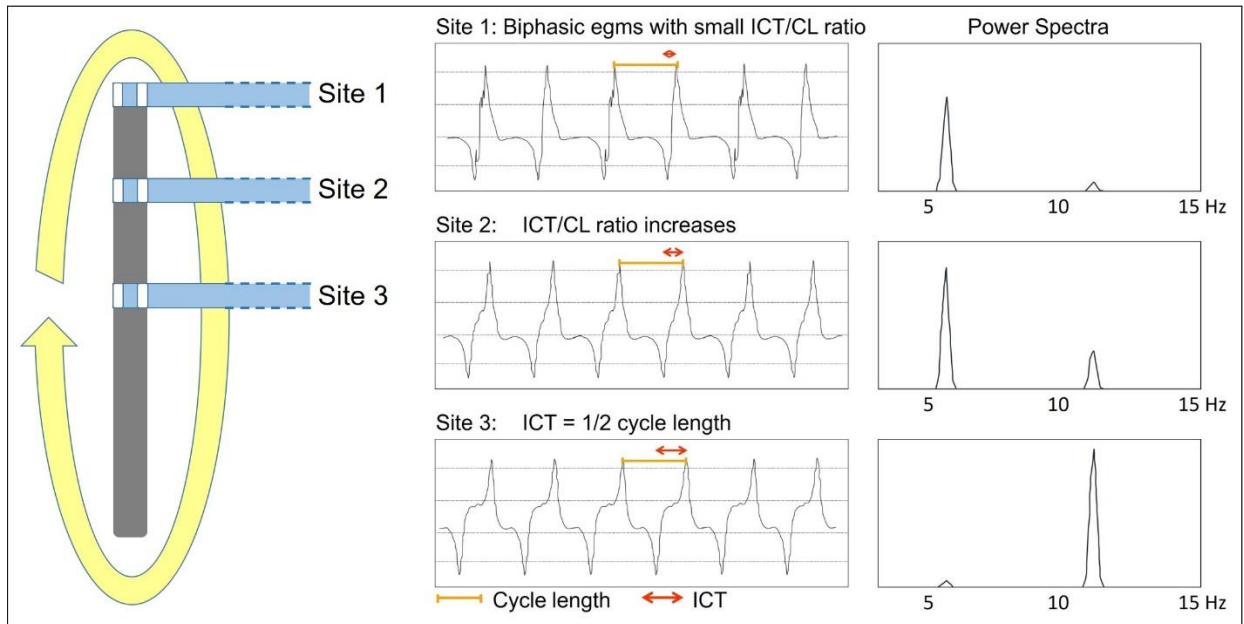
Figure 6.1. Bipolar recordings along a linear scar during single loop reentry (cycle length, CL = 180 ms). The intra-complex peak to peak time (ICT) increases from edge to mid scar. Frequency analysis shows peaks at 5.5 Hz (≈ 1/CL) and 11 Hz. As the ICT/CL ratio approaches 0.5 (moving from edge to mid scar) the power of the 10.99 Hz peak increases.

Similarly, spatial resolution can affect the degree of fractionation, making the acquisition of accurate maps difficult and the comparison of previous studies using different catheter configurations challenging.

The **following two studies** examine the details of electrode resolution and intracardiac electrograms. First, we quantified the effects of electrode characteristics on spatial resolution[43] and found that resolution worsens with increased electrode diameter, length and height above the tissue. We then examined the effects of spatial resolution on fractionation[44] and found that fractionation is a reflection of spatiotemporal variability of tissue excitation within the recording region of an electrode/electrode pair and hence the degree of fractionation can increase as spatial resolution worsens.

Effects of electrode size and spacing on the resolution of intracardiac electrograms[43]

Authors: Justin M. Stinnett-Donnelly, Nathaniel Thompson, Nicole Habel, Vadim Petrov-Kondratov, Daniel D. Correa de Sa, Jason H. Bates, Peter S. Spector

---

Atrial fibrillation (AF) is a cardiac rhythm disturbance frequently associated with coronary artery disease[118], which poses a tremendous healthcare challenge. There are 6.7 million cases in Europe and in the US alone[4], and treatment remains inadequate. Catheter ablation has proven to be less effective for AF compared with other more organized arrhythmias[5,119]. This may, in part reflect the inability to create activation maps of AF using current tools. Activation mapping has been used to tremendous advantage by defining the circuitry of organized rhythms, which facilitates formulation of mechanistically guided ablation strategies. Mapping during AF frequently reveals fractionated electrograms that confound identification of local activation time and therefore preclude activation mapping. We have recently demonstrated that fractionation results from tissue dyssynchrony within the electrode(s) recording region, and is thus proportional to electrode spatial resolution[44].

Optimizing electrode configuration and placement to minimize the area of tissue seen by the electrode is thus crucial to accurate activation mapping of atrial activity, which in turn may facilitate successful ablation of AF. We do not yet have a good understanding of how the characteristics of electrodes currently in clinical use influence spatial resolution. Accordingly, the purpose of the present study was to undertake a formal study of how electrode size, shape, and distance from the tissue affect recording resolution, and how much improvement in resolution might be expected if these design features were optimized relative to the kinds of electrodes currently in clinical use. We conducted our study using a computational model of an electrode situated above a sheet of excitable tissue, validated against in-vitro measurements, in which the effects of electrode dimensions, height above the tissue, and interelectrode spacing (in the case of a bipolar electrode) could be varied over clinically relevant ranges.

METHODS

Theory

We consider an electrode placed inside the heart so that it records a time-varying electric potential, relative to some distant reference, as waves of excitation spread through the nearby heart tissue. The events giving rise to this potential are complex in their details, but in essence can be viewed as arising from patterns of current density that traverse the heart as a result of the transient depolarization and repolarization of the heart cells[120,121]. We model the electric potential field generated by cardiac activation in simple terms as a two-dimensional sheet of tissue in the x-y plane, and consider a point electrode at position (x_0, y_0) and height z_0 above the tissue. The unipolar potential (Φ) recorded by this electrode (relative to a reference of zero) is

$$\Phi(x_0, y_0, z_0) = \frac{1}{2\pi\rho} \iint_{x,y} \frac{I(x,y)}{\sqrt{(x-x_0)^2+(y-y_0)^2+z_0^2}} \, dx \, dy \qquad (1)$$

where ρ is the (assumed constant) resistivity of the blood that fills the space above the tissue and around the electrode and $I(x,y)$ is the current density field in the tissue sheet. $I(x,y)$ is what we would like to be able to measure to accurately map electrical activity but Equation 1 shows that what we actually measure is the convolution[120–122] of $I(x,y)$ with the point spread function

$$P(x, y, z_0) = \frac{1}{\sqrt{x^2+y^2+z_0^2}} \qquad (2)$$

$P(x, y, z_0)$ is a peaked function that increases in width (i.e. causes more blurring of the measured potential as z_0 increases. Furthermore, when the electrode is of finite extent, Equation 1 is averaged over the electrode surface, which further degrades the recorded signal relative to the desired $I(x,y)$. A bipolar electrode recording is obtained as the difference between the signals obtained from two unipolar electrodes spaced a certain (usually small) distance apart.

Computational modeling

Using a custom software (Matlab, The Mathworks Inc., Natick, Massachusetts, USA), we modeled the potential field surrounding a dipole current source to represent the basic unit of electric potential generation from heart tissue, namely, a flow of current from the interior of a cell to the extracellular space

as the cell depolarizes and an equal and opposite currently flow nearby as adjacent cells repolarize. We then calculated the potentials that would be recorded by electrodes of various diameters (d) and lengths (l) placed relative to this dipole source at various positions along the y-axis and at various heights (z_0) when the positive and negative current sources were placed at $y = \pm\, \delta/2$. When we investigated bipolar electrode recordings, the electrodes were separated by a nearest surface distance of Δ. The arrangement is diagrammed in Figure 6.2.
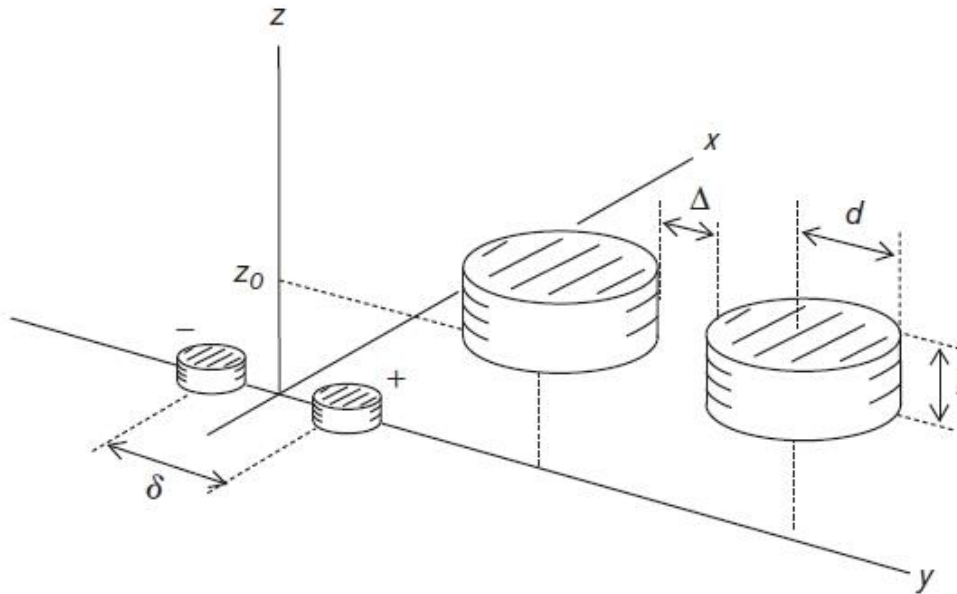

Figure 6.2. Schematic of a dipole current source located $\pm\, \delta/2$ about the origin and a bipolar pair of electrode of diameter d and height l separated by Δ and located at height z_0 along the y-axis.

We set $\delta = 0.25mm$ and $\rho = 1$ (arbitrary units). The electrodes were modeled as hollow cylinders divided into a finite element mesh with 30 elements evenly distributed about the circumference and 15 elements along the length for a total of 450 elements of equal area. Using Equation 1, the electric potential produced by the dipole source was calculated at the center of each element. The potential recorded by the entire unipolar electrode was then calculated as the sum of each element potential multiplied by the element area and divided by the total surface area of the electrode. The bipolar electrogram was obtained simply as the difference in the potentials recorded by two unipolar electrodes.

In-vitro validation

We created an in-vitro apparatus for confirming that commonly used clinical intracardiac electrodes do, in fact, record potentials as our model predicts. A Plexiglas chamber was filled with 0.9% saline. Two 0.3 mm wide copper wires with flat ends were fixed 0.5 mm apart (center to center) into the bath (the x-y plane shown in Figure 6.2) with only their tips exposed to the bath interior. Biphasic square wave impulses (2.4 mV, 10 ms pulse width) were delivered to the electrodes to simulate a dipole source in the heart tissue. Recording electrodes (both unipolar and bipolar) were also placed in the saline bath and positioned with a micromanipulator attached to a machined aluminum base under the bath. The electrode positions could be adjusted with a resolution of ± 0.1 mm over 10 cm.

Unipolar electrode recordings were taken with standard catheters (Biosense Webster Inc., Diamond Bar, California, USA) having electrode tips of width 2.33 mm and lengths of 1, 4, and 8 mm. Bipolar recordings were taking between the tip electrodes on two standard catheters (Biosense Webster Inc.) having a variety of interelectrode spacing (1, 2, 3, 4 mm). The recoding electrodes were oriented to be perpendicular to the bath floor at a height of 1 mm, as diagrammed in Figure 6.2.

The electrograms from the recording electrodes were sampled at 1 kHz and filtered from 0.5 to 250 Hz (Bard EP, Lowell, Massachusetts, USA). Ten recordings were taken using each electrode configuration at 10 positions along the y-axis at intervals of 0.2 mm. The entire set of recordings was repeated five times, with the order of catheter position reversed (and electrodes polished) between runs to minimize effects due to electroplating of the cathode. Signals were exported and analyzed offline with the use of the Matlab software (MathWorks, Natick, Massachusetts, USA).

Figure 6.3 shows examples of unipolar and bipolar space domain electrograms calculated with the computational model and measured in the physical in-vitro model. We examined unipolar electrodes with tips having lengths of 1, 4, and 8 mm (2.33 mm tip diameter) and found correlation coefficients of 0.99 in all cases. These validation experiments thus gave us confidence to proceed with the computational model as a mean to investigate the details of how electrode size, height, and separation determine the spatial resolution of intracardiac electrogram recording.
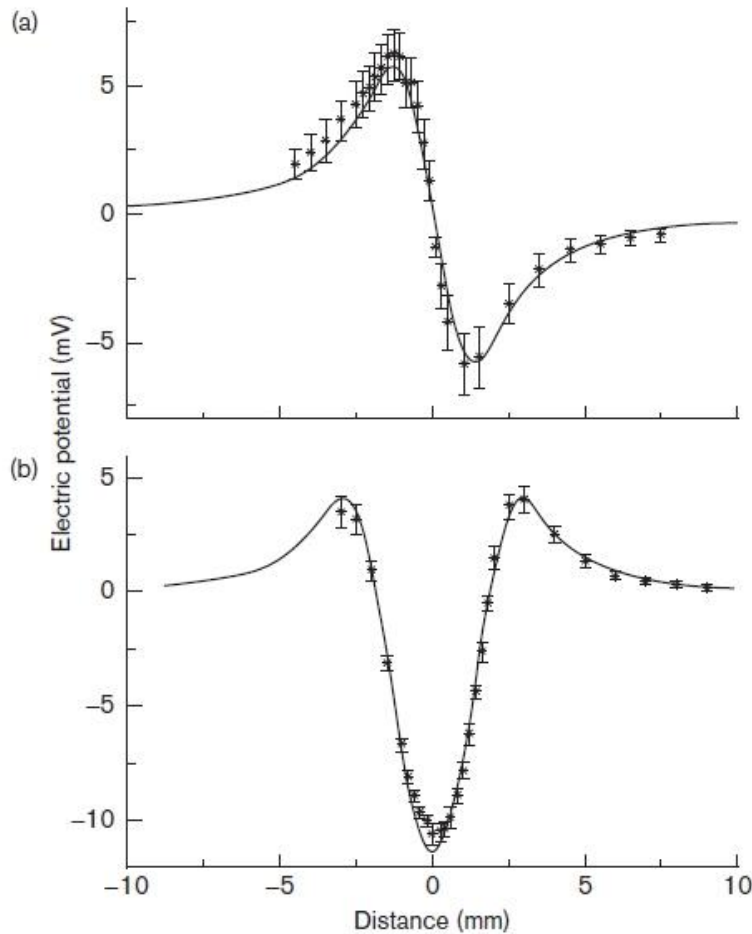
Figure 6.3. (a) Comparison of predicted potential recorded by a unipolar electrode as a function of lateral distance from a dipole current source (solid line) and the potential measured experimentally in a saline bath (filled circles). (b) Corresponding plot for a bipolar recording.

Quantification of spatial resolution

We used two measures of spatial resolution. The first is the conventional distance to half amplitude used to quantify the spread of many measurement functions[123]. The space domain electrogram for unipolar and bipolar electrodes have more than a single peak (Figure 6.3), but the distance to half amplitude concept still usefully applies. Thus, the resolution provided by a unipolar recording of a dipole source was equated to the lateral distance from the dipole center to the point of half maximal amplitude, defined as $W_{1/2}$ (Figure 6.4a). $W_{1/2}$ for bipolar recordings was taken as the distance from its center to the point of half maximum positive deflection (Figure 6.4b).
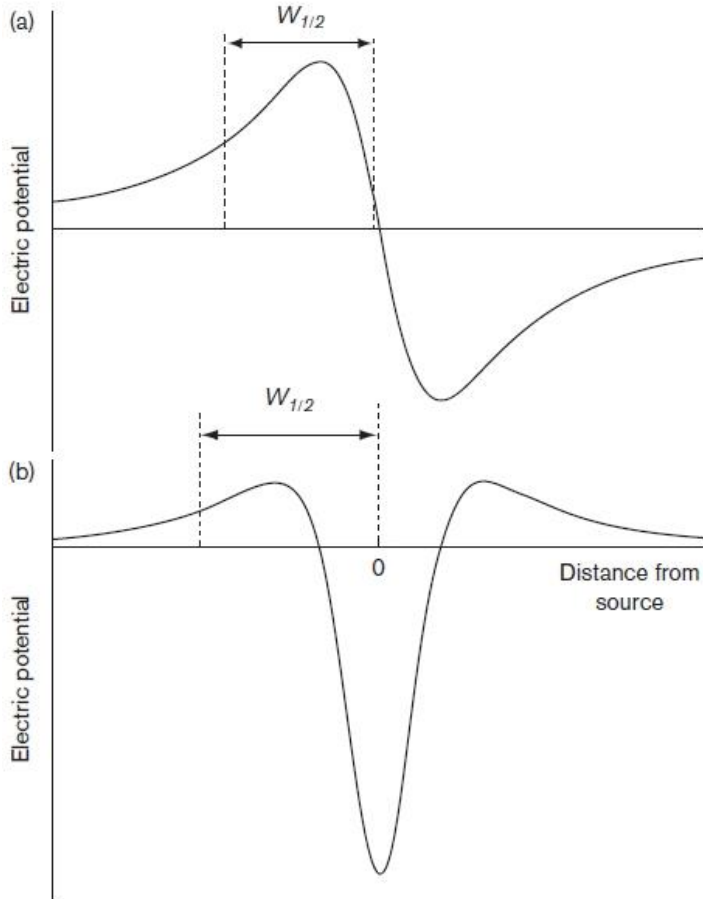
Figure 6.4. (a) The potential due to a dipole current source recorded by a unipolar electrode as a function of lateral distance from the source, showing how resolution is quantified in terms of peak width at half maximum height ($W_{1/2}$). (b) Corresponding plot for a bipolar electrode.

We were concerned that the two and three peaks, respectively, of the unipolar and bipolar point-source electrograms might make the resolution of multiple source more complicated than if they had only single peaks. We, therefore, developed a second measure of spatial resolution designed to detect the minimal resolvable separation between two dipole sources. Considering resolution in the y direction (Figure 6.2), let $\Phi_0(y, z_0)$ be the electrogram measured when the dipole source are separated by a distance of zero (i.e. equivalent to a single dipole source) and $\Phi_{\Delta y}(y, z_0)$ the electrogram measured when the sources are separated by some finite distance Δy. When Δy is small compared with electrode diameter d, $\Phi_0(y, z_0)$ and $\Phi_{\Delta y}(y, z_0)$ are similar. Consequently, their cross correlation achieves a maximum value close to 1, becoming precisely 1 in the limit as Δy approaches zero. When Δy is sufficiently large, $\Phi_{\Delta y}(y, z_0)$ assumes the appearance of two distinct dipole electrograms located at well separated positions, so the cross

correlation between $\Phi_0(y, z_0)$ and $\Phi_{\Delta y}(y, z_0)$ again achieves a relatively high maximum value. At intermediate separations, $\Phi_{\Delta y}(y, z_0)$ consists of two partially overlapping dipole electrograms and thus has a complex morphology that bears little resemblance to that of a single dipole (Figure 6.5a). In this case, the cross correlation between $\Phi_0(y, z_0)$ and $\Phi_{\Delta y}(y, z_0)$ has a relatively low maximum value because the two signals are dissimilar in shape. We, therefore, take as our nominal measure of resolution the value of Δy for which the maximum in the cross correlation between $\Phi_0(y, z_0)$ and $\Phi_{\Delta y}(y, z_0)$ achieves its minimum value. This is defined as C_{min} and is illustrated in Figure 6.5b.
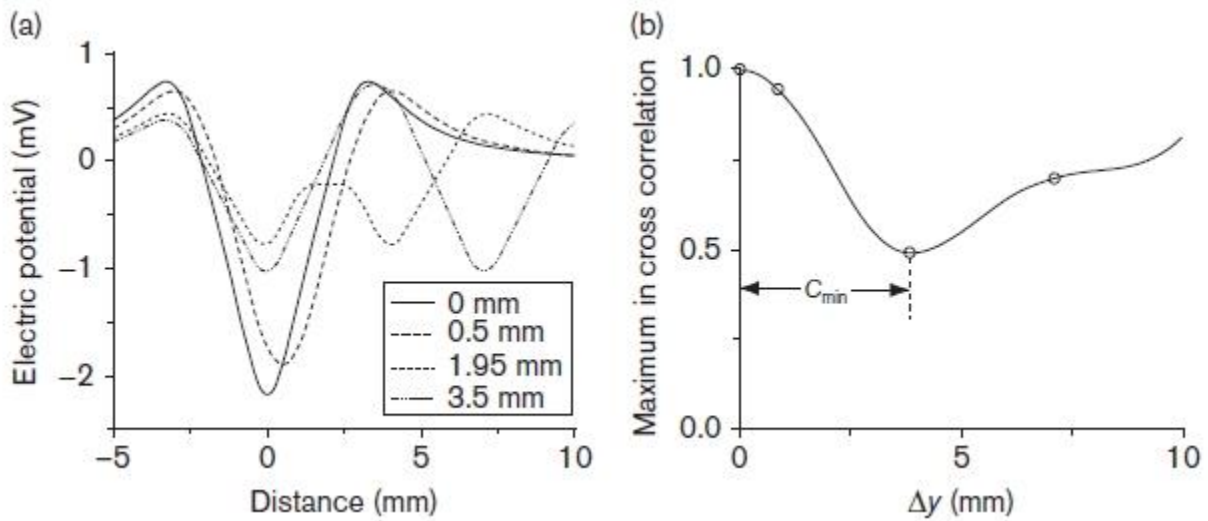

Figure 6.5. (a) Simulated bipolar electrograms (d = 2 mm, l = z = Δ = 1 mm) produced by two dipole sources with Δy = 0, 0.5, 1.95 and 3.5 mm (as indicated in legend). (b) Maximum on the cross correlation between the bipolar electrogram with Δy = 0 and the electrogram with Δy as indicated on the horizontal axis. Open circles correspond to the electrograms shown in (a). This relationship has a maximum for Δy = 0 mm and a miminum for Δy = 3.5 mm = C_{min}.

RESULTS

Figure 6.6 shows how our two measures of spatial resolution, $W_{1/2}$ and C_{min}, vary as functions of electrode dimensions when the potential from a dipole current source is recorded by a unipolar electrode. We set nominal baseline values for the various quantities in question (Figure 6.2) to be $d = 2mm$, $l = 1mm$, and $z_0 = 1mm$, varying each one in turn while the others remained fixed. Not surprisingly, the two measures of resolution are not precisely equal. Nevertheless, they are clearly comparable and exhibit similar trends, both showing that resolution worsens progressively as d, l, and z_0 increase. It is also clear that resolution depends most strongly on z. Figure 6.7 shows corresponding plots for bipolar electrode

recordings, including showing the effects of changing the distance Δ between the two electrodes of a bipolar pair (Figure 6.2).
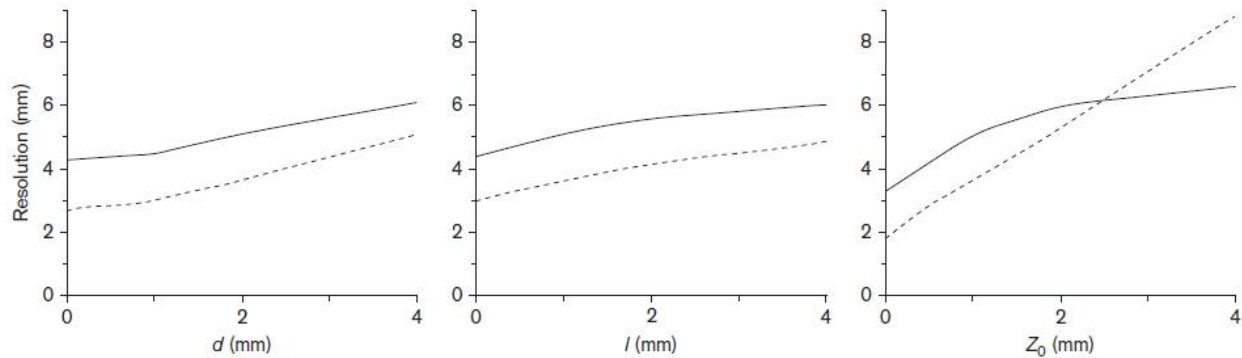

Figure 6.6. Resolution of a unipolar electrode recording of a dipole current source as assessed in terms of C_min (solid lines) and W_1/2 (dashed lines). The three plots show dependence of resolution on electrode diameter (d), length (l), and height above the tissue (z_0). Although each of these quantities was varied, the remaining quantities were held fixed at d = 2 mm, l = 1 mm, and z_0 = 1 mm.

In deciding what conditions correspond to the highest electrogram accuracy that is currently achievable, we need to consider the fact that the myocardial tissue is covered with a layer of endothelial cells that adds to the distance between the active tissue and the closest approach of an electrode tip. Thus, even when an electrode is placed right against the tissue surface, a nominal best case scenario would place it an average of approximately 1 mm from the active tissue. Currently, the smallest clinically available electrodes have diameter and length both of 1 mm. Setting these conditions in our computational model (i.e. $z_0 = d = l = 1\ mm$), we obtained resolution values for a unipolar recoding of $C_{min} = 4.5\ mm$ and $W_{1/2} = 3.0\ mm$. For a bipolar recording (imposing the additional condition that $\Delta = 1\ mm$), we obtained $C_{min} = 2.8\ mm$ and $W_{1/2} = 4.0\ mm$. Reducing d to the relatively negligible value of 0.001 mm while keeping the remaining parameters unchanged, reduced $W_{1/2}$ and C_{min} by factors of between 2 and 4. Conversely, reducing l to 0.001 mm, reduced $W_{1/2}$ and C_{min} by factors of between 1.6 and 2.9. Thus, by reducing an electrode to a single point one would improve resolution over that currently achievable by the product of these two effects, or roughly one order of magnitude.
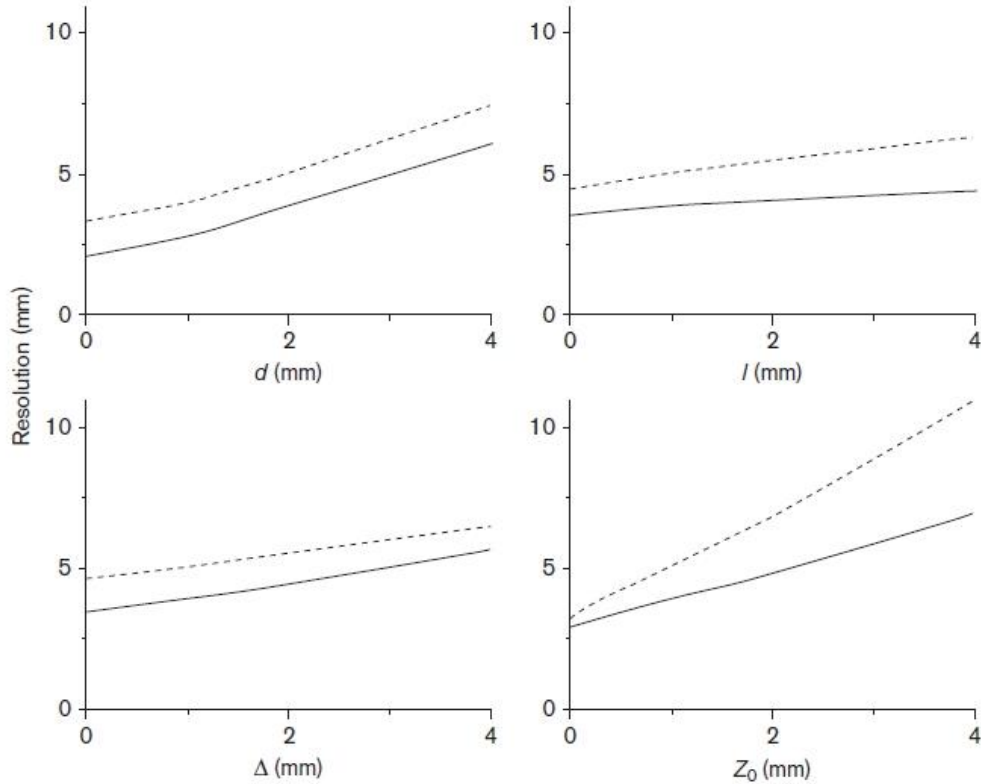
Figure 6.7. Resolution of a bipolar electrode recording of a dipole current source as assessed in terms of C_{min} (solid lines) and $W_{1/2}$ (dashed lines). The four plots show dependence of resolution on electrode diameter (d), length (l), separation (Δ), and height above the tissue (z_0). Although each of these quantities was varied, the remaining quantities were held fixed at d = 2 mm, l = 1 mm, Δ = 1mm, and z_0 = 1 mm.

DISCUSSION

Identification of atrial activation patterns depends crucially on the ability to create spatially accurate maps of atrial electrical activity. The fact that this activity is often complex and nonperiodic would make mapping a significant challenge even if the entire activity pattern could be visualized perfectly. In reality, the practicing cardiac electrophysiologist must make do with nothing more than a series of electrograms from a small number of electrodes placed on the atrial endocardium. The challenge of mapping is further compounded because these electrograms are distance-weighted averages of the activity from an extended region of heart tissue in the vicinity of each electrode. In particular, when different patches of tissue each provide out of phase contributions to the potential measured by a single electrode, the result is a fractionated electrogram. Consequently, it is most desirable to obtain electrograms of the highest achievable spatial resolution.

Here, we used two different measures of resolution (Figure 6.4) to investigate how spatial resolution is affected by the dimensions and configuration of both unipolar (Figure 6.6) and bipolar (Figure 6.7) electrograms. We found that resolution degrades progressively and substantially as electrode width, height, separation (in the case of bipolar), and distance from the tissue are increased. Changes in electrode height had the greatest impact on spatial resolution, however, implying that the most important aspect of electrode design is not related to the electrode itself, but rather the physical proximity of the electrode to the tissue.

There are two principle ways in which the spatial resolution of intracardiac electrode recordings can be diminished: the amount of tissue that is 'near field' [i.e. immediately beneath the electrode(s)] can be increased, and/or the ratio of near-field to far-field tissue can be diminished. An increased electrode diameter results in an effective increase of the electrode's footprint over the myocardial surface, thereby increasing the amount of tissue contributing to the near-field signal. In contrast, an increased electrode height results in greater attenuation of near-field signal relative to far-field signal, resulting in a diminished ability to discriminate between the two. An increased electrode length has a similar effect because it also increases the average height of the electrode above the tissue surface. These various effects are experienced by both unipolar and bipolar electrodes (Figure 6.6 and 6.7), although to a lesser extent by bipolar because taking the difference between two nearby potentials effectively cancels the common far-field components while spatially differentiating the near-field signal.

The theory of intracardiac electrode measurement performance has been known for many years. For example, in 1951 Schaefer et al.[124] outlined the mathematical relationship describing how unipolar and bipolar electrograms are affected by the distance between a dipole source and the recording electrode(s), and observed that bipolar electrodes reduced far-field 'contamination' and that this effect was increased as interelectrode spacing was decreased. Later in the same decade, Durrer et al.[125] investigated methods for measuring electrical activation in the canine left ventricle and made the qualitative observation that only with bipolar recordings '… Can the influence of activity in distant parts of the heart be excluded. They also described unipolar and bipolar electrogram morphologies corresponding closely to those we simulated in the present study (Figure 6.3), and noted that increasing the spacing between bipolar electrodes caused the electrogram morphology to change in the same way as our model simulations predict (Figure 6.5). Similar investigations have been undertaken more recently by other investigators[126,127] and corroborate our findings with respect to unipolar and bipolar electrogram morphologic features.

The notion that various electrode characteristics should affect spatial resolution is also not new. For example, Kimber et al.[128] assessed the ability of unipolar and bipolar recordings to accurately determine local activation time in 'ambiguous' or fractionated signals from ventricular tachycardia mapping studies and found that bipolar recordings were better able to determine local activation time. Nevertheless, to our knowledge, there has been no formal study quantifying how electrode characteristics affect the spatial resolution of intracardiac electrograms, despite the important implications for clinical electrophysiology. The foundation of activation mapping is identification of local activation time, which is dependent on spatial resolution[128]. During organized rhythms, the resolution provided by currently available electrodes is adequate for accurately identifying local activation times. However, this is not always the case for AF in which tissue activation can have high spatiotemporal complexity, changing rapidly with time[42]. This would lead to meaningless maps if local activation time is sampled sequentially with a single mapping electrode.

It would thus appear that accurate mapping of AF will require the use of electrode arrays to provide beat-to-beat activation at multiple sites simultaneously. This raises questions as to the ideal size and spacing of electrodes in the array. Our results indicate that with the smallest electrodes currently available, we cannot expect a resolution of better than about 3-5 mm (Figure 6.6 and 6.7), therefore spacing electrodes any closer than 1mm is unlikely to confer added benefit unless electrode design or methods of digital signal processing such as deconvolution[122] can be used to further enhance resolution.

Finally, we must consider the limitations of our study. Our analysis of the factors affecting spatial resolution was made using a computational model. The close agreement we found with measurements made in an in-vitro experimental system model (Figure 6.3) strongly support the validity of our calculations. Nevertheless, we examined a highly idealized system consisting of a single dipole current source and idealized electrodes. Real electrograms contain measurement noise and are taken from tissue with a complex three-dimensional shape and regional heterogeneities of electrophysiological properties, so the estimate of resolution obtained in the present study represents a best case scenario. In contrast, in practice one deals with a dynamic picture of cardiac activation, so the limited resolution of an electrogram at a given instant may be compensated for substantially by the additional information contained in the way it evolves over time.

In conclusion, we created and validated a computational model for evaluating the impact of electrode size, shape, interelectrode spacing, and height above the tissue on spatial resolution. We used two independent metrics to quantify spatial resolution, both indicating that spatial resolution becomes

degraded roughly in proportion to the above four factors. In particular, we found that electrode height above the tissue has the greatest effect on spatial resolution, so electrode tissue contact is the most important factor impacting resolution. Finally, our calculations suggest that even if electrodes could be constructed to have negligible dimensions compared with those in use today we would increase resolution by at most about one order of magnitude.

Electrogram Fractionation: The relationship between spatiotemporal variation in tissue excitation and electrode spatial resolution[44]

Article in Circulation: Arrhythmia and Electrophysiology, December 2011

Authors: Daniel D. Correa de Sa, Nathaniel Thompson, Justin Stinnett-Donnelly, Pierre Znojkiewicz, Nicole Habel, Joachim G. Müller, Jason H.T. Bates, Jeffrey S. Buzas, Peter S. Spector

---

Fractionated electrograms have attracted the attention of clinical electrophysiologists in the setting of mapping re-entrant rhythms (e.g. ventricular and atrial tachycardia) and more recently mapping of atrial fibrillation. Fractionation in these settings is felt to identify substrate relevant to the arrhythmia circuitry. Although fractionation can identify a critical isthmus in scar-based reentrant ventricular tachycardia circuits[129,130] , the use of fractionated electrograms to guide atrial fibrillation ablation has had conflicting results. Despite the initial successes reported by Nademanne et al.[37], subsequent studies have led to mixed results.[131–136]

Although there is no uniformly accepted definition, the term "complex fractionated atrial electrograms" has been used to describe electrograms with low amplitude and high-frequency deflections. Electrograms measure the changing potential field at the site of a recording electrode.[121] Any pattern of tissue activation within the recording region of an electrode that results in alternation between increasing and decreasing potential will produce electrogram fractionation. Several disparate tissue activation patterns have been shown to result in electrogram fractionation, including meandering rotors[137,138], wave collision[137], discontinuous conduction[139,140] and longitudinal dissociation.[141,142] Using monophasic action potential recordings in patients with atrial fibrillation, Narayan et al. have also demonstrated that complex fractionated atrial electrograms can have multiple etiologies.[143] Because of their nonunique relationship (activation and electrogram), one cannot unambiguously determine a specific tissue activation pattern based solely on the observation of fractionation.

Because fractionation results from tissue dyssynchrony within the electrode recoding region, it follows that the area of tissue that contributes to the electrogram will influence fractionation. Spatial resolution refers to the area of tissue that contributes to the electrogram. Because tissue currents create a potential field that spreads infinitely through space, the "area that contributes to the electrogram" is in fact infinite. However, because potential decreases with distance from a current source, the effective area that

contributes to an electrogram is small and varies with electrode size (length and diameter), configuration (unipolar vs. bipolar), height above the tissue, and interelectrode spacing (IES).[125]

In a series of studies using a computer model of excitable tissue and electrogram recordings from patients with atrial fibrillation, we defined the components that produce electrogram fractionation. We hypothesize that electrogram fractionation can result from either (1) spatiotemporal variation of tissue electric activity; or (2) from temporal variation alone; and that the former (over-counting) is dependent on electrode spatial resolution, whereas the latter (rapid repetitive excitation) is not.

METHODS

Modeling Studies

We studied activation in a 2-dimensional sheet of electrically excitable tissue using a computer model. We calculated the surrounding potential field produced by tissue excitation. With the model we were able to independently vary the temporal and spatiotemporal complexity of tissue excitation. By recording from virtual electrodes of varied size, configuration, and height, we quantified the impact of spatial resolution on fractionation.

Computer Model Design

The model design has been described in detail previously.[58] Briefly, the model is a mono-domain cellular automaton; cells are arranged in a 2-dimensional grid with each cell connected to its 4 neighbors (up, down, left, and right). Cell voltage changes in response to an action potential, external stimulation, or intercellular current flow. The membrane voltage of a cell corresponds to its level of electric depolarization. The resting state of a cell corresponds to quiescence. As a cell gathers current membrane voltage depolarizes, when membrane voltage exceeds voltage threshold, an action potential is initiated. Action potential upstroke velocity and action potential duration are rate-and voltage-dependent conferring restitution as described previously.[58] Cells connect to their immediate neighbors through electrically resistive pathways. The vertical and horizontal resistive constants are R_v and R_h, respectively. Cells exchange current with their neighbors according to first-order kinetics, whereby the voltage of a quiescent cell (j, k) at time t is affected by that of its neighbors according to

$$\frac{dV\,(j,k,t)}{dt} = \frac{1}{R_h}\,[V\,(j-1,k,t) + V\,(j+1,k,t) - 2V\,(j,k,t)]$$

$$+ \frac{1}{R_v}\,[V(j,k-1,t) + V(j,k+1,t) - 2V(j,k,t)]$$

(1)

At each time step in the simulation, all cells have their values of membrane voltage updated according to

$$V(j,k,t) = V(j,k,t-1) + \frac{dV\,(j,k,t)}{dt}\,\delta t + V_{intrinsic} \qquad (2)$$

Where δt is the time step size. A cell may be defined as scar, in which case it is permanently quiescent and electrically isolated from its neighbors.

Tissue Variability

In a flat square sheet of tissue 1 cell thick (10 x 10 mm) without anisotropy, we introduce temporal variation by modulating excitation frequency. Activation wave fronts propagate through the homogeneous tissue at constant conduction velocity.

Spatial variation is created by adding parallel lines of scar alternately extending to the top or bottom edge of the tissue (Figure 6.8; Supplemental Video; http://circ.ahajournal.org). Spatiotemporal variation is then introduced by stimulating in the upper left corner; activation waves proceed through the tissue with a "zig-zag" pattern. Two components of tissue activation complexity can then be independently manipulated: (1) temporal variation can be modulated by changing activation frequency; and (2) spatiotemporal complexity can be increased by increasing the number of parallel lines of scar; that is, increasing the number of separate tissue bundles through which excitation spreads.

Extracellular Potential Recordings

We calculate the potential $\Phi\,(m,n,t)$, that would be recorded by an electrode placed at a height h above a site in the tissue plane (m,n) at each time (t). In the context of the monodomain approximation used, each cell in the tissue makes a contribution to the electrogram that is proportional to the cell's transmembrane current and inversely proportional to its linear distance from the electrode.[120] We assume

that the transmembrane current at a particular cell is the time-derivative of voltage (V), approximated as the difference in V between successive time steps. That is,

$$\Phi\left(m, n, t\right) = \sum_{j=1}^{n} \sum_{k=1}^{n} \frac{V\left(j,k,t\right) - V\left(j,k,t-1\right)}{\sqrt{(j-m)^2 + (k-n)^2 + h^2}} \tag{3}$$

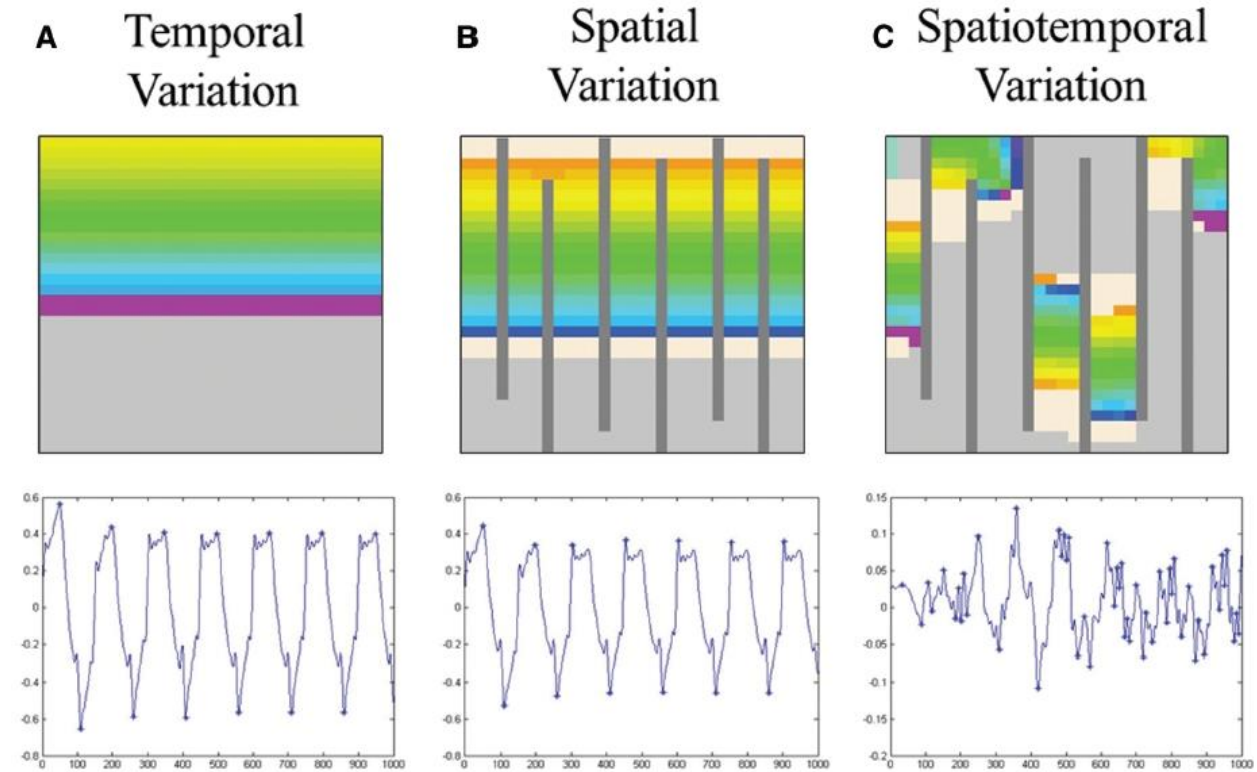where j and k are position indices in the x and y directions.

Figure 6.8. Simulation of temporal, spatial, and spatiotemporal variation of tissue excitation.

Top row, Tissue voltage distribution (single time step; 10 x 10 mm). **A**, Temporal variation: stimulation of the top row of cells (cycle length 150 ms) produced sequential planar waves of excitation. **B**, Spatial variation: although tissue is divided by multiple alternating linear scars, activation proceeds from top to bottom in parallel (secondary to simultaneous stimulation of the top row of cells). **C**, Spatiotemporal variation: stimulation from the top left corner results in sequential excitation of vertical channels between linear scars, producing "zig-zag" activation waves every 150 ms.

Bottom row, Corresponding virtual unipolar electrograms (electrode diameter 1 mm, height 0.5 mm, length 6 mm, oriented horizontally). Turning points are marked with stars. Note that even with linear scars, if activation occurs simultaneously in all bundles, the electrogram is very similar to that seen with in tissue without scar (A versus B). The contributions of each bundle to the potential field occur simultaneously and are hence superimposed in the electrogram (no fractionation).

Virtual Electrograms

We modeled 3-dimensional cylindrical electrodes and varied length, diameter, and height (Figure 6.9). The electrodes were modeled as hollow cylinders divided into a finite element mesh with elements evenly distributed about the circumference and along the length of the electrode. The number of elements varied depending on electrode geometry so no element area was > 1 mm^2. Using Equation 3, the electric potential contribution from each cell was calculated at the center of each element. The potential recorded by the entire unipolar electrode was then calculated as the sum of each element potential multiplied by the element area and divided by the total surface area of the electrode. The bipolar electrogram was obtained simply as the difference in the potentials recorded by the 2 unipolar electrodes. Height was measured from the tissue to the electrode's bottom edge and, for bipolar recording, IES was measured between edges. Electrodes were positioned of the center of the tissue (perpendicular to lines of scar – unipolar; [parallel to lines of scar – bipolar recordings).

Electrode spatial resolution varies inversely with electrode surface area (length and diameter), height above tissue, and IES (for bipolar recordings).
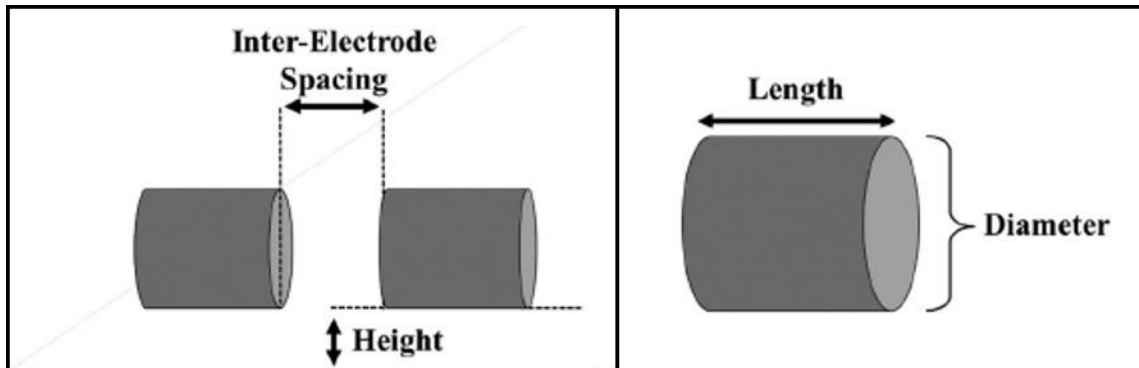

Figure 6.9. Electrode geometry (inset lower left), spacing, and position.

Electrogram analysis

The cellular automaton model evolves through discrete time steps; as a result, electrogram amplitude fluctuates from time step to time step. The electrogram signal was therefore processed with a smoothing function to reduce this artifact. We quantified the number of turning points as the number of peaks and troughs with a 10% tolerance as previously described.[144,145]

Nomenclature Clarification

In this study, temporal variation refers to spatially coordinated changes in the frequency of activation and spatiotemporal variability refers to asymmetrical excitation of various tissue sites in time.

Clinical Studies

We obtained two 60-second unipolar recordings during atrial fibrillation (AF) from the coronary sinus of 20 patients presenting for AF ablation. Average patient age was 59 ± 7 years; 9 patients had paroxysmal and 11 had persistent AF. Unipolar electrograms (indifferent electrode in the inferior vena cava with length = diameter = 2 mm; Bard Electrophysiology, Billerica, MA) were recorded with either a 20-pole (1 mm electrodes, 1-3-1-mm spacing; 10 patients) or a 10-pole (2 mm electrodes, 2-5-2-mm spacing; 10 patients) catheter (Biosense Webster, Diamond Bar, CA). Signals (sampled at 1 kHz, filtered 30-250 Hz) were exported for offline analysis. From these we constructed bipolar electrograms with increasing interelectrode spacing (electrodes 1-2, 1-3, and 1-4). Bipolar signal were analyzed using standard algorithms for average interpotential interval (AIPI) and interval confidence level (ICL).[85] The voltage window for ICL was 0.05 to 0.2 mV; the upper limit of 0.2 mV was selected as an average of values used by different groups.[84,146] The amplitude of electromagnetic noise in each signal was measured in 10 patients (during sinus rhythm). The study was approved by the Institutional Review Committee on Human Research.

Statistical Methods

We used a mixed effects linear model for the analysis of the experimental data for studying fractionation as a function of inter-electrode spacing. Data for each catheter type and each outcome (ICL and AIPI) were analyzed separately. Subjects within a catheter type were treated as random effects, thereby inducing a compound-symmetrical correlation structure among within-subject measurements. Measurements between subjects were independent. IES and time of measurement were treated as fixed effects with time of measurement nested within subject. Analysis was done using PROC MIXED in SAS, Version 9.3.

RESULTS

Modeling Studies

Fractionation as a Function of Temporal Variation

In a series of simulations we stimulated tissue (without linear scars) at progressively shorter cycle lengths (150, 125, 100, and 75 ms). Virtual electrograms were recorded using unipolar electrodes (6 mm length,

1 mm diameter, and 0.5 mm height). Fractionation was directly proportional to tissue frequency; 15, 24, 38, and 93 deflections at cycle lengths of 150, 125, 100, and 75 ms, respectively (Figure 6.10).
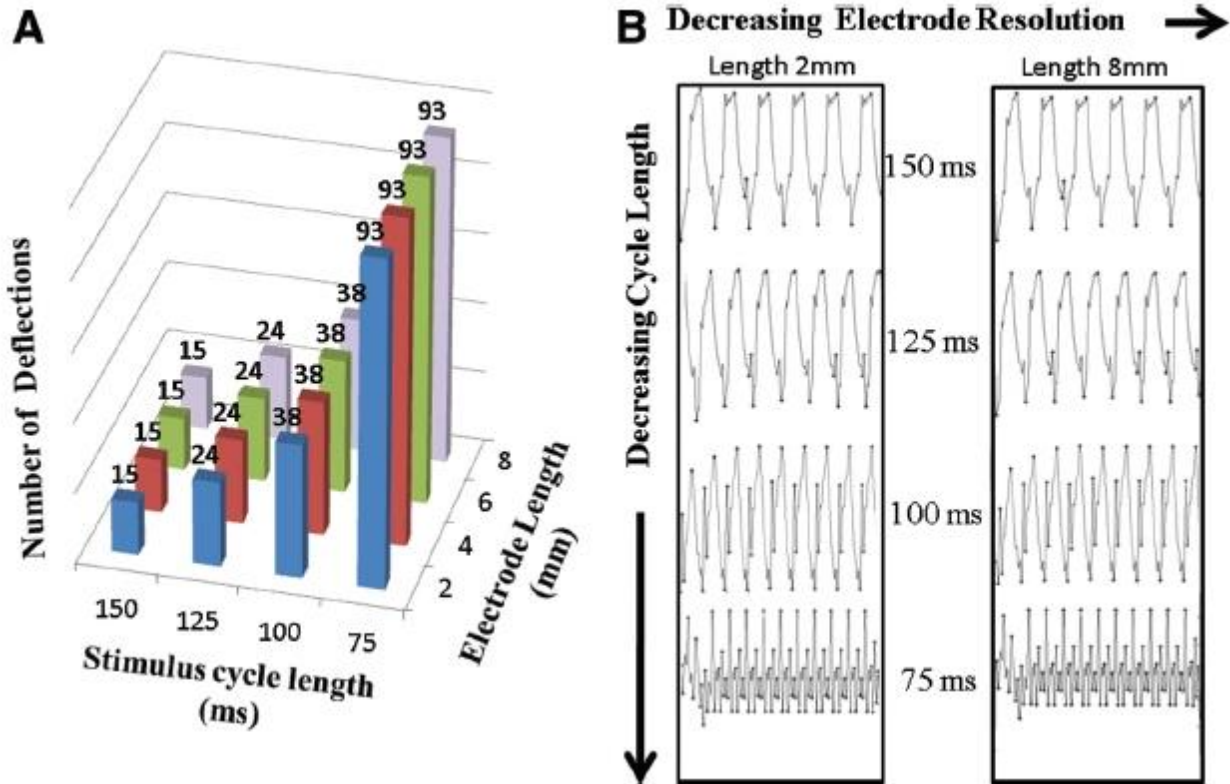

Figure 6.10. Temporal variation: electrogram fractionation is independent of electrode resolution. In a homogeneous sheet of tissue (no linear scar) with planar activation, the number of deflections in the unipolar electrogram was measured at the time of varying cycle length and electrode length. **A**, Number of deflections versus stimulus cycle length; electrode length 2, 4, 6, and 8 mm (diameter 1 mm, height 0.5 mm). **B**, Examples of virtual unipolar electrograms from tissue excited at decreasing cycle lengths: cycle length 150 ms (top) to 75 ms (bottom), recorded with a unipolar electrode of 2 mm (left) and 8 mm (right) in length. Note that number of deflections is independent of electrode size.

Impact of Electrode Spatial Resolution – Temporal Variation

With temporal variation alone, fractionation was independent of electrode spatial resolution (Figure 6.10). In tissue without scars stimulated at 150-ms cycle length, the number of deflections in the unipolar electrogram was independent of electrode length, diameter, or height (15 deflections for electrode length 2, 4, 6 and 8 mm; diameter 1, 2, 3, and 4 mm; height 0.5, 1, 2, and 3 mm). Bipolar recordings (1 mm length and diameter, 0.5 mm height) had 27 deflections regardless of IES (1, 3, 5, and 7 mm).

Fractionation as a Function of Spatiotemporal Variation

To create spatiotemporal variation, tissue was stimulated at a fixed cycle length of 150 ms from the upper left corner resulting in a "zig-zag" activation pattern. When electrode spatial resolution was kept constant, fractionation was directly proportional to the number of linear scars (i.e. spatiotemporal complexity); the number of deflections was 19, 26, 45, and 52 for tissue with 1, 2, 4, and 6 lines of scar, respectively (unipolar 6 mm length, 1 mm diameter, and 0.5 mm height; Figure 6.11). With bipolar recordings (1 mm length and diameter, 0.5 mm height, and 5 mm IES), there were 24, 25, 29, and 32 deflections for tissue with 1, 2, 4 ,and 6 lines of scar, respectively.
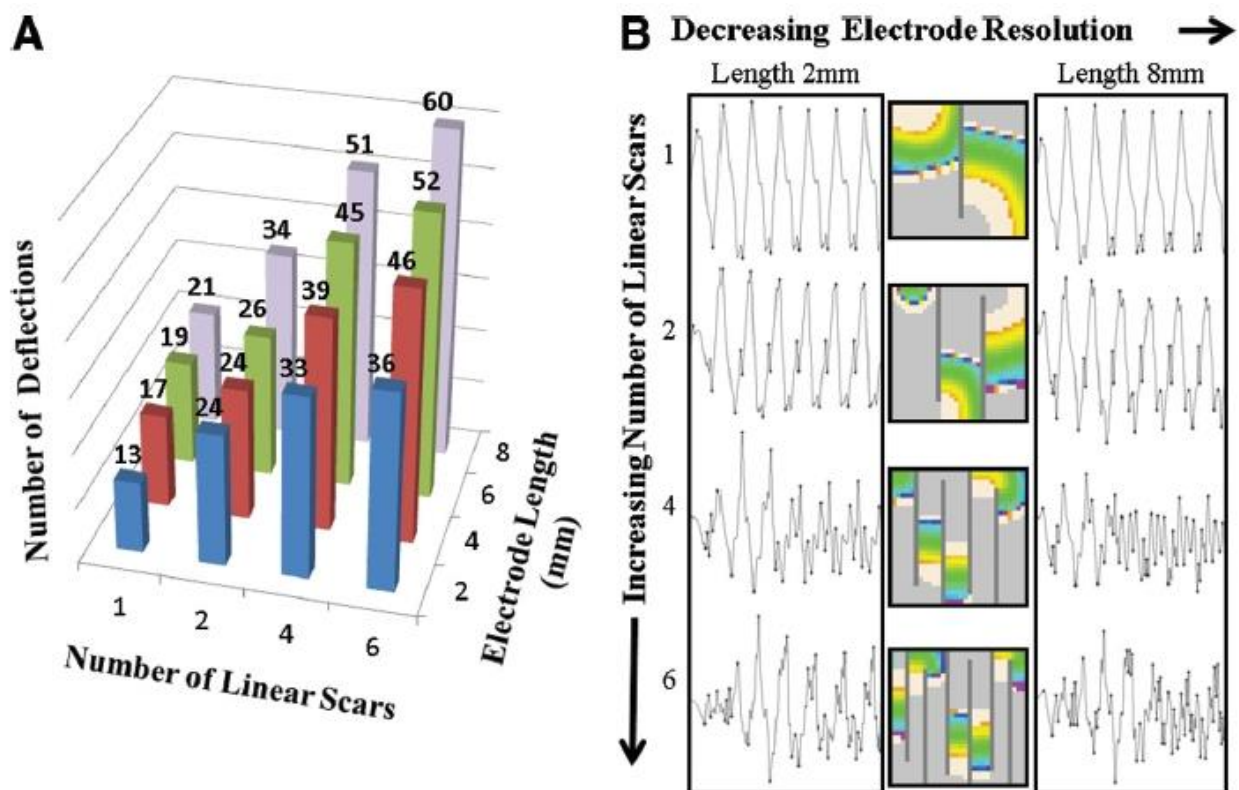

Figure 6.11. Spatiotemporal variation: electrogram fractionation is dependent on electrode resolution. **A**, Graph of number of deflections in unipolar recordings as a function of spatiotemporal variation (no. of scars) and electrode resolution (length; diameter 1 mm, height 0.5 mm). **B**, Examples of virtual electrograms from tissue stimulated every 150 ms with increasing spatiotemporal variation (1 scar [top] to 6 scars [bottom]) recorded with a unipolar electrode (length 2 mm [left] and 8 mm [right]). Note that number of deflections increases with decreased electrode resolution (effect is more prominent as no. of scars increases).

Impact of Electrode Spatial Resolution – Spatiotemporal Variation

In the setting of spatiotemporal variation (cycle length 150 ms, varied number of scars), the number of turning points increased in proportion to unipolar length (diameter 1 mm and height 0.5 mm) and number

of linear scars (Figure 6.11, Table 6.1). In tissue with 6 lines of scar, the number of deflections was proportional to electrode diameter: 52, 66, 74, and 76 deflections for electrodes of 1, 2, 3, and 4 mm diameter, respectively (length 6 mm and height 1 mm). With constant electrode size (length 6 mm and diameter 1 mm), the number of deflections was directly proportional to electrode height: 52, 68, 76, and 84 deflections at heights of 0.5, 1, 2, and 3 mm above the tissue, respectively. Fractionation also increased with increasing IES: 22, 24, 32, and 33 deflections for IES 1, 3, 5, and 7 mm, respectively (1 mm length and diameter, 0.5 mm height).

Table 1.   Fractionation Varies With Electrode Characteristics: Tissue With Spatiotemporal Variation*

Unipolar electrode length				
	2 mm	4 mm	6 mm	8 mm
	36	46	52	60
Unipolar electrode diameter				
	1 mm	2 mm	3 mm	4 mm
	52	66	74	76
Unipolar electrode height				
	0.5 mm	1 mm	2 mm	3 mm
	52	68	76	84
Bipolar interelectrode spacing				
	1 mm	3 mm	5 mm	7 mm
	22	24	32	33

*No. of deflections recorded with electrodes of different characteristics in tissue with spatiotemporal variation (zig-zag activation pattern—6 lines of scar). Note that fractionation increases as spatial resolution decreases. Unipolar electrode: 6 mm length, 1 mm diameter and 0.5 mm height (unless specified). Bipolar electrode: 1-mm length and diameter, 0.5-mm height.

Clinical Studies

Complex Fractionated Atrial Electrogram and Spatial Resolution

Qualitatively the effect of interelectrode spacing on spatial resolution (in sinus rhythm) and fractionation (during AF) is easily appreciated (Figure 6.12). To quantify the effects of spatial resolution on complex fractionated atrial electrogram, we measured ICL and AIPI as a function of IES during AF. Fractionation increased with increased IES (Table 6.2). Average values (and standard errors) were as follows: ICL 10-pole catheter: 5.2 ± 1.0, 8.7 ± 1.0, and 9.5 ± 1.0 for 2, 9, and 13 mm IES, respectively (P < 0.001, 2 versus 9 and 2 versus 13 mm); 20- pole catheter: AIPI confidence level 6.8 ± 1.0, 9.9 ± 1.0, and 10.3 ± 1.0 for 1, 5, and 7 mm). AIPI decreased with increased IES – 10-pole catheter: 207 ± 19, 116 ± 19, and 106 ± 19 for 2, 9,

and 13 mm IES, respectively (P < 0.001, 2 versus 9 mm and 2 versus 13 mm); AIPI 20-pole catheter: 144 ± 13, 99 ± 13, and 92 ± 13 (P < 0.001, 1 versus 5 mm and 1 versus 7 mm). As IES increases, electrodes record signals from locations that are progressively farther apart and are therefore exposed to different electromagnetic noise. Bipolar recordings reflect only the difference between the signals recorded at each electrode; therefore, as the difference in noise recorded at each electrode becomes greater, the amplitude of noise in the bipolar signal becomes larger. As a result, one can expect that noise is progressively increased as IES increases. We measured noise as a function of IES; the mean amplitude of noise increased with IES but remained < 0.05 mV (maximum 0.028 ± 0.01 mV).
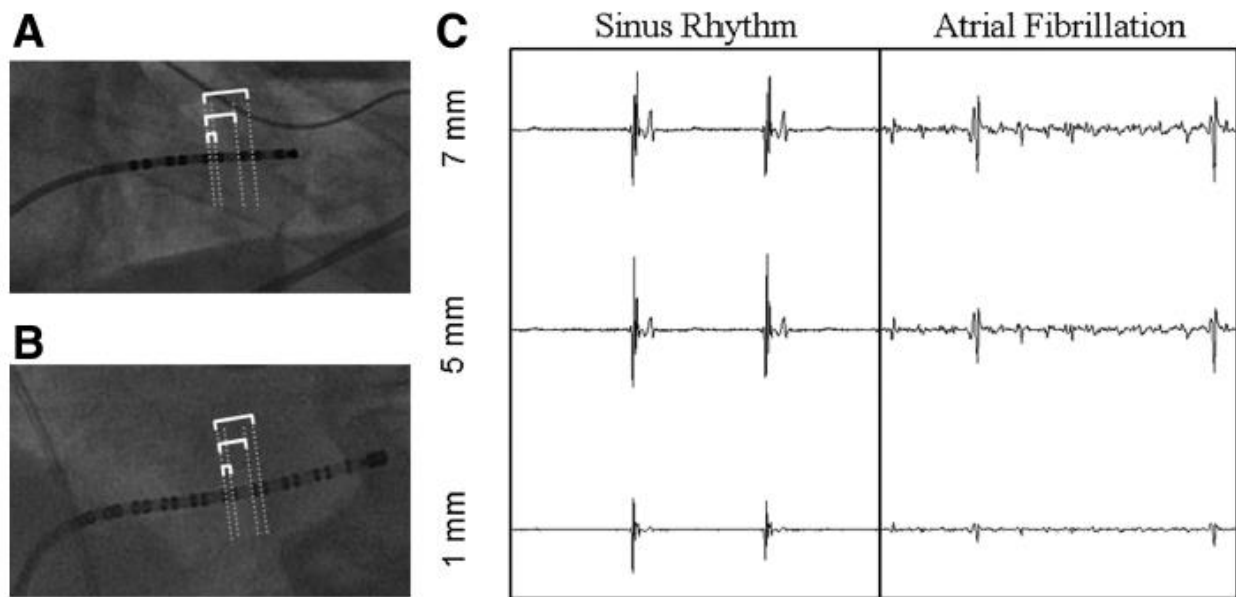

Figure 6.12. Impact of interelectrode spacing on electrograms recorded in the coronary sinus during sinus rhythm and atrial fibrillation. **A**, Fluoroscopic image of 10-pole catheter in the coronary sinus (electrode length 2 mm, interelectrode spacing 2-5-2 mm). Brackets indicate interelectrode spacing used for reconstruction of bipolar recordings. **B**, Fluoroscopic image of 20-pole catheter (electrode length 1 mm, interelectrode spacing 1-3-1 mm). **C**, Simultaneous electrogram recordings (IES as indicated). Note minor increase in baseline noise as IES increases (sinus rhythm) and increased fractionation with increased IES (atrial fibrillation). IES indicates interelectrode spacing.

Table 2. Fractionation Varies With Interelectrode Spacing: Patients With Atrial Fibrillation

ICL average±SEs		
10-Pole Catheter		
2 mm	9 mm	13 mm
5.2 ± 1.0	8.7 ± 1.0 ($P<0.001$)	9.5 ± 1.0 ($P<0.001$)
20-Pole Catheter		
1 mm	5 mm	7 mm
6.8 ± 1.0	9.9 ± 1.0 ($P<0.001$)	10.3 ± 1.0 ($P<0.001$)
AIPI averages±SEs		
10-Pole Catheter		
2 mm	9 mm	13 mm
207 ± 19	116 ± 19 ($P<0.001$)	106 ± 19 ($P<0.001$)
20-Pole Catheter		
1 mm	5 mm	7 mm
144 ± 13	99 ± 13 ($P<0.001$)	92 ± 13 ($P<0.001$)

ICL and AIPI recorded from coronary sinus of patients during atrial fibrillation. Average values presented for 10-pole and 20-pole catheter as interelectrode spacing increases.
ICL indicates interval confidence length; AIPI, average interpotential interval.

DISCUSSION

The fact that electrodes measure electric potential rather than tissue current density creates a possible source of ambiguity in the interpretation of electrograms. Because currents generate a potential field that spreads through space (with amplitude that decreases with distance),[120,121] potential recordings at any site reflect contributions from current sources at multiple sites. This capacity for "far-field" recording has the result that electrogram deflections occur with variation of current density over an area larger than the physical dimensions of the electrode. Electrogram fractionation is generally defined as low-amplitude, high-frequency deflections. As the number of sites contributing to an electrode's potential increases, the number of deflections will increase so long as these sites are excited asynchronously. When sites are excited simultaneously, their impact on the electrogram amplitude is additive but fractionation does not result.

In our study, we used a simple model to independently control each of the components that contribute to fractionation: tissue spatiotemporal variation, tissue temporal variation, and electrode spatial resolution. We made the following observations: (1) fractionation is not observed with spatial variation alone; secondary to temporal superposition, the contributions from spatially disparate currents to the

potential recorded at any electrode location sum to alter amplitude without producing fractionation; (2) fractionation is observed with temporal variation, which is independent of electrode spatial resolution; and (3) fractionation is observed with spatiotemporal variation and in this case is dependent on electrode spatial resolution. Consequently, spatial resolution determines the limit of the ability to distinguish temporal from spatiotemporal variation; that is, increased frequency as a result of overcounting.

Relationship to Previous Studies

Gardner et al.[141] found that fractionated ventricular electrograms in the setting of postinfarct scar results from local dissociation of activation timing between closely spaced muscle bundles separated by fibrous scar. Although their study did not directly assess the relationship between spatial resolution and fractionation, their conclusions were based on comparison of macroscopic recordings (0.3 mm diameter, 0.5-1.0 mm IES) with microscopic recordings (1-5 μm tip, unipolar) and were confirmed with histological examination. De Bakker et al.[147] meticulously demonstrated that "zig-zag" conduction through a "complex network of connected tracts" results in electrogram fractionation in superfused infarcted human papillary muscle. By placing a linear array of high-resolution electrodes (100 μm silver chloride wire) oriented perpendicularly to fiber direction, they were able to demonstrate sequential (asynchronous) activation of between 2 and 35 interconnected fibers. Although they did not systematically examine the relationship between tissue variation and spatial resolution, Jacquemet and Henriquez created a computer model of microfibrosis in which fractionation varied directly with the density of "collagenous" septa and increased when a larger electrode was used.[145] The same results were obtained in a computer model of electric conduction in a study performed by Lesh et al.[142] Kalifa and colleagues demonstrated fractionation at the junction between rapid organized rotors and the surrounding area where wave-break produced variable conduction patterns.[139] Furthermore, it has been demonstrated in computer models, isolated sheep hearts, and monolayers of murine atrial myocytes[137,138] that a meandering rotor generates electrogram fractionation. The common feature in all of these studies is the presence of multiple discretely and asynchronously activating muscle bundles.

To our knowledge, the present study is the first to explicitly and systematically explore and characterize the relationship among tissue spatiotemporal activation, electrode resolution, and electrogram fractionation.

Limitations

Our computer model makes no attempt to reproduce the specific functional and anatomic features of tissue excitation patterns. As a result, our electrograms do not mimic clinically recorded fractionated signals. It was not our intention to investigate the mechanism of any specific instance of physiological fractionation. Instead, our goal was to establish which parameters contribute to fractionation in general and to determine how these parameters interact to produce fractionation. With the use of a simple model, the roles of individual parameters could be independently examined. Our findings are commensurate with a large body of physiological recordings of fractionation resulting from varied activation patterns. We confirmed the general principles elucidated by our computer model in patients with AF. In the clinical experiments, the role of spatial resolution was measured by varying interelectrode spacing (we did not assess the impact of electrode size). We chose IES and not size to vary resolution at the same time as holding tissue spatiotemporal variation fixed. To reduce the confounding influence of spatiotemporal variation during AF, we compared only simultaneous recordings of varied resolution. This was practical only by varying IES, because comparing electrodes of different sizes would have required either sampling from different locations (unacceptable secondary to spatial disparities of tissue variation) or at different times (unacceptable secondary to temporal fluctuation of activation).[42]

CONCLUSION

Electrogram fractionation results from the interaction of 3 components: tissue temporal variation, tissue spatiotemporal variation, and electrode spatial resolution. In the absence of tissue spatiotemporal variation (i.e. temporal variation alone), fractionation is independent of electrode spatial resolution. In a computer model of electrically excitable tissue with spatiotemporal variation and in patients with AF, fractionation increased with decreasing electrode spatial resolution.

Electrograms measure the average potential field at the surface of and electrode over time. As a consequence, multiple different patterns of tissue activation can generate similar electrograms. Analysis of a single fractionated electrogram does not permit differentiation of temporal versus spatiotemporal tissue variation; therefore, one cannot distinguish high-frequency excitation from over-counting. Electrode spatial resolution must be considered when comparing studies of fractionation.

7. SUMMARY

An individualized mechanistic approach to mapping and ablation of human atrial fibrillation remains challenging to date. The standard electrophysiologic approach of mapping local activation time to achieve complete reconstruction of the activation pattern is not feasible outside the research setting. The spatio-temporal complexity of AF would require a large number of electrodes in order to obtain an exact picture of the beat to beat activity. Surrogate markers, such as dominant frequency and complex fractionated atrial electrograms, are thought to identify areas critical to the maintenance of AF and have been employed as an alternative strategy. While initial studies seemed promising, subsequent data did not demonstrate a reliable benefit to targeting DF and CFAE over pulmonary vein isolation alone.[39–41]

Utilizing computational modeling and multi-site simultaneous mapping data from human AF, the present work found several caveats to DF and CFAE mapping, which may explain why substrate modification does not consistently improve outcomes. We examined the temporal stability of DF and CFAE in human AF[42] and found that both are transient phenomena, lasting only an average of 22 and 47 seconds, respectively. As a result of this temporal variability sequentially acquired maps would fail to identify DF sites in 93% and CFAE sites in 38% leading to a significant underestimation of potential areas critical to the perpetuation of AF. Additionally, autonomic withdrawal can have a heterogeneous effect on DF and CFAE[45] further complicating the identification of driver vs. bystander sites. While the previous two studies highlight concerns of under-detecting potential ablation sites, the more dangerous[B] issue arises from falsely labeling areas as high DF or CFAE sites. We demonstrated that measurements of dominant frequency and fractionation are altered by the spatial resolution of electrode recordings[43,113], which in turn is dependent on electrode size, tissue contact (i.e. height above the tissue) and inter-electrode spacing[43].

Future investigations should focus on improving strategies as well as tools used for mapping and ablation of atrial fibrillation. This needs to start with patient selection for and timing of an ablation in order to increase the success rates. Further efforts to identify a diagnostic measure that correlates with the mechanism(s) responsible for the maintenance of AF in the individual patient are warranted. Independently of these goals, mapping tools require optimization to achieve high spatial resolution in

---

[B] Ablation of areas not critical to the perpetuation of the rhythm not only has the potential to be pro-arrhythmic but also increases the risk of procedure-related complications.

order to minimize the variability in the desired measurement and reduce the risk of falsely identifying sites as ablation targets.

REFERENCES

1. Feinberg WM, Blackshear JL, Laupacis A, Kronmal R, Hart RG. Prevalence, age distribution, and gender of patients with atrial fibrillation. Analysis and implications. *Arch Intern Med*. 1995;155(5):469-473.

2. Stewart S, Hart CL, Hole DJ, McMurray JJ. Population prevalence, incidence, and predictors of atrial fibrillation in the Renfrew/Paisley study. *Heart*. 2001;86(5):516-521.

3. Wolf PA, Abbott RD, Kannel WB. Atrial fibrillation as an independent risk factor for stroke: the Framingham Study. *Stroke*. 1991;22(8):983-988.

4. Fuster V, Rydén LE, Cannom DS, et al. ACC/AHA/ESC 2006 Guidelines for the Management of Patients with Atrial Fibrillation: a report of the American College of Cardiology/American Heart Association Task Force on Practice Guidelines and the European Society of Cardiology Committee for Practice . *Circulation*. 2006;114(7):e257-354.

5. Calkins H, Reynolds MR, Spector P, et al. Treatment of atrial fibrillation with antiarrhythmic drugs or radiofrequency ablation: two systematic literature reviews and meta-analyses. *Circ Arrhythm Electrophysiol*. 2009;2(4):349-361.

6. Oral H, Knight BP, Tada H, et al. Pulmonary vein isolation for paroxysmal and persistent atrial fibrillation. *Circulation*. 2002;105(9):1077-1081.

7. Cappato R, Calkins H, Chen S-A, et al. Updated worldwide survey on the methods, efficacy, and safety of catheter ablation for human atrial fibrillation. *Circ Arrhythm Electrophysiol*. 2010;3(1):32-38.

8. Wittkampf FHM, Hauer RNW, Robles de Medina EO. Control of radiofrequency lesion size by power regulation. *Circulation*. 1989;80(4):962-968.

9. Haines DE. Determinants of Lesion Size During Radiofrequency Catheter Ablation: The Role of Electrode-Tissue Contact Pressure and Duration of Energy Delivery. *J Cardiovasc Electrophysiol*. 1991;2(6):509-515.

10. Simmers TA, De Bakker JMT, Coronel R, et al. Effects of intracavitary blood flow and electrode-target distance on radiofrequency power required for transient conduction block in a Langendorff-perfused canine model. *J Am Coll Cardiol*. 1998;31(1):231-235.

11. Haines DE, Watson DP, Verow AF. Electrode radius predicts lesion radius during radiofrequency energy heating. Validation of a proposed thermodynamic model. *Circ Res*. 1990;67(1):124-129.

12. Avitall B, Mughal K, Hare J, Helms R, Krum D. The effects of electrode-tissue contact on radiofrequency lesion generation. *PACE - Pacing Clin Electrophysiol*. 1997;20(12):2899-2910.

13. Yokoyama K, Nakagawa H, Shah DC, et al. Novel contact force sensor incorporated in irrigated radiofrequency ablation catheter predicts lesion size and incidence of steam pop and thrombus. *Circ Arrhythm Electrophysiol*. 2008;1(5):354-362.

14. Shah D. Evolution of Force Sensing Technologies. *Arrhythmia Electrophysiol Rev*. 2017;6(2):75-79.

15. Hai JJ, Tse H-F. Biophysical Principles and Properties of Cryoablation. In: *The Practice of Catheter Cryoablation for Cardiac Arrhythmias*. Oxford, UK: John Wiley & Sons, Ltd; 2013:1-7.

16. Kumar S, Barbhaiya CR, Balindger S, et al. Better Lesion Creation And Assessment During Catheter Ablation. *J Atr Fibrillation*. 2015;8(3):1189.

17. Kolandaivelu A, Zviman MM, Castro V, Lardo AC, Berger RD, Halperin HR. Noninvasive assessment of tissue heating during cardiac radiofrequency ablation using MRI thermography. *Circ Arrhythmia Electrophysiol*. 2010;3(5):521-529.

18. Ranjan R, Kholmovski EG, Blauer J, et al. Identification and Acute Targeting of Gaps in Atrial Ablation Lesion Sets Using a Real-Time Magnetic Resonance Imaging System. *Circ Arrhythmia Electrophysiol*. 2012;5(6):1130-1135.

19. Narayan SM, Krummen DE, Shivkumar K, Clopton P, Rappel W-J, Miller JM. Treatment of Atrial Fibrillation by the Ablation of Localized Sources. *J Am Coll Cardiol*. 2012;60(7):628-636.

20. Benharash P, Buch E, Frank P, et al. Quantitative analysis of localized sources identified by focal impulse and rotor modulation mapping in atrial fibrillation. *Circ Arrhythm Electrophysiol*. 2015;8(3):554-561.

21. Kirchhof P, Benussi S, Kotecha D, et al. 2016 ESC Guidelines for the management of atrial fibrillation developed in collaboration with EACTS. *Eur Heart J*. 2016;37(38):2893-2962.

22. Haïssaguerre M, Jaïs P, Shah DC, et al. Spontaneous Initiation of Atrial Fibrillation by Ectopic Beats Originating in the Pulmonary Veins. *N Engl J Med*. 1998;339(10):659-666.

23. Hwang C, Chen P-S. Ligament of Marshall: Why it is important for atrial fibrillation ablation. *Hear Rhythm*. 2009;6(12):S35-S40.

24. Nakagawa H, Scherlag BJ, Patterson E, Ikeda A, Lockwood D, Jackman WM. Pathophysiologic basis of autonomic ganglionated plexus ablation in patients with atrial fibrillation. *Hear Rhythm*. 2009;6(12):S26-S34.

25. Garrey WE. The nature of fibrillary contraction of the heart. - Its relation to tissue mass and form. *Am J Physiol Content*. 1914;33(3):397-414.

26. Moe GK. On the multiple wavelet hypothesis of atrial fibrillation. *Arch Int Pharmacodyn*. 1962;(140):183-188.

27. Moe GK, Rheinboldt WC, Abildskov JA. A computer model of atrial fibrillation. *Am Heart J*. 1964;67(2):200-220.

28. Allessie M, Lammers W, F B, J H. Experimental evaluation of Moe's multiple wavelet hypothesis of atrial fibrillation. In: Zipes DP, Jalife J, eds. *Cardiac Arrhythmias*. Orlando, FL: Grune & Stratton; 1985:265-276.

29. Schuessler RB, Kawamoto T, Hand DE, et al. Simultaneous epicardial and endocardial activation sequence mapping in the isolated canine right atrium. *Circulation*. 1993;88(1):250-263.

30. Konings KT, Kirchhof CJ, Smeets JR, et al. High-density mapping of electrically induced atrial fibrillation in humans. *Circulation*. 1994;89(4):1665-1680.

31. Jalife J, Delmar M, Anumonwo J, Berenfeld O, Kalifa J. *Basic Cardiac Electrophysiology for the Clinician*. 2nd ed. Wiley-Blackwell; 2009.

32. Jalife J, Berenfeld O, Mansour M. Mother rotors and fibrillatory conduction: A mechanism of atrial fibrillation. *Cardiovasc Res*. 2002;54(2):204-216.

33. Spector P. Principles of cardiac electric propagation and their implications for re-entrant arrhythmias. *Circ Arrhythm Electrophysiol*. 2013;6(3):655-661.

34. Schuessler RB, Grayson TM, Bromberg BI, Cox JL, Boineau JP. Cholinergically mediated tachyarrhythmias induced by a single extrastimulus in the isolated canine right atrium. *Circ Res*. 1992;71(5):1254-1267.

35. Mandapati R, Skanes A, Chen J, Berenfeld O, Jalife J. Stable microreentrant sources as a mechanism of atrial fibrillation in the isolated sheep heart. *Circulation*. 2000;101(2):194-199.

36. Gerstenfeld EP, Sahakian A V, Swiryn S. Evidence for transient linking of atrial excitation during atrial fibrillation in humans. *Circulation*. 1992;86(2):375-382.

37. Nademanee K, McKenzie J, Kosar E, et al. A new approach for catheter ablation of atrial fibrillation: mapping of the electrophysiologic substrate. *J Am Coll Cardiol*. 2004;43(11):2044-2053.

38. Atienza F, Almendral J, Jalife J, et al. Real-time dominant frequency mapping and ablation of dominant frequency sites in atrial fibrillation with left-to-right frequency gradients predicts long-term maintenance of sinus rhythm. *Hear Rhythm*. 2009;6(1):33-40.

39. Atienza F, Almendral J, Ormaetxe JM, et al. Comparison of radiofrequency catheter ablation of drivers and circumferential pulmonary vein isolation in atrial fibrillation: A noninferiority randomized multicenter RADAR-AF trial. *J Am Coll Cardiol*. 2014;64(23):2455-2467.

40. Verma A, Lakkireddy D, Wulffhart Z, et al. Relationship between complex fractionated electrograms (CFE) and dominant frequency (DF) sites and prospective assessment of adding DF-guided ablation to pulmonary vein isolation in persistent atrial fibrillation (AF). *J Cardiovasc Electrophysiol*. 2011;22(12):1309-1316.

41. Providência R, Lambiase PD, Srinivasan N, et al. Is There Still a Role for Complex Fractionated Atrial Electrogram Ablation in Addition to Pulmonary Vein Isolation in Patients With Paroxysmal and Persistent Atrial Fibrillation? Meta-Analysis of 1415 Patients. *Circ Arrhythm Electrophysiol*. 2015;8(5):1017-1029.

42. **Habel N, Znojkiewicz P, Thompson N, et al. The temporal variability of dominant frequency and complex fractionated atrial electrograms constrains the validity of sequential mapping in human atrial fibrillation. *Hear Rhythm*. 2010;7(5):586-593.**

43. **Stinnett-Donnelly JM, Thompson N, Habel N, et al. Effects of electrode size and spacing on the resolution of intracardiac electrograms. *Coron Artery Dis*. 2012;23(2):126-132.**

44. **De Sa DDC, Thompson N, Stinnett-Donnelly J, et al. Electrogram fractionation: The relationship between spatiotemporal variation of tissue excitation and electrode spatial resolution. *Circ Arrhythmia Electrophysiol*. 2011;4(6):909-916.**

45. **Habel N, Müller JG, Znojkiewicz P, et al. The impact of pharmacologic sympathetic and parasympathetic blockade on atrial electrogram characteristics in patients with atrial fibrillation. *Pacing and Electrophysiology.* 2011; 34(11):1460-7.**

46. HODGKIN AL, HUXLEY AF. A quantitative description of membrane current and its application to conduction and excitation in nerve. *J Physiol*. 1952;117(4):500-544.

47. Silva J, Rudy Y. Subunit interaction determines IKs participation in cardiac repolarization and repolarization reserve. *Circulation*. 2005;112(10):1384-1391.

48. Silva JR, Pan H, Wu D, et al. A multiscale model linking ion-channel molecular dynamics and electrostatics to the cardiac action potential. *Proc Natl Acad Sci U S A*. 2009;106(27):11102-11106.

49. Yarov-Yarovoy V, Allen TW, Clancy CE. Computational models for predictive cardiac ion channel pharmacology. *Drug Discov Today Dis Model*. 2014;14:3-10.

50. Courtemanche M, Ramirez RJ, Nattel S. Ionic mechanisms underlying human atrial action potential properties: insights from a mathematical model. *Am J Physiol Circ Physiol*. 1998;275(1):H301-H321.

51. Luo CH, Rudy Y. A model of the ventricular cardiac action potential. Depolarization, repolarization, and their interaction. *Circ Res*. 1991;68(6):1501-1526.

52. Okajima M, Fujino T, Kobayashi T, Yomada K. Computer Simulation of the Propagation Process in Excitation of the Ventricles. *Circ Res*. 1968;000(2):203-212.

53. Virag N, Vesin JM, Kappenberger L. A computer model of cardiac electrical activity for the simulation of arrhythmias. *Pacing Clin Electrophysiol*. 1998;21(11 Pt 2):2366-2371.

54. Trayanova NA. Whole-heart modeling: applications to cardiac electrophysiology and electromechanics. *Circ Res*. 2011;108(1):113-128.

55. Potse M, Dube B, Richer J, Vinet A, Gulrajani RM. A Comparison of Monodomain and Bidomain Reaction-Diffusion Models for Action Potential Propagation in the Human Heart. *IEEE Trans Biomed Eng*. 2006;53(12):2425-2435.

56. Carrick RT, Benson B, Habel N, Bates ORJ, Bates JHT, Spector PS. Ablation of multiwavelet re-entry guided by circuit-density and distribution: maximizing the probability of circuit annihilation. *Circ Arrhythm Electrophysiol*. 2013;6(6):1229-1235.

57. Carrick RT, Bates ORJ, Benson BE, Habel N, Bates JHT, Spector PS. Prospectively quantifying the propensity for atrial fibrillation: a mechanistic formulation. *PLoS One*. 2015;10(3):e0118746.

58. Spector PS, Habel N, Sobel BE, Bates JHT. Emergence of complex behavior an interactive model of cardiac excitation provides a powerful tool for understanding electric propagation. *Circ Arrhythmia Electrophysiol*. 2011;4(4):586-591.

59. Fast VG, Kléber AG. Cardiac tissue geometry as a determinant of unidirectional conduction block: assessment of microscopic excitation spread by optical mapping in patterned cell cultures and in a computer model. *Cardiovasc Res*. 1995;29(5):697-707.

60.	Sasyniuk BI, Mendez C. A mechanism for reentry in canine ventricular tissue. *Circ Res*. 1971;28(1):3-15.

61.	Cabo C, Pertsov AM, Baxter WT, Davidenko JM, Gray RA, Jalife J. Wave-front curvature as a cause of slow conduction and block in isolated cardiac muscle. *Circ Res*. 1994;75(6):1014-1028.

62.	Waldo AL, MacLean WAH, Karp RB, Kouchoukos NT, James TN. Entrainment and interruption of atrial flutter with atrial pacing. Studies in man following open heart surgery. *Circulation*. 1977;56(5):737-745.

63.	Stevenson WG, Khan H, Sager P, et al. Identification of reentry circuit sites during catheter mapping and radiofrequency ablation of ventricular tachycardia late after myocardial infarction. *Circulation*. 1993;88(4 Pt 1):1647-1670.

64.	Courtemanche M, Ramirez RJ, Nattel S. Ionic targets for drug therapy and atrial fibrillation-induced electrical remodeling: insights from a mathematical model. *Cardiovasc Res*. 1999;42(2):477-489.

65.	Dang L, Virag N, Ihara Z, et al. Evaluation of Ablation Patterns Using a Biophysical Model of Atrial Fibrillation. *Ann Biomed Eng*. 2005;33(4):465-474.

66.	Keener J, Panfilow A. Three-dimensional propagation in the heart: the effects of geometry and fiber orientation on propagation in myocardium. In: Zipes D, Jalife J, eds. *Cardiac Electrophysiology*. 2nd ed. Philadelphia, PA: WB Saunders; 1995:335-347.

67.	Jacquemet V, Virag N, Ihara Z, et al. Study of Unipolar Electrogram Morphology in a Computer Model of Atrial Fibrillation. *J Cardiovasc Electrophysiol*. 2003;14(s10):S172-S179.

68.	Beeler GW, Reuter H. Reconstruction of the action potential of ventricular myocardial fibres. *J Physiol*. 1977;268(1):177-210.

69.	Fishler MG, Thakor N V. A Massively Parallel Computer Model of Propagation Through a Two-Dimensional Cardiac Syncytium. *Pacing Clin Electrophysiol*. 1991;14(11):1694-1699.

70.	van Capelle FJ, Durrer D. Computer simulation of arrhythmias in a network of coupled excitable elements. *Circ Res*. 1980;47(3):454-466.

71.	Fitzhugh R. Impulses and Physiological States in Theoretical Models of Nerve Membrane. *Biophys J*. 1961;1(6):445-466.

72.	Winfree AT. Varieties of spiral wave behavior: An experimentalist's approach to the theory of excitable media. *Chaos An Interdiscip J Nonlinear Sci*. 1991;1(3):303-334.

73.	Hunter PJ, Nielsen PM, Smaill BH, LeGrice IJ, Hunter IW. An anatomical heart model with applications to myocardial activation and ventricular mechanics. *Crit Rev Biomed Eng*. 1992;20(5-6):403-426.

74.	Wiener N, Rosenblueth A. The mathematical formulation of the problem of conduction of impulses in a network of connected excitable elements, specifically in cardiac muscle. *Arch Inst Cardiol Mex*. 1946;16(3):205-265.

75. Fast VG, Efimov IR, Krinsky VI. Transition from circular to linear rotation of a vortex in an excitable cellular medium. *Phys Lett A*. 1990;151(3-4):157-161.

76. Gerhardt M, Schuster H, Tyson JJ. A cellular automaton model of excitable media: II. Curvature, dispersion, rotating waves and meandering waves. *Phys D Nonlinear Phenom*. 1990;46(3):392-415.

77. Sanders P, Berenfeld O, Hocini M, et al. Spectral analysis identifies sites of high-frequency activity maintaining atrial fibrillation in humans. *Circulation*. 2005;112(6):789-797.

78. Ng J, Goldberger JJ. Understanding and interpreting dominant frequency analysis of AF electrograms. *J Cardiovasc Electrophysiol*. 2007;18(6):680-685.

79. Josephson ME, Wit AL. Fractionated electrical activity and continuous electrical activity: fact or artifact? *Circulation*. 1984;70(4):529-532.

80. De Bakker JMT, Wittkampf FHM. The pathophysiologic basis of fractionated and complex electrograms and the impact of recording techniques on their detection and interpretation. *Circ Arrhythmia Electrophysiol*. 2010;3(2):204-213.

81. Kalifa J, Jalife J, Zaitsev A V, et al. Intra-atrial pressure increases rate and organization of waves emanating from the superior pulmonary veins during atrial fibrillation. *Circulation*. 2003;108(6):668-671.

82. Krummen DE, Peng KA, Bullinga JR, Narayan SM. Centrifugal gradients of rate and organization in human atrial fibrillation. *Pacing Clin Electrophysiol*. 2009;32(11):1366-1378.

83. Wu J, Estner H, Luik A, et al. Automatic 3D mapping of complex fractionated atrial electrograms (CFAE) in patients with paroxysmal and persistent atrial fibrillation. *J Cardiovasc Electrophysiol*. 2008;19(9):897-903.

84. Scherr D, Dalal D, Cheema A, et al. Automated detection and characterization of complex fractionated atrial electrograms in human left atrium during atrial fibrillation. *Heart Rhythm*. 2007;4(8):1013-1020.

85. Scherr D, Dalal D, Cheema A, et al. Long- and short-term temporal stability of complex fractionated atrial electrograms in human left atrium during atrial fibrillation. *J Cardiovasc Electrophysiol*. 2009;20(1):13-21.

86. Verma A, Wulffhart Z, Beardsall M, Whaley B, Hill C, Khaykin Y. Spatial and temporal stability of complex fractionated electrograms in patients with persistent atrial fibrillation over longer time periods: relationship to local electrogram cycle length. *Heart Rhythm*. 2008;5(8):1127-1133.

87. Go AS, Hylek EM, Phillips KA, et al. Prevalence of diagnosed atrial fibrillation in adults: national implications for rhythm management and stroke prevention: the AnTicoagulation and Risk Factors in Atrial Fibrillation (ATRIA) Study. *JAMA*. 2001;285(18):2370-2375.

88. Benjamin EJ, Wolf PA, D'Agostino RB, Silbershatz H, Kannel WB, Levy D. Impact of atrial fibrillation on the risk of death: the Framingham Heart Study. *Circulation*. 1998;98(10):946-952.

89. Nair GM, Nery PB, Diwakaramenon S, Healey JS, Connolly SJ, Morillo CA. A systematic review of randomized trials comparing radiofrequency ablation with antiarrhythmic medications in patients with atrial fibrillation. *J Cardiovasc Electrophysiol*. 2009;20(2):138-144.

90. Kovacs RJ, Bailey JC. Effects of acetylcholine on action potential characteristics of atrial and ventricular myocardium after bilateral cervical vagotomy in the cat. *Circ Res*. 1985;56(4):613-620.

91. Voigt N, Heijman J, Wang Q, et al. Cellular and molecular mechanisms of atrial arrhythmogenesis in patients with paroxysmal atrial fibrillation. *Circulation*. 2014;129(2):145-156.

92. Scherlag BJ, Yamanashi W, Patel U, Lazzara R, Jackman WM. Autonomically Induced Conversion of Pulmonary Vein Focal Firing Into Atrial Fibrillation. *J Am Coll Cardiol*. 2005;45(11):1878-1886.

93. Moe GK, Abildskov JA. Atrial fibrillation as a self-sustaining arrhythmia independent of focal discharge. *Am Heart J*. 1959;58(1):59-70.

94. Chiou CW, Eble JN, Zipes DP. Efferent vagal innervation of the canine atria and sinus and atrioventricular nodes. The third fat pad. *Circulation*. 1997;95(11):2573-2584.

95. Kovoor P, Wickman K, Maguire CT, et al. Evaluation of the role of I(KACh) in atrial fibrillation using a mouse knockout model. *J Am Coll Cardiol*. 2001;37(8):2136-2143.

96. Pokushalov E, Romanov A, Artyomenko S, et al. Ganglionated plexi ablation for longstanding persistent atrial fibrillation. *Europace*. 2010;12(3):342-346.

97. Wilson R, Mackenzie J. Classics of Cardiology. In: Willius F, Keys T, eds. *Classics of Cardiology*. Volume 2. Krieger Publishing Company; 1983:765-768.

98. Loewi O. On humoral transmission of cardiac-nerve impulses. *Arch Ges Physiol*. 1921;189:239-242.

99. Rushmer R. Functional Anatomy and Control of the Heart. In: *Cardiovascular Dynamics*. 4th ed. Philadelphia, PA: W.B. Saunders Company; 1976.

100. Shepherd J, Vanhoutte P. Neurohumoral Regulation. In: *The Human Cardiovascular System, Facts and Concepts*. New York: Raven Press; 1979.

101. Patterson E, Po SS, Scherlag BJ, Lazzara R. Triggered firing in pulmonary veins initiated by in vitro autonomic nerve stimulation. *Hear Rhythm*. 2005;2(6):624-631.

102. Lu Z, Scherlag BJ, Niu G, et al. Functional Properties of the Superior Vena Cava (SVC)-Aorta Ganglionated Plexus: Evidence Suggesting an Autonomic Basis for Rapid SVC Firing. *J Cardiovasc Electrophysiol*. 2010;21(12):1392-1399.

103. Lin J, Scherlag BJ, Lu Z, et al. Inducibility of Atrial and Ventricular Arrhythmias Along the Ligament of Marshall: Role of Autonomic Factors. *J Cardiovasc Electrophysiol*. 2008;19(9):955-962.

104. Alessi R, Nusynowitz M, Abildskov JA, Moe GK. Nonuniform Distribution of Vagal Effects on the Atrial Refractory Period. *Am J Physiol Content*. 1958;194(2):406-410.

105. Zipes DP, Mihalick MJ, Robbins GT. Effects of selective vagal and stellate ganglion stimulation of atrial refractoriness. *Cardiovasc Res*. 1974;8(5):647-655.

106. Henning RJ, Sawmiller DR. Vasoactive intestinal peptide: cardiovascular effects. *Cardiovasc Res*. 2001;49(1):27-37.

107. Scherlag BJ, Nakagawa H, Jackman WM, et al. Electrical Stimulation to Identify Neural Elements on the Heart: Their Role in Atrial Fibrillation. *J Interv Card Electrophysiol*. 2005;13(S1):37-42.

108. Scherlag B, Patterson E, Po S. The neural basis of atrial fibrillation. *J Electrocardiol*. 2006;39(4 Suppl):S180-183.

109. Spector PS, Noori AM, Hardin NJ, Calame JD, Bell SP, Lustgarten DL. Pulmonary vein encircling ablation alters the atrial electrophysiologic response to autonomic stimulation. *J Interv Card Electrophysiol*. 2007;17(2):119-125.

110. Takahashi Y, O'Neill MD, Hocini M, et al. Characterization of Electrograms Associated With Termination of Chronic Atrial Fibrillation by Catheter Ablation. *J Am Coll Cardiol*. 2008;51(10):1003-1010.

111. Katritsis D, Sougiannis D, Batsikas K, et al. Autonomic modulation of complex fractionated atrial electrograms in patients with paroxysmal atrial fibrillation. *J Interv Card Electrophysiol*. 2011;31(3):217-223.

112. Knecht S, Wright M, Matsuo S, et al. Impact of pharmacological autonomic blockade on complex fractionated atrial electrograms. *J Cardiovasc Electrophysiol*. 2010;21(7):766-772.

113. **Habel N, Znojkiewicz P, Thompson N, et al. Dissociation between Electrogram Frequency and Tissue Frequency. In: *Heart Rhythm Society Meeting*. ; 2010:7:350.**

114. Hirose M, Leatmanoratn Z, Laurita KR, Carlson MD. Partial Vagal Denervation Increases Vulnerability to Vagally Induced Atrial Fibrillation. *J Cardiovasc Electrophysiol*. 2002;13(12):1272-1279.

115. Pappone C, Santinelli V, Manguso F, et al. Pulmonary vein denervation enhances long-term benefit after circumferential ablation for paroxysmal atrial fibrillation. *Circulation*. 2004;109(3):327-334.

116. Pokushalov E, Romanov A, Shugayev P, et al. Selective ganglionated plexi ablation for paroxysmal atrial fibrillation. *Hear Rhythm*. 2009;6(9):1257-1264.

117. Katritsis DG, Giazitzoglou E, Zografos T, Pokushalov E, Po SS, Camm AJ. Rapid pulmonary vein isolation combined with autonomic ganglia modification: A randomized study. *Hear Rhythm*. 2011;8(5):672-678.

118. Schmitt J, Duray G, Gersh BJ, Hohnloser SH. Atrial fibrillation in acute myocardial infarction: a systematic review of the incidence, clinical features and prognostic implications. *Eur Heart J*. 2009;30(9):1038-1045.

119. Spector P, Reynolds MR, Calkins H, et al. Meta-analysis of ablation of atrial flutter and supraventricular tachycardia. *Am J Cardiol*. 2009;104(5):671-677.

120. Plonsey R, Barr R. *Bioelectricity. A Quantitative Approach*. 3rd ed. New Yrok: Springer; 2007.

121. Kootsy J, Johnson E. Origin of the electrocardiogram: relationship between transmembrane potential and the electrocardiogram. In: Nelson C, DB G, eds. *Theor Basis Electrocardiol*. London: Oxford University Press; 1976:21-43.

122. Bates JHT, Spector PS. On the ill-conditioned nature of the intracardiac inverse problem. In: *2009 Annual International Conference of the IEEE Engineering in Medicine and Biology Society*. Vol 2009. IEEE; 2009:3929-3931.

123. Bogunović H, Loncarić S. Blood flow and velocity estimation based on vessel transit time by combining 2D and 3D X-ray angiography. *Med Image Comput Comput Assist Interv*. 2006;9(Pt 2):117-124.

124. Schaefer H, Trautwein W. Further experiments on the nature of the excitation wav in the myocardium of the dog. *Pflugers Arch Gesamte Physiol Menschen Tiere*. 1951;(253):152-164.

125. Durrer D, Van Der Tweel LH. Excitation of the left ventricular wall of the dog and goat. *Ann N Y Acad Sci*. 1957;65(6):779-803.

126. Berbari EJ, Dyer J, Lander P, Geselowitz DB. Simulation of intracardiac electrograms with a moving dipole source. Role of electrode geometry and high-pass filtering. *J Electrocardiol*. 1994;27(SUPPL. 1):146-150.

127. Fontaine G, Pierfitte M, Tonet J, Fillette F, Frank R, Grosgogeat Y. Interpretation of afterpotentials registered from epicardium, endocardium and body surface in patients with chronic ventricular tachycardia. In: Hombach V, Helger H, eds. *Signal Averaging Technique in Clinical Cardiology*. Stuttgart, New York; 1981:177.

128. Kimber S, Downar E, Masse S, et al. A comparison of unipolar and bipolar electrodes during cardiac mapping studies. *Pacing Clin Electrophysiol*. 1996;19(8):1196-1204.

129. Stevenson WG, Weiss JN, Wiener I, et al. Fractionated endocardial electrograms are associated with slow conduction in humans: Evidence from pace-mapping. *J Am Coll Cardiol*. 1989;13(2):369-376.

130. Brunckhorst CB, Delacretaz E, Soejima K, et al. Ventricular Mapping During Atrial and Right Ventricular Pacing: Relation of Electrogram Parameters to Ventricular Tachycardia Reentry Circuits After Myocardial Infarction. *J Interv Card Electrophysiol*. 2004;11(3):183-191.

131. Elayi CS, Fahmy TS, Martin DO, et al. Atrial fibrillation ablation strategies for paroxysmal patients randomized comparison between different techniques. *Circ Arrhythmia Electrophysiol*. 2009;2(2):113-119.

132. Elayi CS, Verma A, Di Biase L, et al. Ablation for longstanding permanent atrial fibrillation: Results from a randomized study comparing three different strategies. *Hear Rhythm*. 2008;5(12):1658-1664.

133. Khaykin Y, Skanes A, Champagne J, et al. A randomized controlled trial of the efficacy and safety of electroanatomic circumferential pulmonary vein ablation supplemented by ablation of complex fractionated atrial electrograms versus potential-guided pulmonary vein antrum isolation guided by intracardiac ultrasound. *Circ Arrhythm Electrophysiol*. 2009;2(5):481-487.

134. Oral H, Chugh A, Yoshida K, et al. A Randomized Assessment of the Incremental Role of Ablation of Complex Fractionated Atrial Electrograms After Antral Pulmonary Vein Isolation for Long-Lasting Persistent Atrial Fibrillation. *J Am Coll Cardiol*. 2009;53(9):782-789.

135. Li W, Bai Y, Zhang H, et al. Additional ablation of complex fractionated atrial electrograms after pulmonary vein isolation in patients with atrial fibrillation: a meta-analysis. *Circ Arrhythm Electrophysiol*. 2011;4(2):143-148.

136. Porter M, Spear W, Akar JG, et al. Prospective Study of Atrial Fibrillation Termination During Ablation Guided by Automated Detection of Fractionated Electrograms. *J Cardiovasc Electrophysiol*. 2008;19(6):613-620.

137. Umapathy K, Masse S, Kolodziejska K, et al. Electrogram fractionation in murine HL-1 atrial monolayer model. *Hear Rhythm*. 2008;5(7):1029-1035.

138. Zlochiver S, Yamazaki M, Kalifa J, Berenfeld O. Rotor meandering contributes to irregularity in electrograms during atrial fibrillation. *Hear Rhythm*. 2008;5(6):846-854.

139. Kalifa J, Tanaka K, Zaitsev A V, et al. Mechanisms of Wave Fractionation at Boundaries of High-Frequency Excitation in the Posterior Left Atrium of the Isolated Sheep Heart During Atrial Fibrillation. *Circulation*. 2006;113(5):626-633.

140. Berenfeld O, Zaitsev A V, Mironov SF, Pertsov AM, Jalife J. Frequency-dependent breakdown of wave propagation into fibrillatory conduction across the pectinate muscle network in the isolated sheep right atrium. *Circ Res*. 2002;90(11):1173-1180.

141. Gardner PI, Ursell PC, Fenoglio JJ, Wit AL. Electrophysiologic and anatomic basis for fractionated electrograms recorded from healed myocardial infarcts. *Circulation*. 1985;72(3):596-611.

142. Lesh MD, Spear JF, Simson MB. A computer model of the electrogram: what causes fractionation? *J Electrocardiol*. 1988;21 Suppl:S69-73.

143. Narayan SM, Wright M, Derval N, et al. Classifying fractionated electrograms in human atrial fibrillation using monophasic action potentials and activation mapping: evidence for localized drivers, rate acceleration, and nonlocal signal etiologies. *Hear Rhythm*. 2011;8(2):244-253.

144. Lellouche N, Buch E, Celigoj A, et al. Functional Characterization of Atrial Electrograms in Sinus Rhythm Delineates Sites of Parasympathetic Innervation in Patients With Paroxysmal Atrial Fibrillation. *J Am Coll Cardiol*. 2007;50(14):1324-1331.

145. Jacquemet V, Henriquez CS. Genesis of complex fractionated atrial electrograms in zones of slow conduction: a computer model of microfibrosis. *Hear Rhythm*. 2009;6(6):803-810.

146. Nademanee K, Schwab M, Porath J, Abbo A. How to perform electrogram-guided atrial fibrillation ablation. *Hear Rhythm*. 2006;3(8):981-984.

147. de Bakker JM, van Capelle FJ, Janse MJ, et al. Slow conduction in the infarcted human heart. "Zigzag" course of activation. *Circulation*. 1993;88(3):915-926.

DEUTSCHE KURZFASSUNG

Einführung

Vorhofflimmern (VHF) ist eine der häufigsten Herzrhythmusstörungen, von der über 6,8 Millionen Menschen in Europa und den Vereinigten Staaten betroffen sind.[1,2] Obwohl Vorhofflimmern per se nicht lebensbedrohlich ist, so ist es mit einem erhöhten Schlaganfallrisiko verbunden und kann zu Tachykardie-induzierter Kardiomyopathie führen.[3] Die Symptome reichen von Herzrasen, Palpitationen, zu Schwindelgefühl, Angina pectoris und Atemnot, welche Patienten mit Vorhofflimmern deutlich beeinträchtigen können. Die Frequenz und Dauer von Vorhofflimmer-Episoden schwankt deutlich zwischen Patienten und kann einen progredienten Verlauf nehmen. Medikamentöse Behandlung erzielt Rhythmuskontrolle in 52% der Patienten, allerdings kann ihre Anwendung durch Nebenwirkungen erheblich eingeschränkt sein.[5] Katheterablation mit Pulmonalvenen Isolation allein hingegen erreicht eine Erfolgsrate von etwa 70%.[6] Die Erfolgsquoten sinken jedoch mit einer erhöhten Belastung an Vorhofflimmern. Selbst wenn umfangreichere Ablationsverfahren für persistierendes oder permanentes Vorhofflimmern angewandt werden, bleiben die Erfolgsraten relativ gering (64,8 % bzw. 63,1 %).[7]

Die Faktoren, die zu diesem unbefriedigendem Ergebnis beitragen, sind, dass bestehende Ablationsstrategien entweder nicht erfolgreich umgesetzt werden und/oder dass, die derzeitigen Strategien mangelhaft sind:

(1) Inadäquate Ausführung: Unvollständige Ablationslinien führen nicht nur zum Versagen einer interventionellen Behandlung, sondern haben auch das Potenzial, pro-arrhythmisch zu sein. Trotz Fortschritten in der Biophysik der Ablation und dem Einsatz von Kathetern mit Kraftsensoren[14] fehlt uns nach wie vor die Möglichkeit, Läsionsgrößen intraoperativ und dreidimensional genau und zuverlässig zu beurteilen.[16] Die Anwendung einer MR-Thermographie[17] und des Echtzeit-MRT[18] wird derzeit untersucht.

(2) Mangelhafte Strategien: Die allgemeine medizinische Praxis beruht auf einer diagnostischen Maßnahme, deren Ergebnisse die darauffolgende Behandlung informieren. Leider kommt dieses Prinzip bei der Behandlung von Vorhofflimmern derzeit nicht routinemäßig zum Einsatz. Während das Mapping von Rotoren der neueste Ansatz ist, um arrhythmogene Areale ausfindig zu machen, ist das Verfahren fehleranfällig und dazu durchgeführte Studien zeigen unterschiedliche Ergebnisse.[19,20] Das derzeitige Behandlungsvorgehen beim Vorhofflimmern beinhaltet die Pulmonalvenenisolation, eine

lineare Läsionen, die das chirurgische MAZE-Verfahren simulieren und häufig auch eine "Substratmodulation", z. B. Ablation von dominanten Frequenzen (DF) oder komplexen fraktionierten atrialen Elektrogrammen (CFAE).[21]

Probleme beim Mapping von menschlichem Vorrhofflimmern

Es ist bekannt, dass Erregungen, die von den Pulmonalvenen ausgehen, ein wesentlicher Beitrag zur Entstehung von Vorhofflimmern sind. Pulmonalvenen Isolation ist darauf ausgerichtet, diese „Trigger" unter Quarantäne zu stellen.[22] Wenn Vorhofflimmern nach Pulmonalvenen Isolation allerdings weiterhin fortbesteht, ist der anschließende Therapieansatz nicht genau definiert. Leider ist die Erregung der Vorhöfe so komplex, dass das Mapping von lokalen Aktivierungszeiten nicht angewandt werden kann, da man hunderte von dicht beieinander liegenden Elektroden bräuchte, um das gesamte atriale Endokardium genau zu kartieren („Mapping"). Stattdessen wurde vorgeschlagen, dass man Ersatzmarker wie dominante Frequenzen (DF) und „complex fractionated atrial electrograms" (CFAE) nutzt, um kritische Areale zu identifizieren, die zum Aufrechterhalten des Vorhofflimmerns beitragen.[37,77] Die initialen Studien lieferten vielversprechende Ergebnisse – Ablation von CFAE erreichte nach einem Jahr 91% Freiheit vom Vorhofflimmern[37] und Ablation von hochfrequenten DF Arealen erzielte Freiheit vom Vorhofflimmern bei 88% der paroxysmalen und bei 56% der persistenten VHF-Patienten (bei einer durchschnittlichen Nachbeobachtung von 9,3 +/- 5,4 Monaten).[38] Spätere Studien[39,40] und eine Metaanalyse[41] hingegen kamen zu dem Schluss, dass weder die Ablation von DF noch von CFAE einen zusätzlichen Nutzen gegenüber alleiniger Pulmonalvenen Isolation bietet.

Studienziele

Die folgende Reihe von Studien ist darauf ausgerichtet, die Grenzen des Mapping von DF und CFAE mit heutigen Methoden zu erforschen. Außerdem untersuchen wir die fundamentalen Komponenten der räumlichen Auflösung von Elektroden[43], sowie deren Einfluss auf die Messwerte von Frequenz[113] und Fraktionierung[44]. Zunächst stellen wir ein Computermodell[58] vor, das für die Untersuchung der Erregungsausbreitung und des daraus resultierenden Potentialfeldes entwickelt wurde. Dieses Modell wird dann in den folgenden Studien angewendet.

Computermodell: Simulation der Erregungsausbreitung

Das Ziel der Studie **"Emergence of complex behavior: An interactive model of cardiac excitation provides a powerful tool for understanding electric propagation"** [58] war die Entwicklung eines physikalischen Zellautomaten, welcher uns erlaubt, die Erregungsausbreitung im zweidimensionalen Raum und das entstehende Potentialfeld zu untersuchen. Das Potentialfeld kann mit Elektroden individueller Konfiguration (z.B. unterschiedliche Elektrodengröße, Interelektrodenabstand, unipolare oder bipolare Aufzeichnung) getestet werden. Dadurch ist eine direkte Korrelation von Elektrogrammen und dem Verhalten der Kardiomyozyten im Gewebsverband möglich. Natürlich ist jedes Computermodell nur eine Annäherung an Herzgewebe, und dieses Modell wurde darauf ausgerichtet, die Simulationsgeschwindigkeit zu maximieren, während der Kompromiss akzeptiert wird, bestimmte Details auszulassen, wie z.B. den Strom durch einzelne Ionenkanäle.[55] Stattdessen werden Zellen so simuliert, dass sie mehrere Phasen haben (z.B. Ruhezustand, Erregungszustand mit Modulation der absoluten und relativen Refraktärzeit) und elektrisch über einen modulierbaren Widerstand miteinander verbunden sind. Die folgende Studie zeigt, dass trotz der begrenzten Regeln, ein komplexes Gewebeverhalten entstehen kann. Dies ist vergleichbar mit detaillierteren Computermodellen, allerdings mit dem Vorteil, Experimente in schneller Folge und ohne Änderung der Startbedingungen von einem Experiment zum anderen durchführen zu können. Darüber hinaus erlaubt dieses Modell die direkte Kenntnis der Gewebeeigenschaften (z.B. Aktionspotentialdauer) und ermöglicht es, verschiedene Bestandteile unabhängig voneinander zu verändern.

Dieses Computermodell wurde unter anderem angewandt, um den Effekt zeitlicher und räumlicher Variabilität, sowie den Effekt des Interelektrodenabstandes auf Elektrogrammfraktionierung [44] und die Wellendynamik bei Vorhofflimmern zu studieren.[56,57]

Zeitliche Variabilität von dominanter Frequenz und komplex fractionierten atrialen Electrogrammen

Mapping der dominanten Frequenz (DF)

Ein Mapping von hochfrequenten Arealen soll auf Grund der Erkenntnisse einer Studie von Mandapati[35] am Schafmodell arrhythmogene Bereiche identifizieren, die für die Aufrechterhaltung von Vorhofflimmern verantwortlich sind. Die komplexe Erregungsausbreitung bei Vorhhofflimmern führt zu Schwankungen in der Signalamplitude und Signalmorphologie, sodass die zeitliche Signalanalyse (d.h. die Messung der lokalen Aktivierungszeit zur Bestimmung der Aktivierungsrate) nicht möglich ist. Um diese

Einschränkung zu überwinden, wird die Frequenzanalyse eingesetzt. Ein Elektrogramm kann hierbei als Summierung verschiedener sinusförmiger Signale (Fourier-Analyse) betrachtet werden. Weist das Signal über einen längeren Zeitraum eine gewisse Regelmäßigkeit (d.h. Periodizität) auf, wird die Amplitude dieser Frequenz im Amplitudenspektrum größer. Die dominante Frequenz ist als höchster Punkt im Amplitudenspektrum definiert.[78] Ein Vorbehalt zur Frequenzanalyse von Vorhofflimmerelektrogrammen sind die Variabilität der Erregungsintervalle und die Morphologie- Schwankungen zwischen einzelnen Komplexen (z.B. gespaltene Doppelpotentiale). Das führt dazu, dass diese Signale nur schwer an Sinuswellen angepasst werden können und damit mehrere Höhepunkte im Amplitudenspektrum erscheinen. Dies wiederum erschwert die Bestimmung der dominanten Frequenz. Der Regelmäßigkeitsindex, definiert als das Verhältnis der Fläche im dominanten Frequenzband zur Fläche des gesamten Frequenzbandes, wird als Messwert verwendet, um die Zuverlässigkeit der dominanten Frequenz als "wahre" Vorhoffrequenz zu bestimmen.

Mapping von komplex fraktionierten atrialen Elektrogrammen (CFAE)

Die Fraktionierung, definiert als repetitives Hochfrequenzsignal mit niedriger Amplitude, wird als wichtige Kennzeichnung für Arrhythmien, bzw. für ein Kreisen von Erregungswellen gewertet - analog zum Mapping von narbenbedingter ventrikulärer Tachykardie.[79] Wie wir anschließend aufzeigen werden, gibt es mehrere Ursachen, die zum Phänotyp der Fraktionierung führen können[44,80] ; damit sind nicht alle CFAE-Bereiche geeignete Ziele der Ablation.

Die Voraussetzung für die Berücksichtigung von DF und CFAE als Ablationsziele ist, dass sie zeitlich stabil sein müssen, um eine umfangreiche Kartierung (Mapping) der Vorhöfe in sequenzieller Weise zu erlauben. Optisches Mapping von Kalifa et al.[81] zeigte Vorhofflimmerepisoden, die sehr periodisch sind; allerdings war die Dauer der Beobachtung nur auf Sekunden beschränkt. In ähnlicher Weise wurde das Mapping von DF und CFAE beim menschlichen Vorhofflimmern in fünf bis zehn Sekundenintervallen durchgeführt. Mit der Studie **"The temporal variability of dominant frequency and complex fractionated atrial electrograms constrains the validity of sequential mapping in human atrial fibrillation"** [42] wollten wir unter Anwendung von „multi-site simultaneous" Mapping herausfinden, ob DF und CFAE über einen Zeitraum von fünf Minuten erkennbare Schwankungen aufweisen. Wir stellten fest, dass sowohl DF- als auch CFAE-Bereiche, die im Rahmen bestehender Protokolle zur Ablation verwendet werden, innerhalb von fünf Minuten sehr stark variieren. Dementsprechend kommen wir zu der Schlussfolgerung, dass DF und CFAE nicht zuverlässig in sequenzieller Weise erfasst werden können.

__Autonomer Tonus verändert dominante Frequenz und komplex fraktionierte atriale Elektrogramme in unvorhersehbarer Weise__

Die Herzfunktion wird durch das autonome Nervensystem stark moduliert. Zahlreiche Studien der zellulären Physiologie haben gezeigt, dass sowohl die sympathische, als auch die parasympathische Stimulation einen pro-arrhythmischen Einfluss auf das atriale Myokard haben können, indem sie z. B. die Aktionspotentialdauer verkürzen oder die Heterogenität der Refraktärzeit verstärken.[90,91] Tierstudien zeigten weiterhin, dass die Modulation des autonomen Nervensystems die Induzierbarkeit von Vorhofflimmern verändern kann.[92] Zum Beispiel, kann ein Vorhofflimmern bei Hunden durch andauernde Stimulation des Nervus vagus aufrecht erhalten werden[93], und im umgekehrten Fall kann nach vagaler Nervenablation kein VHF mehr induziert werden.[94] Ähnlich dazu, zeigen die I_{KACh}-Knockout-Mäuse kein Vorhofflimmern. [95]

Diese Ergebnisse lassen vermuten, dass die Ausschaltung autonomer Einflüsse durch eine Ablation intrinsischer Herzganglien zu einer Beseitigung oder zumindest einer Reduzierung der VHF-Auslöser führt, oder zu einer Substratveränderung beiträgt, was dann die Wahrscheinlichkeit, dass VHF aufrechterhalten werden kann, deutlich verringert. Während klinische Studien zuversichtliche Ergebnisse für diesen Ansatz geliefert haben[24,96], muss man bedenken, dass die Ablation von Herzganglien nicht nur das autonome Nervensystem verändert, sondern auch direkt das anliegende Myokard modifiziert. Daher ist die Wirkung der alleinigen Ausschaltung des autonomen Nervensystems auf das Verhalten vom menschlichen Vorhofflimmern noch ungenügend untersucht.

Die Studie **"The impact of pharmacologic sympathetic and parasympathetic blockade on atrial electrogram characteristics in patients with atrial fibrillation"[45]** war darauf ausgerichtet, die Auswirkugen des pharmakologischen Nervenblocks auf die Surrogate der VHF-Dynamik (DF und CFAE) zu untersuchen. Studiert man den Einfluss des autonomen Nervensystems auf die zellulären elektrophysiologischen Eigenschaften, so würde man erwarten, dass eine pharmakologische Nervenblockierung zur Verminderung der dominanten Frequenz und zur Verringerung der Fraktionierung führt. Interessanterweise ist dies nicht in allen Vorhofregionen der Fall. Wir fanden eine Beschleunigung von DF in 32% der Standorte und eine erhöhte Dys-synchronisation (d.h. mehr Fraktionierung) in 29% aller Messpunkte.

Auflösungsvermögen von Elektroden und der Einfluss auf intrakardiale Elektrogramme

Eine räumliche Auflösung bezieht sich auf die Fähigkeit, zwischen zwei Entitäten unterscheiden zu können. Im Zusammenhang mit der Elektrophysiologie bedeutet das, zwischen getrennten Erregungen innerhalb des Aufzeichnungsbereichs einer Elektrode zu differenzieren. Das Aufzeichnungsgebiet einer Elektrode überschreitet deren physikalische Dimension, da sich das elektrische Potentialfeld, welches von der Elektrode gemessen wird, durch den Raum ausbreitet. Hierbei nimmt die Stärke des Potentialfeldes mit der Entfernung vom Ursprung der elektrischen Erregung ab. Beispielsweise kann eine Elektrode, die sich im Vorhof befindet, sowohl die lokale Vorhofaktivierung als auch die ferne ventrikuläre Erregung aufzeichnen.

Das elektrische Potential hängt nicht nur von den ihm zu Grunde liegenden Strömen ab, sondern ändert sich auch mit der Konfiguration der Elektrode (bei bipolaren Elektroden: Elektrodengröße, Gewebekontakt und Interelektrodenabstand). Daraus ergibt sich das Problem, dass die zugrunde liegende Gewebeaktivierung nicht einfach aus dem Elektrogramm rekonstruiert werden kann. Es ist ein Phänomen, das mathematisch als inverses Problem bekannt ist. Insbesondere beim Mapping von Vorhofflimmern machen es die komplexen Aktivierungsmuster schwierig, ein genaues Bild der elektrischen Aktivität zu erstellen. Dys-Synchronie innerhalb des Aufzeichnungsbereichs einer Elektrode führt zur Fraktionierung und macht damit die Identifizierung der lokalen Aktivierungszeit unmöglich. Anstelle des „Aktivierungsmapping" wurden Ersatzmarker wie dominante Frequenz[77] oder komplex fraktionierte atriale Electrogramme[37] als Ablationsziele vorgeschlagen. Die räumliche Auflösung der Elektrode kann jedoch die Messung der dominanten Frequenz und Fraktionierung beeinflussen. Eine geringe räumliche Auflösung kann dazu führen, dass zwei getrennte Erregungen nicht diskriminiert werden können und damit z. B. hochfrequente Bereiche nicht erfasst werden. Das Gegenteil ist auch möglich, d. h. mangelnde Klarheit zwischen Nahfeld- und Fernfeld-Erregungen kann die Zahl der Erregungen erhöhen und damit fälschlicher Weise Vorhofbereiche als Hochfrequenzareale identifiziern.[113]

In ähnlicher Weise kann die räumliche Auflösung den Grad der Fraktionierung beeinflussen. Das erschwert ein genaues Mapping und kompliziert den Vergleich zwischen einzelnen CFAE-Studien, da diese Studien oft unterschiedliche Katheter-Konfigurationen benutzen. Die folgenden zwei Studien untersuchen die Details der Elektrodenauflösung und deren Einfluss auf intrakardiale Elektrogramme. Die Studie: "**Effects of electrode size and spacing on the resolution of intracardiac electrograms"** [43] quantifiziert die Auswirkungen von Elektrodeneigenschaften auf die räumliche Auflösung der intra-kardialen Elektrogramme und stellte fest, dass sich die Auflösung mit größerem Elektrodendurchmesser, größerer

Elektrodenlänge und Elektrodenabstand vom Gewebe verschlechtert. Die Studie "**Electrogram Fractionation: The relationship between spatiotemporal variation in tissue excitation and electrode spatial resolution**" [44] untersucht die Auswirkungen der räumlichen Auflösung auf die Fraktionierung. Wir fanden heraus, dass Fraktionierung eine Reflexion der räumlich-zeitlichen Variabilität der Gewebeerregung innerhalb des Aufzeichnungsbereichs einer Elektrode, d. h. eines Elektrodenpaares, ist. Somit kann sich der Grad der Fraktionierung erhöhen, wenn sich die räumliche Auflösung verschlechtert.

Zusammenfassung

Ein individualisierter, mechanistischer Ansatz zur Kartierung (Mapping) und Ablation von menschlichem Vorhofflimmern (VHF) stellt nach wie vor eine Herausforderung dar. Der übliche Ansatz der Elektrophysiologie – das Mapping der lokalen Aktivierungszeit zur vollständigen Rekonstruktion eines Aktivierungsmusters - ist außerhalb der Forschung nicht realisierbar. Die räumlich-zeitliche Komplexität von VHF würde eine große Anzahl von Elektroden erfordern, um ein genaues Bild der gesamten Vorhoferregung zu erstellen. Ersatzparameter, wie dominante Frequenz (DF) und komplex fraktionierte atriale Elektrogramme (CFAE) wurden verwendet, um kritische Bereiche zu identifizieren, die für die Aufrechterhaltung von VHF ausschlaggebend schienen. Während die initialen Studien vielversprechend waren, zeigten spätere Daten keinen zuverlässigen Vorteil von DF- und CFAE Ablation gegenüber der alleinigen Pulmonalvenenisolation.[39–41]

Daten von Computersimulationen und „Multisite simultaneous Mapping" vom menschlichen VHF sind in der vorliegenden Arbeit dargestellt, und sie zeigen verschiedene Probleme beim Mapping von DF und CFAE auf. Die in der Arbeit dargestellten Ergebnisse können erklären, warum eine Substratmodifikation die Ablationsergebnisse beim Vorhofflimmern nicht verbessert. Wir untersuchten die zeitliche Stabilität von DF und CFAE bei menschlichem VHF[42] und stellten fest, dass beide Parameter vorübergehende Phänomene sind, die durchschnittlich nur 22 bzw. 47 Sekunden andauern. Als Folge dieser zeitlichen Variabilität würden sequenziell erworbene Mapping-Karten 93% der DF-Standorte und 38% der CFAE-Standorte nicht identifizieren, was zu einer erheblichen Unterschätzung potenzieller Ablationsgebiete führen würde. Darüber hinaus kann eine autonome Nervenblockierung eine heterogene Wirkung auf die Messung von DF und CFAE[45] haben, wodurch eine Identifizierung von arrhythmogenen und passiven Bereichen weiter erschwert wird. Während unsere letzten zwei Studien Fehler durch Unterschätzung potentieller Ablationsareale aufzeigen, ergibt sich ein weitaus größeres Problem aus der fälschlichen

Kennzeichnung von Hochfrequenz- oder CFAE-Bereichen. Die Ablation von Gewebe, das für das Fortbestehen des Vorhofflimmerns nicht ausschlaggebend ist, hat nicht nur das Potential pro-arrhythmisch zu sein, sondern erhöht auch das Risiko behandlungsbedingter Komplikationen. Weiterhin konnten wir zeigen, dass Messungen der dominanten Frequenz und Fraktionierung vom Auflösungsvermögen der Elektroden abhängig ist.[43,113] Die zeitlich-räumliche Auflösung wiederum ist abhängig von der Elektrodengröße, dem Gewebekontakt und dem Interelektrodenabstand.[43]

Zukünftige Studien sollten sich auf die Verbesserung von Mapping Strategien, Mapping-Kathetern und Mapping Systeme konzentrieren. Dies sollte durch geeignete Patientenauswahl und dem richtigen Zeitpunkt einer Ablation geschehen, um die Erfolgsquoten bei der Behandlung von Vorhofflimmern zu erhöhen. Es erscheint wichtig, diagnostische Marker zu identifizieren, die mit den Mechanismen des Flimmerns korrelieren und die für die Aufrechterhaltung des VHF im individuellen Patientenverantwortlich sind. Unabhängig von diesen Bedingungen benötigen wir Mapping-Katheter mit einem höheren Auflösungsvermögen, um die Variabilität des gewünschten Messwertes zu minimieren und um das Risiko zu verringern, falsche Lokalisationen als Ablationsziele zu identifizieren.

ACKNOWLEDGEMENTS

Erklärung zur strafrechtlichen Verurteilung

Ich erkläre hiermit, nicht wegen einer Straftat verurteilt worden zu sein, die Wissenschaftsbezug hat.

Colchester Vermont (USA), den 28. Januar 2020

Nicole Habel

Curriculum vitae

Nicole Habel, MD
Cardiology Fellow, University of Vermont Medical Center

PROFESSIONAL TRAINING

07/2018 – 06/2021	**Cardiology Fellow at the University of Vermont Medical Center (Burlington, VT)**
11/2020	Advanced Heart Failure Rotation at Massachusetts General Hospital (Boston, MA)
07/2015 – 06/2018	**Internal Medicine Resident at Carilion Clinic & Virginia-Tech Carilion School of Medicine (Roanoke, VA)**
02/2017	Away Elective - Cardiology at the University of Utah (Salt Lake City, UT)
09/2016	Away Elective - Cardiac Electrophysiology at Virginia Commonwealth University (Richmond, VA)
11/2012 – 06/2015	**Post-doctoral Fellow at the University of Vermont**

EDUCATION

10/2004 – 11/2012	**Medical School, Otto-von-Guericke University of Magdeburg (Magdeburg, Germany)**
10/2010 – 11/2012	Clinical Training Part II
05/2012 – 07/2012	Acting Internship, University of Vermont (Burlington, VT) Anesthesiology & Critical Care Medicine
02/2012 – 05/2012	Acting Internship, University of California San Diego (San Diego, CA) Cardiology/Cardiac Electrophysiology Pulmonary Physiology/Clinical Pulmonology
12/2011 – 02/2012	Acting Internship, University of Vermont (Burlington, VT) Cardiology/Cardiac Electrophysiology
11/2011 – 12/2011	Research Fellowship, Yale University/Aortic Institute (New Haven, CT) Project: Natural history and the role of pain in thoracic aortic aneurysm (Supervisor: John Elefteriades, MD)
10/2011 – 12/2011	Acting Internship, Yale University (New Haven, CT) Cardiac Surgery and Vascular Surgery
07/2011 – 12/2011	Acting Internship, University of North Carolina Chapel Hill (Chapel Hill, NC) Abdominal Transplant Surgery and Plastic Surgery
08/2008 – 09/2010	**Research Fellowship** Cardiac Electrophysiology, University of Vermont (Burlington, VT) Thesis: Mapping of Human Atrial Fibrillation – Constraints of Dominant Frequency and Complex Fractionated Atrial Electrograms (Supervisor: Peter Spector, MD; Helmut U. Klein, MD)

10/2004 – 07/2008   Medical School, Basic Science & Clinical Training Part I

09/2003 – 08/2004   **Research Fellowship, Humbolt University/Robert-Roessle Clinic (Berlin, Germany)**
Applied Physics & Radiation Therapy
Project: Radiofrequency hyperthermia as adjunct therapy in cancer treatment
Supervisor: Waldemar Wlodarczyk, PhD

08/1996 – 08/2004   **Lew-Landau Gymnasium (Weisswasser, Germany)**
Acceptance Qualification for Medical School (2004)

PROFESSIONAL NON-ACADEMIC WORK POSITIONS

11/2020 – Present   **Internal Medicine Hospitalist (per diem)**, Central Vermont Medical Center (Berlin, VT)

10/2020 – Present   **Consultant, CoreMap Inc.**

11/2012 – Present   **Founding Member and Educational Product Manager at Visible Electrophysiology, LLC**
VisibleEP is an interactive teaching tool for trainees of Cardiac Electrophysiology. The simulation software enables users to observe the spread of electrical activity through the heart and to interact with the rhythm. Pacing maneuvers, 3D-electronanatomic mapping and ablation can be practiced in this virtual environment.

11/2012 – Present   **Consultant & Educational Workshop Instructor, Biosense Webster Inc**

07/2019 – 06/2021   **Member of the Program Evaluation Committee**
General Cardiology Fellowship, University of Vermont Medical Center

07/2016 – 06/2018   **Member of the Institutional Review Board**, Carilion Clinic (Roanoke, VA)

07/2016 – 06/2018   **Elected Member of the Quality and Patient Safety Subcommittee,** Carilion Clinic (Roanoke, VA)

07/2016 – 06/2018   **Standing member of the Joint Quality Committee**, Carilion Clinic (Roanoke, VA)

09/2014 – 09/2017   **Advisory Board Member, Loma Linda University**
Cardiac Electrophysiology Technician Program (Loma Linda, CA)

11/2012 – 12/2016   **Consultant & Educational Workshop Instructor, Medtronic Inc**

HONORS and AWARDS

10/2016 Carilion Clinic Compassion Value Award Winner
In recognition of your concern for the patient experience and your compassion and caring attitude towards others.

02/2011 Deutsche Studienstiftung - German National Academic Foundation Scholarship
Awarded for outstanding academic achievements, creative approaches in teaching, interdisciplinary dialogue, and great social responsibility.

LICENSURE/BOARD CERTIFICATION

2020   Vermont Licensure Internal Medicine
2018   Board Certification Internal Medicine (ABIM)
2012   Full Registration/Licensure Deutsche Ärztekammer, Germany

TEACHING EXPERIENCE

TEACHING

07/2018 – Present **Students**	**Cardiology Service Teaching: Junior Fellows, Residents, UVM Medical**
	University of Vermont Medical Center (Burlington, VT) Including: Bedside Cardiac Ultrasound for Residents (Hands-on Workshop)
07/2015 – 06/2015 **Students**	**Medical Service Teaching: Junior residents, VTCSOM and VCOM Medical**
	Carilion Clinic & Virginia Tech Carilion School of Medicine (Roanoke, VA)
11/2012 – Present **Fellows**	**Educational Workshop Instructor for Cardiology and Electrophysiology**
10/2005 – 08/2007	**Teaching Assistant (Applied Physics in Medicine)** Otto-von-Guericke University Magdeburg (Magdeburg, Germany)

MENTORING

2020 – Present:	Advisor for Women in Medicine Applying to Cardiology Fellowship

SCHOLARSHIP

PEER-REVIEWED PUBLICATIONS

1. Infeld M, Avram R, Wahlberg K, Silverman DN, **Habel N**, Lustgarten DL, Pletcher M, Olgin JE, Marcus G, Meyer M. An approach towards individualized lower rate settings for pacemakers. *Heart Rhythm O2* 2020; 1(5):P390-393

2. Wall A, **Habel N**. Extensive myocarditis masquerading as lateral ST elevation myocardial infarction. *NASCI Case in point* 2020

3. Carrick R, Bates ORJ, Benson BE, **Habel N**, Bates JHT, Spector PS. Prospectively Quantifying the Propensity for Atrial Fibrillation: A Mechanistic Formulation. *PLoS One* 2015; 10(3):e0118746

4. Benson BE, Carrick R, **Habel N**, Bates ORJ, Bates JHT, Bielau P, Spector PS. Mapping multi-wavelet reentry without isochrones: an electrogram-guided approach to define substrate distribution *Europace* 2014; 16 Suppl4:iv102-iv109

5. Spector PS, **Habel N**. Principles of Differential Diagnostic Pacing Maneuvers: Serial vs. Parallel Conduction. *Pacing Clin Electrophysiol* 2014; 37(7):909-22

6. Thompson NC, Stinnett-Donnelly, **Habel N**, Benson B, Bates JHT, Sobel BE, Spector PS. Improved spatial resolution and electrogram wave direction independence with the use of an orthogonal electrode configuration. *J Clin Monit Comput* 2014 Apr; 28(2):157-163

7. Carrick R, Benson B, **Habel N**, Bates O, Bates JHT, Spector PS. Ablation of Multi-Wavelet Reentry Guided by Circuit Density and Distribution: Maximizing the Probability of Circuit Annihilation. *Circ Arrhythm Electrophysiol* 2013; 6(6):1229-35

8. Elefteriades JA, **Habel N**, Sun W, Sang AX, Kuzmik GA. The aortic wall: Four questions and insights. *J Thorac Cardiovasc Surg* 2013; 145(3):S130-134

9. Spector PS, Correa de Sa, Tischler ES, Thompson NC, **Habel N**, Stinnett-Donnelly, Benson BE, Bielau P, Bates JHT. Ablation of Multi-Wavelet Reentry: General Principles and in silico analyses. *Europace* 2012; 14 Suppl 5:v106-111

10. Stinnett-Donnelly JM, Thompson N, **Habel N**, Petrov-Kondratov V, Correa de Sa DD, Bates JHT, Spector PS. Effects of electrode size and spacing on the resolution of intracardiac electrograms. *Coron Artery Dis* 2012; 23(2):126-32

11. Correa de Sa DD, Thompson N, Stinnett-Donnelly J, Znojkiewicz P, **Habel N**, Müller JG, Bates JHT, Buzas JS, Spector PS. Electrogram fractionation: the relationship between spatiotemporal variation of tissue excitation and electrode spatial resolution. *Circ Arrhythm Electrophysiol* 2011; 4(6):909-16

12. **Habel N**, Müller JG, Znojkiewicz P, Thompson N, Calame J, Calame S, Noori A, Gallo A, Lustgarten DL, Sobel BE, Spector PS. The impact of pharmacologic sympathetic and parasympathetic blockade on atrial electrogram characteristics in patients with atrial fibrillation. *Pacing Clin Electrophysiol* 2011; 34(11):1460-7

13. Spector PS, **Habel N**, Sobel BE, Bates JHT. Emergence of complex behavior: an interactive model of cardiac excitation provides a powerful tool for understanding electric propagation. *Circ Arrhythm Electrophysiol* 2011; 4(4):586-91

14. **Habel N**, Znojkiewicz P, Thompson N, Müller JG, Mason B, Calame J, Calame S, Sharma S, Mirchandani G, Janks D, Bates J, Noori A, Karnbach A, Lustgarten DL, Sobel BE, Spector PS. The temporal variability of dominant frequency and complex fractionated atrial electrograms constrains the validity of sequential mapping in human atrial fibrillation. *Heart Rhythm* 2010; 7(5):586-93

PUBLICATIONS (non-reviewed)
Habel N. Computer Modeling in EP Education. EP Lab Digest 2014; 14(7)

BOOK CHAPTERS
1. **Habel N,** Lustgarten DL. His Bundle Pacing in Cardiac Electrophysiology: Clinical Case Review, 2nd edition. 2020 (Natale, Wang, Al-Ahmad, Estes)

2. **Habel N,** Lustgarten DL. His Bundle Pacing vs. Biventricular Pacing for CRT in Device Therapy for Cardiac Arrhythmias. 2019 (Steinberg, Epstein)

NATIONAL PRESENTATIONS
1. **Quality Improvement Project: Improving medication reconciliation to reduce the risk of medication errors.** Carilion Clinic and Virginia Tech Carilion School of Medicine (May 2018)

2. **Quality Improvement Project: Medication Refills in the Internal Medicine Resident Clinic.** Carilion Clinic and Virginia Tech Carilion School of Medicine (May 2017)

3. **Habel N**, Znojkiewicz P, Thompson N, Müller JG, Noori A, Calame J, Calame S, Sobel BE, Spector PS. The Effects of Pharmacologic Autonomic Blockade on Frequency and Fractionation in Human Atrial Fibrillation. *Heart Rhythm Society Meeting* 2010

INVITED LECTURES
1. **Case Presentation: PVC-induced Cardiomyopathy**
   ACC.21 Annual Scientific Session Meeting, May 2021

2. **EP Fellows Conference: From Ion Channels to Clinical Electrophysiology**
   Virginia Commonwealth University, September 2016

3. **Cardiology Core Conference: Arrhythmia Mechanisms**
   Virginia Commonwealth University, September 2016

4. **Cardiology Core Conference: From Ion Channels to Clinical Electrophysiology**
   Virginia Commonwealth University, September 2016

POSTER PRESENTATIONS
1. Infeld M, Meagher S, Nicoli C, Wayne S, Irvine B, Tomkins B, Betageri O, **Habel N**, Lobel R, Lustgarten DL. Bachmann Bundle Pacing is associated with decreased incidence of atrial arrhythmias. *Heart Rhythm Society Meeting* 2020

2. Infeld M, Nicoli C, Meagher S, Wayne S, Tomkins B, Irvine B, Betageri O, **Habel N**, Lustgarten DL. Electrically Guided Bachmann Bundle Pacing is associated with increased freedom from atrial arrhythmias. *Heart Rhythm Society Meeting* 2020

3. Wahlberg K, **Habel N.** Dynamic Left Ventricular Outflow Tract Obstruction, Severe Mitral Regurgitation and Cardiogenic Shock Precipitated by Stress Cardiomyopathy. *ACC 2020 World Congress of Cardiology*

4. **Habel N,** Bhowansingh R. Unusually large exophytic penile mass. *National ACP Meeting 2018*

5. **Habel N,** Spector PS. Augmented Entrainment Mapping: Response at Non-Pacing Sites Reveals Proximity to Reentrant or Focal Source. *Heart Rhythm Society Meeting 2016*

6. Carrick R, Benson B, Bates O, **Habel N**, Bates JHT, Spector PS. Ablation of Multi-Wavelet Reentry Guided by Circuit Density. *Biomedical Engineering Society Meeting 2013*

7. Benson B, Carrick R, **Habel N**, Bielau P, Bates O, Spector PS. Mapping Atrial Fibrillation: High Resolution Electrograms Identify Circuit Density. *Biomedical Engineering Society Meeting 2013*

8. Benson B, **Habel N**, Carrick R, Bielau P, Spector PS. Tissue Activation Frequency Identifies Rotor Density in Multi-Wavelet Reentry. *Heart Rhythm Society Meeting 2013*

9. Thompson N, Stinnett-Donnelly J, **Habel N**, Bates JHT, Spector PS. Orthogonal Close Unipolar Recording: Improved Spatial Resolution without Direction Dependence. *Heart Rhythm Society Meeting 2011*

10. Znojkiewicz P, Thomspon N, **Habel N**, Müller JG, Spector PS. Complex Fractionated Atrial Electrogram Detection and Inter-Electrode Spacing. *Heart Rhythm Society Meeting 2011*

11. **Habel N**, Znojkiewicz P, Thompson N, Karnbach A, Sobel BE, Bates JHT, Spector PS. Dissociation between Electrogram Frequency and Tissue Frequency. *Heart Rhythm Society Meeting 2010*

RESEARCH SUPPORT
05/27/2020 – Present Medtronic Investigator Initiated Research Grant 12047
                     Principal Investigator: Daniel L. Lustgarten
                     Physiologic accelerated pacing as a treatment in patients with heart failure with preserved ejection fraction (PACE HFpEF)
                     NCT04546555 (enrolling)
                     Role: Co-Investigator

MEMBERSHIP IN PROFESSIONAL SOCIETIES/ORGANIZATIONS

11/2012 – Present   Alumni Deutsche Studienstiftung – German National Academic Foundation
07/2018 – Present   ACC Member
03/2019 – Present   HRS Member
07/2015 – 06/2018   ACP Resident Member
07/2015 – 06/2018   AMA Resident Member

Colchester Vermont (USA), den 22. April 2021

Nicole Habel